Sulphur isotope fractionation in modern and ancient sediments: field and laboratory experiments

Thi Hao Bui

Department of Earth and Planetary Sciences

McGill University

Montreal, Quebec

April, 2014

A thesis submitted to McGill University in partial fulfillment of the requirements of the degree of Doctor of Philosophy

DEDICATION

I dedicate this thesis to my husband, Xuan Tuan Le, to my son, Minh Le, and to my little daughter, Anh Minh Le. Thank you for your love and support. Time with you is never enough.

ACKNOWLEDGEMENTS

My first and foremost acknowledgement is to my supervisor, Professor Boswell Wing, who gave me a chance to come back to academia. I thank him for his guidance in science as well as his financial support, and especially for his patience in correcting my writing. I also appreciate his understanding and sympathy in personal life.

I would like to acknowledge co-authors for their contribution into my thesis:

(1) Michael Riedel and Laura L. Lapham, who collected Cascadia porewater samples for my first project and helped me with mapping and describing study site,

(2) John W. Pohlman, who contributed lots of valuable inputs to better understand and to explain the sulphur isotope data of Cascadia samples,

(3) Andre Pellerin, who was always willing spending time discussing about writing and modeling.

I would like to thank Jean-Francois Helie and Agnieszka Adamowicz-Walczak at GEOTOP, UQAM for the help on sample preparation and carbon isotope measurements. I would like to thank Grant Cox for his help with writing skills and software skills. I also thank all members of PROPS (Precambriam Research group) at McGill and EPS administration group for your great help and enthusiasm.

TABLE OF CONTENTS

ABSTRACT

Modern and ancient sediments are complex biogeochemical systems where multiple sulphur isotopes may be useful in tracing previously unseen processes. Multiple sulphur isotope signatures of pore water sulphate from methane-rich marine sediments indicate different microbial pathways involved in the overall sulphur cycling. Particularly in chapter 2, we found that sulphate reduction is the only microbial process controlling the sulphur cycling at station 12 but at station 5 up to 60% of sulphide produced from sulphate reduction re-oxidizes back to sulphate. We are only able to tell this difference with multiple sulphur isotopes. (Chapter 2- *Hidden sulphur cycle stimulates the microbial methane biofilter in deep marine sediments*)

Beside biological processes, transport of material may cause isotope fractionation. We analyze multiple sulphur isotope composition of dissolved sulphate and sulphide when these ions diffused through an acrylamide gel column. The experimental results showed that the diffusion-associated isotope fractionation of ion sulphate is insignificant within the study size (~20 cm length) but the diffusion-associated isotope fractionation of ion sulphide is clearly observable ($^{34}\alpha = 0.9990 \pm 0.0005$). With that fractionation factor, when sulphide diffuses 1 meter away from the source, it is at least 10‰ lighter than the original isotope composition. (Chapter 3 - *Sulphur isotope effects of SO_4^{2-} and HS^- diffusion in water*)

In chapter 4, we apply multiple sulphur isotope techniques to study the sulphur cycling during the end-Permian mass extinction. Minor sulphur isotope signature suggests the mixing of at least two distinct sulphur sources during that time period. We have proposed possible sulphur sources even though further studies are required in order to identify exactly which sources contributed to the sulphur enrichment at Permian-Triassic period. (Chapter 4 - *Sulphur and carbon isotope records across the terrestrial Permian-Triassic (P-T) boundary*)

RÉSUMÉ

Les signatures isotopiques du soufre, dans les sédiments marins riches en méthane indiquent que différents processus microbiens jouent un rôle important dans le cycle global du soufre. En particulier dans le chapitre 2, nous avons constaté que la réduction de sulfate est le seul processus microbien qui contrôle le cycle de soufre à la station 12, mais à la station 5 à 60% du soufre réduit est ré-oxydé en sulphate *in-situ*. Cette conclusion est seulement possible grâce à la mesure de plusieurs isotopes du soufre (*Chapitre 2 - Hidden sulphur cycle stimulates the microbial methane biofilter in deep marine sediments*).

À part les processus biologiques, le simple transport par diffusion peut aussi causer un fractionnement isotopique. La composition isotopique du soufre de sulfate et de sulfure dissous varie lorsque ces ions diffusent à travers une colonne de gel d'acrylamide. Les résultats expérimentaux ont montré que le fractionnement isotopique associé à la diffusion d'ion sulfate est négligeable à l'intérieur de la plage d'étude (~20 cm de longueur) mais que le fractionnement isotope associé à la diffusion du sulfure est mesurable ($^{34}\alpha = 0.9990 \pm 0.0005$). Avec ce facteur de fractionnement, lorsque le sulfure diffuse à 1 mètre de la source, il est d'au moins 10‰ plus léger que la composition isotopique d'originale (*Chapitre 3 - Sulphur isotope effects of* SO_4^{2-} *and* HS^- *diffusion in water*).

Au chapitre 4, nous appliquons techniques de plusieurs isotopes du soufre pour étudier le cycle global du soufre au cours de l'extinction à la fin du Permien. Le soufre analysé dans les sédiments du basin Karoo, un bassin de provenance terrestre, reflète la signature atmosphérique globale du soufre lors de cette époque. Les signatures isotopiques suggèrent la présence de deux sources distinctes de soufre. Dans cette thèse, nous proposons un nombre de sources de soufre possibles, même si d'autres études sont nécessaires pour identifier précisément les sources du soufre atmosphérique lors de la période du Permien-Trias. (*Chapitre 4 - Sulphur and carbon isotope records across the terrestrial Permian-Triassic (P-T) boundary*)

CONTRIBUTIONS OF AUTHORS

The main body of this thesis consists of three chapters (Chapter 2 to Chapter 4). In chapter 2, we utilize multiple sulphur isotope data to investigate the different microbiological pathways controlling the sulphur cycle in Cascadia marine sediment. Chapter 3 describes the sulphate and sulphide diffusion experiments, as well as, the modeling work that allows estimating sulphur isotope fractionation associated with diffusion. Chapter 4 uses the sulphur and carbon isotope signatures of terrestrial sediments collected in Karoo Basin to investigate the possible sources of sulphur injected into the system ~ 252Ma ago. An introduction and overview is provided in Chapter 1, and conclusions to the work are provided in Chapter 5.

Chapter 2 is the manuscript *Hidden sulphur cycle stimulates the microbial methane biofilter in deep marine sediments* by Thi Hao Bui, John W. Pohlman, Laura L. Lapham, Michael Riedel, André Pellerin and Boswell Wing.

John W. Pohlman, Laura L. Lapham and Michael Riedel provided samples. André Pellerin provided input on the reoxidation model. Thi Hao Bui analyzed the samples, interpreted the data and wrote the manuscript. Boswell Wing supervised the interpretation and the writing.

Chapter 3 is the manuscript *Sulphur isotope fractionation produced by diffusions of dissolved sulphate and sulphide in an acrylamide gel system* by Thi Hao Bui and Boswell Wing.

Thi Hao Bui set up the experiments, analyzed the samples, interpreted the data and wrote the manuscript. Boswell Wing supervised the interpretation and the writing.

Chapter 4 is the manuscript *Sulphur and carbon isotope records across the terrestrial Permian-Triassic (P-T) boundary* by Thi Hao Bui and Boswell Wing.

Thi Hao Bui analyzed the samples, interpreted the data and wrote the manuscript. Boswell Wing provided samples, supervised the interpretation and the writing.

LIST OF TABLES

LIST OF FIGURES

CHAPTER 1

Introduction

1.1 Overview

Methane concentration in the atmosphere is orders of magnitude smaller than that of carbon dioxide but its global warming potential is much higher than carbon dioxide. Similar to carbon dioxide, increasing global methane concentrations have been noted (Blake and Rowland 1986; Steele, Fraser et al. 1987). Therefore it is critical to understand the sources of methane and the mechanisms that control methane release to the atmosphere.

Marine seepage is a major geological source of methane, which releases 20Tg per year (Etiope 2012). Methane concentrations in marine sediments are at milimolar levels but little of this methane apparently makes its way to the oceans and eventually to the atmosphere. Microbially-driven anoxic oxidation processes consume much of the methane before it leaves the sedimentary environment (Reeburgh 2007). Among these processes, sulphate reduction plays an important role due to the high sulphate concentrations in the modern ocean compared to other potential oxidants (Niewöhner, Hensen et al. 1998; Jørgensen, Weber et al. 2001).

In this thesis, I focus on the sedimentary sulphur cycle in methane-rich, organic matter-poor sediments at a well-studied gas hydrate site on the Cascadia margin off the west coast of Canada. In this environment, most sulphate reduction is coupled with the anaerobic oxidation of methane, and I use it as a case study to investigate how sulphur isotopes can constrain the microbial processes that enhance the capacity of sulphate to oxidize methane. Although biological processes impart significant sulphur isotope signals, abiotic processes like diffusion may also affect these signals. As a result I also present in this thesis an experimental calibration of how ionic diffusion affects sulphur isotopes.[1]

[1] The third part of this thesis was a project that I started when I began my PhD as a way to learn how to perform S isotope analyses. It is tangential to the main research questions in the thesis but included as a chapter here on terrestrial S isotope records during the Permian-Triassic mass extinction.

1.2 The biogeochemical sulphur cycle in marine sediments

1.2.1 Microbial sulphate reduction

Sulphate is the second most abundant anion in ocean water, after chloride, with the average concentration of ≈28mM (Canfield and Farquhar 2009). With a volume of 3.8×10^6 km^3, ocean water is an essentially infinite source of sulphate for anoxic microbial sulphate reduction. In the upper sediment layers, sulphate reduction is coupled with organic matter oxidation by the following net reaction:

$$2CH_2O + SO_4^{2-} \rightarrow HS^- + 2HCO_3^- + H^+$$

During this "organoclastic" sulphate reduction, rates are highest at the top of anoxic zone and decrease exponentially with depth (Berner, Leeuw et al. 1985). As a result, sulphate concentration profiles in sedimentary pore waters have a characteristic concave-down shape (Berner 1964).

In methane-rich, organic matter-poor sediments, sulphate is consumed in a narrow region in the deep sediment layers that is called the sulphate-methane transition zone (SMTZ) (Iversen and Jørgensen 1985). Here, sulphate diffusing downwards from seawater meets and reacts with methane diffusing upwards from deep biological or geological sources, leading to a net reaction like:

$$CH_4 + SO_4^{2-} \rightarrow HS^- + HCO_3^- + H_2O$$

This process is mediated by a consortium of archaea and sulphate reducing bacteria (Boetius, Ravenschlag et al. 2000). Sulphate reduction rates associated with this process are peaked with the maximum rate at the depth of the SMTZ (Iversen and Jørgensen 1985), which also corresponds to the maximum of sulfide production (Niewöhner, Hensen et al. 1998). Because sulphate concentrations in this situation are only driven by ionic diffusion from the seawater-sediment interface to the SMTZ, sulphate concentrations in sedimentary pore waters have a characteristic straight-line profile at steady state (Borowski, Paull et al. 1997; Borowski, Paull et al. 1999). This characteristic has been used to distinguish the relative influences of organoclastic sulphate reduction versus sulphate reduction associated with the anaerobic oxidation of methane.

1.2.2 Sulphide reoxidation and disproportionation

Sulphide, as a product of sulphate reduction, can be trapped in sediments in the forms of iron monosulphide (FeS) and pyrite (FeS_2). However, only a small fraction of sulphide is permanently buried within sediments (5%-20%) (Canfield and Teske 1996; Schippers and Jørgensen 2002) because the production of sulphide by microbial sulphate reduction is much greater than the sedimentary supply of reactive iron phases (Raiswell and Canfield 1998). The remaining sulphide is gradually oxidized back to sulphate by abiotic and biotic processes (Aller and Rude 1988; Schippers and Jørgensen 2002; Jørgensen and Nelson 2004).

Some of these processes are unlikely in typical marine environments. For example, the direct oxidation of sulphide by oxygen only happens under special conditions, such as when sulphide production is so high that oxidants and metal oxides are rapidly consumed leading to the escape of sulphide out of the sediments. In another situations, oxygen can be injected directly into the sulphide zone by bioirrigation (Jørgensen and Nelson 2004). Oxygen chemically oxidizes sulphide to sulphate by following reaction:

$$HS^- + O_2 \rightarrow SO_4^{2-} + H^+$$

However, in typical marine sediments, dissolved sulphide and oxygen are normally separated by an intermediate sub-oxic zone where iron and manganese oxides form a barrier that oxidizes and traps sulfide diffusing up from below (Jørgensen and Nelson 2004).

In this sub-oxic zone, sulphide can be reoxidized completely to sulphate or partially to intermediate oxidation state sulphur compounds through biotic or abiotic processes (Yao and Millero 1996; Schippers and Jørgensen 2001) by reactions like:

$$FeS_2 + 7.5MnO_2 + 11H^+ \rightarrow Fe(OH)_3 + 2SO_4^{2-} + 7.5Mn^{2+} + 4H_2O$$

$$3H_2S + 2FeOOH \rightarrow S^o + 2FeS + 4H_2O$$

$$FeS + 1.5MnO_2 + 3H^+ \rightarrow Fe(OH)_3 + S^o + 1.5Mn^{2+}$$

The intermediate sulphur compounds later can be disproportionated back to sulphate and sulphide without the requirement of external oxidants or reductants (Bak and Pfennig 1987) through microbially-driven reactions like:

$$S_2O_3^{2-} + H_2O \rightarrow HS^- + SO_4^{2-} + H^+$$

$$4SO_3^{2-} + 2H^+ \rightarrow 3SO_4^{2-} + HS^-$$

As the disproportionation reactions require microbial catalysis, they are only energetically favorable at low sulphide concentrations (Thamdrup, Finster et al. 1993).

1.3 Multiple sulphur isotopes as tracers of biogeochemical processes in the marine sulphur cycle

1.3.1 Multiple sulphur isotope systematics

Sulphur has four stable isotopes with ^{32}S being the most abundant (95.04%), followed by ^{34}S (4.20%), ^{33}S (0.75%) and ^{36}S (0.015%) (Ding, Valkiers et al. 2001). The sulphur isotope composition of a sample is reported relative to the international standard V-CDT (Vienna Canyon Diablo Troilite) in delta notation ($\delta^{3x}S$):

$$\delta^{3x}S\ (‰) = \left\{ \frac{{}^{3x}S_{sample} / {}^{32}S_{sample}}{{}^{3x}S_{V-CDT} / {}^{32}S_{V-CDT}} - 1 \right\} \times 1000$$

where 3*x* can be 33, 34 or 36. On this scale, the sulphur isotope composition of the international reference material (IAEA-S-1, Ag_2S) is defined as $\delta^{34}S_{V\text{-}CDT} = -0.3‰$.

During multiple sulphur isotope measurements, we obtain three delta values ($\delta^{33}S$, $\delta^{34}S$, and $\delta^{36}S$) for each sample. Under conditions of high-temperature equilibrium, these values are related to each other by their relative mass differences such that:

$$\delta^{33}S \approx 0.515 \times \delta^{34}S$$

$$\delta^{36}S \approx 1.9 \times \delta^{34}S$$

However, these relationships will change if the measured sample was involved in geological or biological processes that are different than high-temperature equilibration. The deviation of $\delta^{33}S$ values from the "predicted" $\delta^{33}S$ value assuming high-temperature equilibration is defined as $\Delta^{33}S$ where:

$$\Delta^{33}S(‰) = \delta^{33}S - \left[\left(\frac{\delta^{34}S}{1000} + 1 \right)^{\wedge 0.515} - 1 \right] \times 1000$$

Although similar arguments can be used to define $\Delta^{36}S$ values, I do not discuss them here. The abundance of ^{36}S is lower than any other sulphur isotope, which leads to the relatively higher

uncertainty in $\delta^{36}S$ measurements. As a result, $\Delta^{36}S$ values don't add any additional information than can be obtained from the more precise $\Delta^{33}S$ measurements.

The effectiveness of processes that separate or "fractionate" sulphur isotopes can be characterized by a fractionation factor, α. In this notation, fractionation between two sulphur pools, A and B, is defined:

$$^{3x}\alpha_{AB} = \frac{\left({}^{3x}S/{}^{32}S\right)_A}{\left({}^{3x}S/{}^{32}S\right)_B}$$

where 3*x* can be 33, 34 or 36. These α values are always very close to 1. They are often expressed as relative differences in ‰ in order to isolate those parts that are different from 1, such as: $(^{3x}\alpha_{AB} - 1) \times 1000$. There are characteristic 'slopes' between $^{3x}\alpha_{AB}$ values that are characterized as:

$$^{33}\lambda = \frac{ln\left(^{33}\alpha\right)}{ln\left(^{34}\alpha\right)}$$

In this notation, high-temperature equilibrium has a $^{33}\lambda$ value that is very close to 0.515.

1.3.2 Multiple sulphur isotope fractionation by sedimentary biogeochemical processes

Pure cultures of sulphate reducing bacteria produce a large range of isotope fractionation, from 2‰ to 47‰, even at the optimum growth conditions for each species (Detmers, Brüchert et al. 2001; Brüchert 2004). But the fractionation observed in natural systems can be much higher, up to 75‰ (Wortmann, Bernasconi et al. 2001; Canfield, Farquhar et al. 2010). This large isotope fractionation has been interpreted as the result of extracellular sulphide reoxidation and microbial sulphur disproportionation (Canfield and Thamdrup 1994; Canfield and Teske 1996). However, recent work has shown that sulphate reduction alone can produce a large fractionation, up to 66‰ (Sim, Bosak et al. 2011). Therefore it is difficult to distinguish these microbial processes by measuring traditional ^{34}S fractionation.

On the contrary, sulphide oxidation and subsequent disproportionation produce distinct multiple sulphur isotope signatures that are different from microbial sulphate reduction. Particularly, the $^{33}\lambda$ value obtained from microbial sulphate reduction ranges from 0.5090 to 0.5145 (Johnston, Farquhar et al. 2005; Sim, Bosak et al. 2011; Sim, Ono et al. 2011). As this is

less than the reference $^{33}\lambda$ value corresponding to high-temperature equilibration, this results a negative trend on a $\Delta^{33}S$-$\delta^{34}S$ plot. On the other hand, microbial disproportionation is characterized by $^{33}\lambda$ values that are larger (≥ 0.515) leading to a neutral to positive slope on a $\Delta^{33}S$-$\delta^{34}S$ plot (Johnston, Farquhar et al. 2005).

According to kinetic theory, an object with lower mass moves faster than an object with higher mass and the relationship between the velocity and mass is described by the inversed square root equation:

$$\frac{v_1}{v_2} = \left(\frac{m_2}{m_1}\right)^{0.5}$$

Applying this theory for isotopes results the fractionation during diffusion because light isotope-substituted isotopologue diffuses faster than heavy isotope-substituted isotopologue. In fact, various studies on diffusion of ionic species in aqueous systems obtained fractionations ≤1‰, with exponential factors order of magnitude smaller than 0.5 (Richter, Mendybaev et al. 2006; Eggenkamp and Coleman 2009). Therefore the contribution of diffusion to isotope fractionation is usually ignored when studying reaction-transport processes (Bourg 2008; Wortmann and Chernyavsky 2011), although recent work has suggested that diffusive fractionations are up to 10‰. These conflicting results can only be resolved by a well-designed laboratory experiment to determine the magnitude of sulphur isotope fractionation produced by sulphate and sulfide diffusion. Modelling the interaction of all these specific isotope fractionations and measuring the overall isotope fractionation in natural samples will enable new constraints the magnitude of sulphur recycling, and methane consumption, in natural sedimentary systems.

1.4 Research objectives

This thesis includes three main chapters to address three major questions:

1. Does sulfide reoxidation happen in methane-rich anoxic sediments? How is it important to the regulation of the methane flux from sediments into the ocean?

Up to 90% of the sulphide produced in sediments is reoxidized in oxic and suboxic zones (Jørgensen and Nelson 2004). But sulphide oxidation in anoxic sulphate-methane transition zone

has never been reported. In this study, we measure concentrations and multiple sulphur isotope signatures of dissolved sulphate and sulphide in pore water samples collected in the Cascadia margin, offshore Vancouver Island. We develop a box model to describe the effect of sulphide reoxidation on isotope fractionation and use this model to quantify the magnitude of sulphide recycling. Based on that, we evaluate the enhanced capacity of sulphate to prevent methane escape from sediments.

2. What is the magnitude of sulphur isotope fractionation by sulfate and sulfide diffusion? What is its impact on the sulphur isotope records in marine sediments?

In this study, we design a series of experiment to examine the sulphur isotope fractionation produced by sulphate and sulphide diffusion in aqueous environment. The result helps to validate the assumption we have made in the sulphide reoxidation model (in the previous chapter), that the sulphur isotope fractionation in marine sediments is only driven by microbial processes. Moreover, this work offers the first hard evidence that transport-associated sulphur isotope fractionation is negligible.

3. Can we see the input of sulfur from Siberian traps into the surface earth system at the Permian-Triassic boundary?

We evaluate the potential relationship of eruption of the Siberian traps and the Permian-Triassic mass extinction event by studying the sulphur isotope geochemistry of two terrestrial sediment sections from the Karoo Basin, South Africa. The two studied sections are correlated with each other and with other terrestrial Permian-Triassic sections in Karoo Basin by carbon isotope excursions. We determine the variation of sulphur content to find out the injections of sulphur into the sediments at the Permian-Triassic boundary, constraining possible sources of sulphur to this sulphur-poor terrestrial environment.

1.5 References

Aller, R. C. and P. D. Rude (1988). "Complete oxidation of solid phase sulfides by manganese and bacteria in anoxic marine sediments." Geochimica et Cosmochimica Acta **52**(3): 751-765.

Bak, F. and N. Pfennig (1987). "Chemolithotrophic growth of Desulfovibrio sulfodismutans sp. nov. by disproportionation of inorganic sulfur compounds." Archives of Microbiology **147**(2): 184-189.

Berner, R. A. (1964). "An idealized model of dissolved sulfate distribution in recent sediments." Geochimica et Cosmochimica Acta **28**(9): 1497-1503.
Berner, R. A., J. W. D. Leeuw, et al. (1985). "Sulphate Reduction, Organic Matter Decomposition and Pyrite Formation [and Discussion]." Philosophical Transactions of the Royal Society of London. Series A, Mathematical and Physical Sciences **315**(1531): 25-38.
Blake, D. R. and F. S. Rowland (1986). "World-wide increase in tropospheric methane, 1978–1983." Journal of atmospheric chemistry **4**(1): 43-62.
Boetius, A., K. Ravenschlag, et al. (2000). "A marine microbial consortium apparently mediating anaerobic oxidation of methane." Nature **407**(6804): 623-626.
Borowski, W. S., C. K. Paull, et al. (1997). "Carbon cycling within the upper methanogenic zone of continental rise sediments; An example from the methane-rich sediments overlying the Blake Ridge gas hydrate deposits." Marine Chemistry **57**(3–4): 299-311.
Borowski, W. S., C. K. Paull, et al. (1999). "Global and local variations of interstitial sulfate gradients in deep-water, continental margin sediments: Sensitivity to underlying methane and gas hydrates." Marine Geology **159**(1–4): 131-154.
Bourg, I. C. (2008). "Comment on "Modeling sulfur isotope fractionation and differential diffusion during sulfate reduction in sediments of the Cariaco Basin" by M.A. Donahue, J.P. Werne, C. Meile and T.W. Lyons." Geochimica et Cosmochimica Acta **72**(23): 5852-5854.
Brüchert, V. (2004). "Physiological and ecological aspects of sulfur isotope fractionation during bacterial sulfate reduction." Geological Society of America Special Papers **379**: 1-16.
Canfield, D. E. and J. Farquhar (2009). "Animal evolution, bioturbation, and the sulfate concentration of the oceans." Proceedings of the National Academy of Sciences **106**(20): 8123-8127.
Canfield, D. E., J. Farquhar, et al. (2010). "High isotope fractionations during sulfate reduction in a low-sulfate euxinic ocean analog." Geology **38**(5): 415-418.
Canfield, D. E. and A. Teske (1996). "Late Proterozoic rise in atmospheric oxygen concentration inferred from phylogenetic." Nature **382**: 11.
Canfield, D. E. and A. Teske (1996). "Late Proterozoic rise in atmospheric oxygen concentration inferred from phylogenetic and sulphur-isotope studies." Nature **382**(6587): 127-132.
Canfield, D. E. and B. Thamdrup (1994). "The production of 34S-depleted sulfide during bacterial disproportionation of elemental sulfur." Science **266**(5193): 1973-1975.
Detmers, J., V. Brüchert, et al. (2001). "Diversity of sulfur isotope fractionations by sulfate-reducing prokaryotes." Applied and environmental microbiology **67**(2): 888-894.
Ding, T., S. Valkiers, et al. (2001). "Calibrated sulfur isotope abundance ratios of three IAEA sulfur isotope reference materials and V-CDT with a reassessment of the atomic weight of sulfur." Geochimica et Cosmochimica Acta **65**(15): 2433-2437.
Eggenkamp, H. and M. L. Coleman (2009). "The effect of aqueous diffusion on the fractionation of chlorine and bromine stable isotopes." Geochimica et Cosmochimica Acta **73**(12): 3539-3548.
Etiope, G. (2012). "Climate science: Methane uncovered." Nature Geosci **5**(6): 373-374.
Iversen, N. and B. Jørgensen (1985). "Anaerobic methane oxidation rates at the sulfate-methane transition in marine sediments from Kattegat and Skagerrak (Denmark)." Limnol. Oceanogr **30**(5): 944-955.

Johnston, D. T., J. Farquhar, et al. (2005). "Multiple sulfur isotope fractionations in biological systems: a case study with sulfate reducers and sulfur disproportionators." American Journal of Science **305**(6-8): 645-660.
Jørgensen, B. B. and D. C. Nelson (2004). "Sulfide oxidation in marine sediments: Geochemistry meets microbiology." Geological Society of America Special Papers **379**: 63-81.
Jørgensen, B. B., A. Weber, et al. (2001). "Sulfate reduction and anaerobic methane oxidation in Black Sea sediments." Deep Sea Research Part I: Oceanographic Research Papers **48**(9): 2097-2120.
Niewöhner, C., C. Hensen, et al. (1998). "Deep sulfate reduction completely mediated by anaerobic methane oxidation in sediments of the upwelling area off Namibia." Geochimica et Cosmochimica Acta **62**(3): 455-464.
Niewöhner, C., C. Hensen, et al. (1998). "Deep Sulfate Reduction Completely Mediated by Anaerobic Methane Oxidation in Sediments of the Upwelling Area off Namibia." Geochimica et Cosmochimica Acta **62**(3): 455-464.
Raiswell, R. and D. E. Canfield (1998). "Sources of iron for pyrite formation in marine sediments." American Journal of Science **298**(3): 219-245.
Reeburgh, W. S. (2007). "Oceanic Methane Biogeochemistry." Chemical Reviews **107**(2): 486-513.
Richter, F. M., R. A. Mendybaev, et al. (2006). "Kinetic isotopic fractionation during diffusion of ionic species in water." Geochimica et Cosmochimica Acta **70**(2): 277-289.
Schippers, A. and B. Jørgensen (2001). "Oxidation of pyrite and iron sulfide by manganese dioxide in marine sediments." Geochimica et Cosmochimica Acta **65**(6): 915-922.
Schippers, A. and B. B. Jørgensen (2002). "Biogeochemistry of pyrite and iron sulfide oxidation in marine sediments." Geochimica et Cosmochimica Acta **66**(1): 85-92.
Sim, M. S., T. Bosak, et al. (2011). "Large Sulfur Isotope Fractionation Does Not Require Disproportionation." Science **333**(6038): 74-77.
Sim, M. S., S. Ono, et al. (2011). "Effect of electron donors on the fractionation of sulfur isotopes by a marine< i> Desulfovibrio</i> sp." Geochimica et Cosmochimica Acta **75**(15): 4244-4259.
Steele, L., P. Fraser, et al. (1987). The global distribution of methane in the troposphere. Scientific Application of Baseline Observations of Atmospheric Composition (SABOAC), Springer**:** 417-463.
Thamdrup, B., K. Finster, et al. (1993). "Bacterial disproportionation of elemental sulfur coupled to chemical reduction of iron or manganese." Applied and environmental microbiology **59**(1): 101-108.
Wortmann, U. G., S. M. Bernasconi, et al. (2001). "Hypersulfidic deep biosphere indicates extreme sulfur isotope fractionation during single-step microbial sulfate reduction." Geology **29**(7): 647-650.
Wortmann, U. G. and B. M. Chernyavsky (2011). "The significance of isotope specific diffusion coefficients for reaction-transport models of sulfate reduction in marine sediments." Geochimica et Cosmochimica Acta **75**(11): 3046-3056.
Yao, W. and F. J. Millero (1996). "Oxidation of hydrogen sulfide by hydrous Fe(III) oxides in seawater." Marine Chemistry **52**(1): 1-16.

CHAPTER 2

Hidden sulphur cycle stimulates the microbial methane biofilter in deep marine sediments

Thi Hao Bui, John W. Pohlman, Laura L. Lapham, Michael Riedel, André Pellerin,

and Boswell Wing

2.1 Abstract

Marine seepage is a major geological source of methane which releases ~20Tg methane per year[1]. However, it is only a small fraction of the methane generated marine sediments because most of this methane is oxidized in sediments and the water column by microbially-mediated processes[2]. Microbial sulphate reduction, in particular, plays an important role in regulating the methane flux out of marine sediments, and ultimately from the ocean to the atmosphere[3]. Stoichiometric coupling of the mutualistic anaerobic oxidation of methane (AOM) and bacterial sulphate reduction (BSR) in a 1:1 consumption ratio has enabled dissolved sulphate profiles in marine sediments to constrain sedimentary methane fluxes. Here, we show that reoxidative sulphur cycling can dictate the methane flux out of marine sediments. This process is effectively hidden from conventional geochemical techniques, but is revealed through its effects on the multiple sulphur isotope composition of sulphate from pore waters above methane-bearing marine sediments. Existing theoretical approaches[4] are able to quantify the reoxidative throttle identified here, and so could improve the estimation of the methane fluxes.

2.2 Main text

In methane-rich sediments, an upward flux of methane from depth drives a downward flux of sulphate from the overlying water column. A metabolic mutualism between the anaerobic oxidation of methane (AOM) and sulphate reduction[5] draws both methane and sulphate concentrations to near zero within the sulphate-methane transition zone (SMTZ)[6]. The stoichiometric simplicity of this arrangement, where the removal of each molecule of methane is linked to the removal of one molecule of sulphate[5], enables straightforward estimates of methane fluxes and SMTZ depths[6]. With a primary sink within the SMTZ, sulphate in the overlying

sedimentary pore waters is essentially a passive tracer of the rate of AOM, leading to characteristic linear profiles of sulphate concentration with depth[6,7].

Although AOM is the final sulphate sink, organoclastic sulphate reduction may also occur in sediments above the SMTZ[8], provided enough metabolizable organic substrates and a lack of oxidants associated with higher metabolic energy yields than sulphate[9]. The localization of AOM beneath this oxidant biofilter is consistent with the common observation of diagenetic enrichment of iron sulphide minerals in SMTZ sediments[10]. A protective overlying redox gauntlet and a ready sink for sulphide both suggest that the sulphur cycle in methane-rich sediments is essentially a unidirectional reductive process, responding largely to the magnitude of methane flux into the SMTZ. Reoxidative sulphur cycling, whereby sulphide is ultimately oxidized back to sulphate through a multi-step pathway including disproportionation[11], is common when the SMTZ has essentially intersected the sediment-water interface[12] but would be surprising within the anoxic sediments of a deeply buried SMTZ. However, reoxidative sulphur cycling can strongly influence elemental and energetic budgets in unexpected environments, in which either a tight coupling to sulphate reduction[13] or the exploitation of latent oxidants[14] mask its effects. We took advantage of distinctive multiple sulphur-isotope signatures ($^{33}S/^{32}S$ and $^{34}S/^{32}S$) produced by sulphate-reducing bacteria and sulphur-disproportionating bacteria[15] to reveal the influence of deep reoxidative sulphur cycling in methane-rich sediments offshore of Vancouver Island, Canada.

The northern Cascadia active margin off Canada's West coast hosts one of the best studied marine gas hydrate provinces worldwide, with intensive cold-vent monitoring starting over a decade ago[16]. We collected sediment cores in the area of a major cold seep (referred to as Bullseye Vent) in an on-slope basin at a water depth of ≈1260 m (Fig. 2.1). In this area, methane appears to be largely sourced from microbial CO_2 reduction within the offshore accretionary prism[17]. Migration of methane-bearing fluids through vertical fracture networks sustains gas hydrate 'caps' about 2 to 8 m below the seafloor, above which vents are sporadically developed[16]. We measured the concentrations and full sulphur isotope compositions of dissolved sulphate and sulphide in pore waters squeezed from the sediment cores.

Dissolved sulphate concentrations decrease with depth to near-zero values, while $\delta^{34}S$ values increase with depth in an exponential fashion (Fig. 2.2). These features are consistent with

microbial reduction of sulphate in a transport-limited system. Both profiles also possess similar geometries, with an upper portion where dissolved sulphate concentrations and sulphur isotope compositions remain relatively constant and close to those typical of seawater sulphate ($[SO_4^{2-}] \approx$ 28mM[18], $\delta^{34}S \approx +21‰$ V-CDT[18], $\Delta^{33}S \approx +0.04‰$ V-CDT[19]). These homogeneous layers, which extend nearly 1m in both profiles, are related to bioirrigation or recent deposition from surrounding regions with much shallower sulphate gradients[7]. Below the homogeneous layers, sulphate concentrations decrease linearly with depth in both profiles, reaching the SMTZ at ≈ 4m at station 5 and at ≈ 2m at station 12. Linear sulphate concentration profiles are consistent with sulphate consumption by AOM in a deep SMT rather than in the overlying sediment column[6].

We evaluated the hypothesis of AOM-driven sulphate consumption by comparing our pore water sulphate profiles with the results of a minimal model of sulphate transport, consumption, and isotope fractionation. Our simple diagenetic model assumes steady-state, diffusion-dominated sulphate transport into the SMTZ, where AOM is the only process driving sulphur isotope fractionation. The geochemical homogeneity of the upper sediments sets the concentration and sulphur isotope composition of sulphate entering the modeled sediment column. The sulphate profile, then, is controlled by one free parameter: the sulphate concentration (C_{SMT}) at the top of the modeled SMTZ. The $\delta^{34}S$ profile, in turn, is set by C_{SMT} and a second free parameter: the fractionation factor ($^{34}\alpha$) associated with sulphate reduction rates across the SMTZ. With nearly equivalent C_{SMT} values (3.1 mM for station 5; 2.3 mM for station 12) and the same $^{34}\alpha$ values (0.95), the model reproduces profiles of sulphate concentrations and $\delta^{34}S$ values at both stations (Fig. 2.2). The estimated $^{34}\alpha$ values correspond to an isotope fractionation of 50‰, which is not unusual for marine settings and well within the range reported for pure cultures of sulphate-reducing bacteria[20]. Overall, the fit is remarkable given the simplicity of the model, and suggests that SMT depths or, equivalently, methane fluxes, are the only differences between the two stations.

Sulphate-reducing bacteria and archea produce characteristic fractionations between ^{33}S and ^{32}S that accompany ^{34}S and ^{32}S fractionations[21]. The enzymatic reaction network that supports the respiratory sulphate metabolism limits the full thermodynamic expression of these fractionations, resulting in an intrinsic negative correlation between $\Delta^{33}S$ and $\delta^{34}S$ values associated with intracellular sulphate reduction[22]. For an $^{34}\alpha$ value of 0.95, the experimentally derived slopes that characterize these correlations range from 0.5117 to 0.5139 (Supplementary

Fig. S2.1). We included these isotope effects in our model, and reproduced the $\Delta^{33}S$-$\delta^{34}S$ systematic of station 12 without any additional adjustments to C_{SMT} or $^{34}\alpha$ (Fig. 3a). Replication of this station's full sulphate concentration and isotopic dataset by a model with only two free parameters strongly validates our initial model assumptions.

In particular, it appears that sulphate reduction via AOM and, by extension, methane flux into the SMTZ completely control the sulphur dynamics at station 12. This is consistent with the sulphur isotope composition of pore water sulphide below the SMTZ, which rapidly approaches the isotope composition of sulphate entering the top of the sediment column (Fig. 2.2d, Supplementary Fig. S2.2). Similarly, the lack of sulphate below the SMTZ implies the simple unidirectional reduction of sulphate via AOM. Finally, the parabolic pattern outlined by the measured sulphate $\Delta^{33}S$-$\delta^{34}S$ values (Fig. 2.3a) suggests a binary mixing process[19], reasonably interpreted as diffusive exchange of sulphate from the overlying homogenous layer with sulphate originating from the SMTZ, without any intervening biogeochemical modification. We note that the estimated $^{34}\alpha$ value is consistent with those measured in pure and enriched cultures of sulphate-reducing bacteria[20]. While physiological adaptations must accompany co-feeding within AOM consortia[23], our results imply that they do not come with abnormal isotopic consequences for sulphate-reducing bacteria. This prediction should be testable though a S isotope assay of *in-vitro* incubations of methane-seep sediments.

Under similar model assumptions, the deeper SMTZ at station 5 implies a weaker methane flux, driving a slower AOM rate that enables sulphate to penetrate further into the sediment column. However, despite producing an equally exceptional fit to pore water sulphate concentrations and $\delta^{34}S$ values at both stations, a model built on these expectations predicts $\Delta^{33}S$-$\delta^{34}S$ trajectories at station 5 that are antithetical to those we measured (Fig. 2.3b). Instead of the parabolic predictions indicative of passive mixing of pore water sulphate, the measured $\Delta^{33}S$ and $\delta^{34}S$ values define a clear linear pattern, with a positive correlation. The high precision $\Delta^{33}S$ isotope technique we have employed demonstrates geochemical complexity in the sulphur cycle that is undetectable by conventional pore water geochemistry and traditional sulphur isotope analysis.

Classical models that couple pore water sulphate reduction with organic matter oxidation[24] can generate a positive correlation between $\Delta^{33}S$ and $\delta^{34}S$ values (Fig. S2.3e,f).

Under the condition that sulphate is depleted much more rapidly than organic matter, such models can also mimic a nearly linear profile of pore water sulphate concentrations[8] (Fig. S2.3a,b). In contrast, simple models of organoclastic sulphate reduction in the sediments above the SMTZ can only attain the $\delta^{34}S$ values measured here by incorporating isotope fractionations of 75‰, outside the range reported for pure cultures of sulphate-reducing bacteria[20]. The $\delta^{34}S$ profile produced by these models is also linear with depth (Fig. S2.3c,d) in strong contrast to the exponential profiles presented here. Exponential $\delta^{34}S$ profiles appear to require a significant contribution from sulphate reduction via AOM[4]. These features suggest that organoclastic sulphate reduction is not a viable explanation for the cryptic sulphur cycling identified at station 5[25].

A positive correlation between $\Delta^{33}S$ and $\delta^{34}S$ values is also produced during the microbial disproportionation of sulphur compounds[15]. The oxidation of porewater sulphide, and subsequent disproportionation of the resulting sulphur compounds of intermediate oxidation state (e.g., S_0, $S_2O_3^{2-}$ [11,26]) to sulphate and sulphide, is a potential source of the $\Delta^{33}S$ and $\delta^{34}S$ trajectories we observe in pore water sulphate at station 5 (Fig. 2.3b). While this reoxidative sulphur cycling could take place in the sediments above the SMTZ, the linear sulphate profile there would require a reductive sulphate sink that perfectly balances the reoxidative sulphate source. A simpler explanation is that reoxidative sulphur cycle occurs at the SMTZ, where it is directly coupled to sulphide production by sulphate-dependent AOM. Under this scenario, the modeled sulphur isotope fractionation implies that ≈ 60% or more of the sulphide in this system was ultimately reoxidized during synchronous sulphate reduction and sulphide reoxidation at the SMTZ (Section 2.3 Appendix and Fig. S2.4 and S2.5). Regeneration of sulphate in this quantity is sufficient to consume a methane flux nearly two and a half times larger than that estimated from the sulphate concentration profile at station 5 alone (see section 2.3.6 Appendix).

Sulphur disproportionation has been observed in enrichment cultures of Deltaproteobacteria and a specific clade of anaerobic methanotrophic archaea (ANME-2) without the requirement of external oxidants[27]. In this process, sulphate is reduced to S^0 by ANME-2, and then transported to the extracellular environment where it reacts to form disulphide, which is then disproportionated to sulphate and sulphide in a 1:7 ratio[27]. An isotope fractionation model for this process is unable to reproduce the net multiple sulphur isotope fractionations observed at station 5 (Section 2.3.6 Appendix and Fig. S6), using experimentally

determined isotope fractionations for sulphate reduction and disproportionation. It may be that the archeal reduction of sulphate to S^0 and the reaction to disulphide produces unique isotope fractionations. These, however, have not been experimentally investigated yet. In absence of this information, we suggest that sulphide reoxidation at station 5 happens in the presence of external oxidants.

Pore water trace metals suggest that transport of oxidant-bearing minerals into the SMT sustains the reoxidative sulphur cycling identified here. Although sampling constraints limited our ability to quantify dissolved iron in the pore waters, the dissolved manganese profile at station 5 (Fig. S2.7a) exhibits a complex structure, likely associated with the latent redox processing of Mn(IV)[28]. Elevated dissolved manganese above and below the modeled SMTZ ($C_{SMT} \approx$ 2-3 mM) may result from chemical oxidation of sulphide to S^0 by manganese oxides[29]. This elemental sulphur would then be available for disproportionation to sulphate and sulphide through microbial catalysis[11]. Although some of the Mn(IV) that makes its way into the SMTZ may couple to AOM[30], the pore water sulphate $\Delta^{33}S$ and $\delta^{34}S$ trajectory requires that a significant portion must be dedicated to sulphide reoxidation at station 5. The absence of dissolved Mn in station 12 porewaters (Fig. S2.7b), combined with the isotopic closure exhibited by the accumulated dissolved sulphide there, provides compelling, albeit indirect, supporting evidence that metal oxides are critical to sustain sulphide reoxidation within the SMTZ.

A deep reoxidative sulphur cycle provides a unifying explanation for several enigmatic observations of methane-rich sediment biogeochemistry. Dissolved sulphide and sulphate concentrations in cold seep fluids often form arrays with slopes less than one, taken to reflect sequestration of sulphide by reactive iron or microbial sulphide consumption at the seafloor[31]. These imbalances may instead reflect the compounding effects of in-situ sulphide oxidation and sulphate regeneration. At cold seeps, directly measured process rates show that maximum AOM activity can be uncoupled from sulphate reduction[32]. Likewise, careful measurements of pore water methane contents show that sedimentary methane fluxes into the SMTZ can exceed sulphate fluxes by up to 30%[33]. Regenerated sulphate re-entering the AOM loop offers a viable origin for both phenomena. When these observations are viewed in light of the results reported here, it appears that sulphide reoxidation can provide a deep throttle for sedimentary methane fluxes.

2.3 Appendix

This appendix contains multiple S isotope data of dissolved sulphate and sulphide in pore waters extracted from 3 sedimentary cores (Table S2.1). It details the geological environment of the studied sediment cores, the methods used to sample sediments, and the analytical methods for geochemical and isotopic analysis. We also discuss the presence of peculiar sulphate $\delta^{34}S$ and $\Delta^{33}S$ values below the SMTZ in station 12, and we describe our models of sulphate reduction coupled with either AOM or organic matter oxidation. The sulphur geochemistry of dissolved sulphate at station 6 is also presented here.

2.3.1 Geologic environment

The area of study is generally speaking part of the central slope region of the northern Cascadia accretionary complex[34] linked to the Juan de Fuca subduction zone. The present Juan de Fuca plate configuration had its origin in a major reorganization of the northeast Pacific plate regime in the Eocene, ~43 million years ago. Since this time, convergence has been continuous and approximately orthogonal to the coast along the northern portion of the Cascadia margin with a present rate of convergence of ~46 mm/y[35]. In 1985, widely spaced marine seismic survey lines were acquired across the continental shelf and slope off Vancouver Island as part of the Frontier Geoscience program of the Geological Survey of Canada to study the accretionary complex. As part of the site survey for ODP Leg 146, additional data were acquired in 1989[36]. Within this set of regional seismic lines, a first discovery was made of a gas-hydrate-related bottom-simulating reflector (BSR). Since this early discovery, the area offshore central Vancouver Island has been the subject of many interdisciplinary studies on gas hydrates. The work focused initially on mapping the regional distribution of BSRs and determining the associated regional concentrations of underlying free gas or overlying gas hydrate[36,37]. The more recent studies focused on cold-vent structures with high, near-seafloor concentrations of gas hydrate. Studies were especially focused on a vent field on the mid-continental slope near ODP Site 889/890[38,39]. The best-studied area of the vent field is referred to as Bullseye Vent, which also has been the site of IODP Expedition 311 drilling, with 5 boreholes of Site U1328 penetrating the upper 300 meters of sediments below seafloor[40]. Recent new mapping of the area

around Bullseye Vent was conducted with an autonomous underwater vehicle (AUV) and revealed a complex structure of Bullseye Vent resembling that of an elongated pockmark[41]. The same AUV survey also lead to the discovery of multiple formerly unknown cold-vents based on a characteristic rugged seafloor morphology related to carbonate outcrops and small pockmarks. An almost East-West-oriented transect consisting of several piston cores across Bullseye Vent was collected in 2002 for detailed geochemical pore-water analyses and measurements of physical properties[42,43]. Selected core sites from this early transect were re-visited in a recent expedition in 2008[44] allowing further in-depth geochemical and microbiological sample analyses as reported in this study.

2.3.2 Sampling methods

Details about sample collection and processing were described in a previous publication[45]. Pore water samples were squeezed and filtered from sediment cores shipboard and immediately preserved in 4% w/w zinc acetate (ZnAce) solution to avoid oxidation of any aqueous sulphide to sulphate. Samples then were stored frozen at -20°C until the analyses performed here.

2.3.3 Analytical methods

S isotope analysis: Precipitates of zinc sulphide (ZnS) were separated from the sulphate-bearing solution by filtration on 0.2µm filters and rinsed 3 times with ~15mL Milli-Q water. ZnS was then converted to silver sulphide (Ag_2S) by adding ~1mL of 0.1N silver nitrate ($AgNO_3$). The remaining sulphate solution was acidified to pH of ~3 by adding drops of 0.5N hydrochloric acid (HCl) and gently heated to ~60°C. About 2mL of 10% barium chloride ($BaCl_2$) solution was added to convert dissolved sulphate to barium sulphate ($BaSO_4$) precipitate. The $BaSO_4$ powder was then converted to hydrogen sulphide (H_2S) through reaction with a 'Thode' reduction solution consisting of 250 mL HI 48%, 410 mL HCl 38%, and 121 mL H_2PO_4[46]. The produced H_2S was brought to a ZnAce trap by a stream of pure N_2 where it precipitated as ZnS. After all $BaSO_4$ was reacted and recovered as ZnS, the addition of a few drops of 0.1N $AgNO_3$ solution preserved the sulphate S as Ag_2S. The solution was left to react overnight. The Ag_2S end-product

of either sulphide or sulphate was then rinsed with ~2mL of 0.1N ammonium hydroxide solution and 30 mL of Milli-Q water and dried overnight at 60°C.

The Ag_2S was weighed in cleaned aluminum pouches and reacted in a nickel reaction vessel overnight at ~250°C in the presence of excess F_2 to produce SF_6. The resulting SF_6 was purified first cryogenically and then with a gas chromatograph. Purified SF_6 was introduced to a Thermo Finnigan MAT 253 dual-inlet gas-source mass spectrometer where sulphur isotope abundances were measured by monitoring the $^{32}SF^{5+}$, $^{33}SF^{5+}$, $^{34}SF^{5+}$, and $^{36}SF^{5+}$ ion beams at mass to charge ratio (m/z) = 127, 128, 129 and 131, respectively. Uncertainties are calculated as the standard deviation (1σ) for $\delta^{34}S$, $\Delta^{33}S$ and $\Delta^{36}S$ values from multiple measurements of an in-house standard (MSS-1).

Isotope compositions are reported as delta values:

$$\delta^{3x}S = \left(\frac{R^{3x}_{Sample}}{R^{3x}_{V-CDT}} - 1\right) \times 1000$$

where 3x is 33, 34 or 36.

Minor isotopic signatures are reported as capital delta values[47,48]

$$\Delta^{33} = \delta^{33}S - \left[\left(1 + \frac{\delta^{34}S}{1000}\right)^{0.515} - 1\right] \times 1000$$

The data are reported relative to the V-CDT scale. On this scale, $\delta^{34}S$ value of IAEA-S-1 is defined as -0.3‰. We take the $\Delta^{33}S$ value of IAEA-S-1 to be 0.094‰ V-CDT.

2.3.4 Model of sulphate reduction coupled with AOM at the SMTZ

Under the boundary conditions of constant concentration at the top of the sediment column and constant removal rate across the SMTZ at depth and pure diffusion between the two boundaries, the steady-state solution to the diagenetic equation for dissolved species is a straight line[49]. Straight sulphate concentration profiles for individual isotopomers can be represented as:

$$^{3x}C(z) = \quad ^{3x}A \times z + \quad ^{3x}B$$

where $^{3x}C(z)$ is concentration of the sulphate isotopomer ($^{32}SO_4^{2-}$, $^{33}SO_4^{2-}$ and $^{34}SO_4^{2-}$) at the sediment depth z, ^{3x}A is the slope of the concentration profile, and ^{3x}B is the initial sulphate concentration of the sulphate isotopomer.

At the kink in the sulphate concentration profiles, the concentration of $^{32}SO_4^{2-}$, $^{33}SO_4^{2-}$ and $^{34}SO_4^{2-}$ were calculated from measured sulphate concentrations, $\delta^{33}S$ values, and $\delta^{34}S$ values. These concentrations reflect the ^{3x}B terms above. At the SMTZ depth, the flux of each sulphate isotopomer (^{3x}Q) was calculated from the following definition of the fractionation factor associated with sulphate reduction via AOM:

$$^{3x}\alpha = \frac{^{3x}Q/\ ^{32}Q}{^{3x}C/\ ^{32}C}$$

The slopes of sulphate concentration profiles (^{3x}A terms above) were calculated as ^{3x}Q-D ratios where D is an effective diffusion coefficient of sulphate. We neglected the effects of isotopic mass on the effective sulphate diffusion coefficient.

In terms of actual model implementation, we assumed that the slope of $^{32}SO_4^{2-}$ is equal to the slope of total sulphate concentration profile because $^{32}SO_4^{2-}$ is the dominant isotopomer. The slope of $^{34}SO_4^{2-}$ concentration profile was then controlled by two free parameters: (1) the sulphate concentration at the SMT (C_{SMT}); and (2) $^{34}\alpha$. These parameters were varied in order to best fit the $\delta^{34}S$ profiles at each station, using the definition of $\delta^{34}S$ defined above. Although they were free parameters in our model, the resulting values were in the range of observed sulphate concentrations at the SMTZ in natural systems[50,51] and the $^{34}\alpha$ values were in the published range for pure cultures of sulphate-reducing bacteria[52,53].

In order to investigate the minor isotope consequences of our minimal model, the C_{SMT} and $^{34}\alpha$ values from the original fit were used, along with the relationship $^{33}\alpha = \left(^{34}\alpha\right)^{^{33}\lambda}$ and published $^{33}\lambda$ values for sulphate-reducing bacteria (Fig. S2.1). Since there were no free parameters, the modeled $\Delta^{33}S$-$\delta^{34}S$ results were truly predictive.

2.3.5 Model of sulphate reduction coupled with organic matter oxidation

In systems where sulphate reduction is coupled with organic-matter oxidation, sulphate concentrations usually decrease exponentially with depth[24,54]. Here we apply a classical

formulation of a diagenetic model[24] for a system in which sulphate disappears quickly before organic matter. To make the model physically meaningful, we only apply the model to the depth range where sulphate concentration is greater than or equal to zero.

The fictive sulphate concentration at infinite depth and the ratio of sulphate reduction rate (k) to sedimentation rate (w) were treated as free parameters. These parameters were adjusted so that the model fit the measured concentration profiles. Next, the fractionation factor ($^{34}\alpha$) was varied so that the model best fit the $\delta^{34}S$ profiles. Finally, the $^{33}\lambda$ values corresponding to the chosen $^{34}\alpha$ values were used to predict $\Delta^{33}S - \delta^{34}S$ trajectories.

While it is mathematically possible for this model to produce exponentially increasing $\delta^{34}S$ values with depth, this pattern is only evident at very high k-w ratios. These situations are reached either when the sulphate reduction rate is very fast or the sedimentation rate is very slow. In either case, organic matter is depleted much faster than sulphate and sulphate concentrations remain greater than zero at depth. This situation is not relevant to the sulphate profiles reported here.

2.3.6 Model to quantify sulphide reoxidation at station 5

We built a simple box model to understand the specific combinations of sulphate reduction and sulphide reoxidation that are capable of producing the observed isotope fractionations. In this model, we assume a tight coupling between sulphate reduction and sulphide reoxidation when sulphate enters the SMT. The loss term used to account for sulphate flux out of the sedimentary column above the SMT can then be represented by an open system balance among three pools of sulphur: sulphate, sulphide and sequestered sulphur. Three transfers link these pools: (1) sulphate to sulphide by microbial sulphate reduction (*MSR*); (2) sulphide to sulphate through reoxidation (*REOX*); and (3) sulphide to a permanently sequestered form of sulphur (*SEQ*). The net fractionation factor (α_{NET}) extracted from the sulphate profile reflects the specific fractionations associated with sulphate reduction (α_{MSR}) and sulphide reoxidation (α_{REOX}), along with the relative magnitude of sulphur transfer along each pathway. The sulphur sequestration process is assumed to be isotopically non-selective. We define $\alpha_{MSR} = \frac{R_{H_2S,\ MSR}}{R_{SO_4^{2-}}}$, where $R_{H_2S,\ MSR}$ represents the isotopic ratio of the sulphide leaving the

sulphate pool through the sulphate reduction pathway, and define $\alpha_{REOX} = \frac{R_{H_2S}}{R_{SO_4^{2-},\ REOX}}$, where $R_{SO_4^{2-},\ REOX}$ represents the isotopic ratio of the sulphate leaving the sulphide pool through the reoxidation pathway. The relative magnitudes of sulphur transfer through the reoxidation pathway or leaving the reaction site through sequestration as a fraction (f) of transfer of sulphide into the system through sulphate reduction. These terms, f_{SEQ} and f_{REOX}, are therefore a function of each other ($f_{SEQ} = 1 - f_{REOX}$). The net fractionation recorded by the pore water sulphate is:

$$\alpha_{NET} = \frac{\alpha_{MSR}}{\left(\alpha_{REOX} f_{REOX} + (1 - f_{REOX})\right)}$$

A similar box model including three sulphur pools: sulphide, intermediate S and reoxidizing sulphate, was built to understand the reoxidation process. Based on that model, the α_{REOX} can be expressed as:

$$\alpha_{REOX} = \frac{\alpha_{OX}\ \alpha_{IA}}{\left(\alpha_{IH} f_{IH} + \alpha_{IA}(1 - f_{IH})\right)}$$

where f_{IH} is the relative magnitude of the sulphide oxidation flux that is returned to the pore water sulphide pool. We define $\alpha_{OX} = \frac{R_{S,\ OX}}{R_{H2S}}$, where $R_{S,\ OX}$ represents the isotopic ratio of the intermediate S leaving the sulphide pool through the sulphide oxidation pathway, define $\alpha_{IH} = \frac{R_{H2S,\ IH}}{R_S}$, where $R_{H2S,\ IH}$ represents the isotopic ratio of sulphide leaving the intermediate S pool through S disproportionate pathway, and define $\alpha_{IA} = \frac{R_{SO_4^{2-},\ IA}}{R_S}$, where $R_{R_{SO_4^{2-},\ IA}}$ represents the isotopic ratio of sulphate leaving the intermediate S pool through S disproportionate pathway.

The α_{NET} calculation is performed with characteristic $^{34}\alpha$ and $^{33}\alpha$ values for microbial sulphate reduction and reoxidation. The specific minor isotope fractionations associated with each process are expressed as exponential factors ($^{33}\lambda$) such that $^{33}\alpha = \left(^{34}\alpha\right)^{^{33}\lambda}$.

We applied this model for station 5 to explore the amount of sulphide recycling through the system. The model of sulphate reduction coupled with AOM fits measurement data with $^{34}\alpha_{NET} = 0.95$ and $^{33}\lambda_{NET} = 0.518$. Because the zero-valent sulphur (S^0) is the key intermediate in marine methane oxidation[27], the relative magnitude of the sulphide oxidation flux (f_{IH}) is 0.75

($4S^0 + 4H_2O \leftrightarrow 3HS^- + SO_4^{2-} + 5H^+$). Experiment of S^0 disproportionation have shown that the intermediate S disproportionation to SO_4^{2-} process produces $^{34}\alpha_{IA} = 1.018530$ and $^{33}\lambda_{IA} = 0.519507$, the intermediate S disproportionation to H_2S process produces $^{34}\alpha_{IH} = 0.993823$ and $^{33}\lambda_{IH} = 0.516468$, and the $^{34}\alpha_{OX}$ varies within a narrow range from 0.995 to 1.001539 for H_2S oxidation with different mechanisms[55]. Here we choose $^{34}\alpha_{OX} = 1$ and $^{33}\lambda_{OX} = 0.515$ for the H_2S to S^0 oxidation process. With those experimentally determined values, we can only reproduce our data point ($^{34}\alpha_{NET} = 0.95$ and $^{33}\lambda_{NET} = 0.518$) by: (1) increasing $^{34}\alpha_{IA}$ and/or decreasing $^{34}\alpha_{IH}$ and (2) increasing $^{33}\lambda_{IA}$ and/or $^{33}\lambda_{IH}$. In the first scenario, the MSR fractionation is relatively low ($^{34}\alpha_{MSR} > 0.985$) and the reoxidation fraction is greater than 60% ($f_{REOX} > 0.6$) (Fig. S2.4). In the second scenario, the model suggests the MSR fractionation from 30‰ to 38‰ and the reoxidation fraction from 70% to 100% (Fig. S2.5). So, in any case, ~60% or more of sulphide was reoxidized in to sulphate. It means that the real methane flux in station 5 is at least 2.5 times greater than the flux estimated from sulphate concentration profile (1/(1-0.6)=2.5).

Disproportionation by Deltaproteobacteria produces sulphate and sulphide in a 7:1 ratio ($4HS_2^- + 4H_2O \leftrightarrow 7HS^- + SO_4^{2-} + 5H^+$)[27]. We define $\alpha_{MSR} = \frac{R_{HS_2^-,\ MSR}}{R_{SO_4^{2-}}}$, where $R_{HS_2^-,\ MSR}$ represents the isotopic ratio of the disulphide leaving the sulphate pool through the sulphate reduction pathway, define $\alpha_{REOX1} = \frac{R_{SO_4^{2-},\ REOX}}{R_{HS_2^-}}$, where $R_{SO_4^{2-},\ REOX}$ represents the isotopic ratio of the sulphate leaving the disulphide pool through the reoxidation pathway, and define $\alpha_{REOX2} = \frac{R_{H_2S,\ REOX}}{R_{HS_2^-}}$, where $R_{H_2S,\ REOX}$ represents the isotopic ratio of the sulphide leaving the disulphide pool through the reoxidation pathway. The relative magnitudes of sulphur transfer through the reoxidation pathway back to sulphate or sulphide (f) of transfer of disulphide into the system through sulphate reduction. These terms, $f_{SO_4^{2-},\ REOX}$ and $f_{H_2S,\ REOX}$, are therefore a function of each other ($f_{SO_4^{2-},\ REOX} + f_{H_2S,\ REOX} = 1$) and according to the 1:7 stoichiometry of the reaction, $f_{SO_4^{2-},\ REOX} = 0.125$ and $f_{H_2S,\ REOX} = 0.875$.The model for this process produces the net fractionation recorded by the pore water sulphate as following:

$$\alpha_{NET} = \frac{8\alpha_{MSR}\alpha_{REOX2}}{(7\alpha_{REOX2} + \alpha_{REOX1})}$$

Here we assume that sulphate reduction to disulphide produces similar isotope fractionations as traditional MSR. By varying the α_{REOX1} and α_{REOX2} in a reasonable range ($\varepsilon_{SO_4^{2-}-H_2S}$ < 80‰) and varying the λ_{REOX2} and λ_{REOX1} from 0.515 to 0.535[55,56], the model is unable to reproduce $^{34}\alpha_{NET}$ = 0.95 and $^{33}\lambda_{NET}$ = 0.518 observed in station 5 (Fig. S2.6).

2.3.7 Station 6

Like the geochemical profiles at stations 12 and 5, the profiles at station 6 show a relatively homogeneous zone from shallow depths (≈ 100 cm) to the seawater-sediment interface. Unlike the other stations, however, station 6 preserves changes in slope with depth in both the sulphate concentration profile and $\delta^{34}S$ profile (Fig. S2.8a,b). These features coincide with the appearance of fracture-filling biofilms, which are associated with the local presence of AOM[57]. Operation of AOM in the vicinity of these biofilms will provide local sulphate sinks, greatly complicating any application of our minimal digenetic model to the geochemical profiles at station 6. We note, however, that even with the increased variability present at station 6, the $\Delta^{33}S$-$\delta^{34}S$ trajectory for pore water sulphate (Fig. S8c) resembles the pattern at station 5 more than the pattern at station 12. It appears that deep sulphur reoxidation is operating at station 6 as well, despite the lack of evidence in the sulphate concentration and $\delta^{34}S$ profiles. The lower slope of the $\Delta^{33}S$-$\delta^{34}S$ trajectory at station 6 compared to station 5 indicates that the sulphur recycling capacity is likely less at station 6. This may reflect the local consumption of sulphate within the biofilms that perform AOM.

2.3.8 Peculiar sulphur isotope signatures of dissolved sulphate below the SMT

Pore water sulphate below the SMTZ is extremely rare, and always occurs at very small (<< 1 mM) concentrations. The rarity of sub-SMTZ sulphate, plus the susceptibility of small reservoirs to mixing and fractionation, makes the isotopic characteristics of these samples difficult to interpret. The sub-SMTZ sulphate always has lower $\delta^{34}S$ values than the overlying pore water sulphate, and possesses negative $\Delta^{33}S$ values. These characteristics are also unlike the coexisting pore water sulphide when it is present (Fig. S2.2a), indicating that trace oxidation of pore water sulphide is not the source of the sub-SMTZ sulphate. Although mixing curves within

a $\Delta^{33}S$-$\delta^{34}S$ coordinate system are parabolic, it is not possible to reproduce the $\Delta^{33}S$ and $\delta^{34}S$ values of the sub-SMTZ sulphate at station 12 by any mixture of the measured pore water sulphide and sulphate, suggesting that oxidation of pore water sulphide and mixing with overlying sulphate is not the origin of the sub-SMTZ sulphate. It is unlikely that the sub-SMTZ sulphate results from the dissolution of barite after it passed below the SMTZ as the barite typically preserves the sulphur isotopic characteristics of overlying seawater. Evidently an undocumented sulphur source is needed to explain the trace sulphate found below the SMTZ. We suggest that potential sources could either be sulphate supplied by the advection of deep brines or, perhaps more likely, the oxidation of trace H_2S (one of the earliest identified clathrate 'hilfsgase'[58]) released during gas-hydrate dissociation.

2.4 References

1 Etiope, G. Climate science: Methane uncovered. *Nature Geoscience* **5**, 373-374 (2012).

2 Reeburgh, W. S. Oceanic Methane Biogeochemistry. *Chemical Reviews* **107**, 486-513, doi:10.1021/cr050362v (2007).

3 Joye, S. B. Microbiology: A piece of the methane puzzle. *Nature* **491**, 538-539 (2012).

4 Dale, A., Bruchert, V., Alperin, M. & Regnier, P. An integrated sulphur isotope model for Namibian shelf sediments. *Geochimica Et Cosmochimica Acta* **73**, 1924-1944, doi:DOI 10.1016/j.gca.2008.12.015 (2009).

5 Reeburgh, W. Oceanic methane biogeochemistry. *Chemical Reviews* **107**, 486-513, doi:DOI 10.1021/cr050362v (2007).

6 Borowski, W. S., Paull, C. K. & Ussler, W., III. Marine pore-water sulphate profiles indicate in situ methane flux from underlying gas hydrate. *Geology* **24**, 655-658, doi:10.1130/0091-7613(1996)024<0655:mpwspi>2.3.co;2 (1996).

7 Hensen, C. *et al.* Control of sulphate pore-water profiles by sedimentary events and the significance of anaerobic oxidation of methane for the burial of sulphur in marine sediments. *Geochimica Et Cosmochimica Acta* **67**, 2631-2647, doi:10.1016/s0016-7037(03)00199-6 (2003).

8 Malinverno, A. & Pohlman, J. Modeling sulphate reduction in methane hydrate-bearing continental margin sediments: Does a sulphate-methane transition require anaerobic oxidation of methane? *Geochemistry Geophysics Geosystems* **12**, -, doi:ARTN Q07006

DOI 10.1029/2011GC003501 (2011).

9 Regnier, P. *et al.* Quantitative analysis of anaerobic oxidation of methane (AOM) in marine sediments: A modeling perspective. E*arth-Science Reviews* 1**06,** 105-130, doi:DOI 10.1016/j.earscirev.2011.01.002 (2011).

10 Riedinger, N. *et al.* Diagenetic alteration of magnetic signals by anaerobic oxidation of methane related to a change in sedimentation rate. G*eochimica Et Cosmochimica Acta* 6**9,** 4117-4126, doi:10.1016/j.gca.2005.02.004 (2005).

11 Jorgensen, B. B. & Nelson, D. C. Sulphide oxidation in marine sediments: Geochemistry meets microbiology. Sulphur *Biogeochemistry-Past and Present* S**pecial Paper 379,** 63-82 (2004).

12 Sommer, S. *et al.* Efficiency of the benthic filter: Biological control of the emission of dissolved methane from sediments containing shallow gas hydrates at Hydrate Ridge. G*lobal Biogeochemical Cycles* 2**0,** -, doi:ARTN GB2019

DOI 10.1029/2004GB002389 (2006).

13 Canfield, D. e*t al. A* Cryptic Sulphur Cycle in Oxygen-Minimum-Zone Waters off the Chilean Coast. Sc*ience 3*3**0,** 1375-1378, doi:DOI 10.1126/science.1196889 (2010).

14 Holmkvist, L., Ferdelman, T. & Jorgensen, B. A cryptic sulphur cycle driven by iron in the methane zone of marine sediment (Aarhus Bay, Denmark). Ge*ochimica Et Cosmochimica Acta 7*5**,** 3581-3599, doi:DOI 10.1016/j.gca.2011.03.033 (2011).

15 Johnston, D. T. e*t al. M*ultiple sulphur isotope fractionations in biological systems: A case study with sulphate reducers and sulphur disproportionators. Am *J Sci 3*0**5,** 645-660, doi:10.2475/ajs.305.6-8.645 (2005).

16 Riedel, M. e*t al. G*eophysical and geochemical signatures associated with gas hydrate-related venting in the northern Cascadia margin. Ge*ological Society of America Bulletin 1*1**8,** 23-38, doi:10.1130/b25720.1 (2006).

17 Pohlman, J. W. e*t al. M*ethane sources in gas hydrate-bearing cold seeps: Evidence from radiocarbon and stable isotopes. Ma*rine Chemistry 1*1**5,** 102-109, doi:10.1016/j.marchem.2009.07.001 (2009).

18 Rees, C. E., Jenkins, W. J. & Monster, J. Sulphur isotope composition of ocean water sulphate. Ge*ochimica Et Cosmochimica Acta 4*2**,** 377-381 (1978).

19 Johnston, D. T. e*t al. A*ctive microbial sulphur disproportionation in the Mesoproterozoic. Sc*ience 3*1**0,** 1477-1479 (2005).

20 Sim, M., Bosak, T. & Ono, S. Large Sulphur Isotope Fractionation Does Not Require Disproportionation. Sc*ience 3*3**3,** 74-77, doi:DOI 10.1126/science.1205103 (2011).

21 Farquhar, J. e*t al. M*ultiple sulphur isotopic interpretations of biosynthetic pathways: implications for biological signatures in the sulphur isotope record. Ge*obiology 1*, 27-36 (2003).

22 Johnston, D. T. e*t al. M*ultiple sulphur isotope fractionations in biological systems: A case study with sulphate reducers and sulphur disproportionators. Am*erican Journal of Science 3*0**5,** 645-660 (2005).

23 Boetius, A. e*t al. A* marine microbial consortium apparently mediating anaerobic oxidation of methane. Na*ture 4*0**7,** 623-626 (2000).

24 Berner, R. A. An idealized model of dissolved sulphate distribution in recent sediments. Ge*ochimica et Cosmochimica Acta 2*8**,** 1497-1503, doi:Doi: 10.1016/0016-7037(64)90164-4 (1964).

25 Pohlman, J. W., et al. (submitted).

26 Jorgensen, B. B. The Sulphur Cycle of a Coastal Marine Sediment (Limfjorden, Denmark). Li*mnology and Oceanography 2*2**,** 814-832 (1977).

27 Milucka, J. e*t al. Z*ero-valent sulphur is a key intermediate in marine methane oxidation. Na*ture 4*9**1,** 541-546 (2012).

28 Valentine, D. Emerging Topics in Marine Methane Biogeochemistry. An*nual Review of Marine Science, Vol 3 3*, 147-171, doi:DOI 10.1146/annurev-marine-120709-142734 (2011).

29 Burdige, D. J. The biogeochemistry of manganese and iron reduction in marine sediments. Ea*rth-Science Reviews 3*5**,** 249-284, doi:Doi: 10.1016/0012-8252(93)90040-e (1993).

30 Beal, E., House, C. & Orphan, V. Manganese- and Iron-Dependent Marine Methane Oxidation. Sc*ience 3*2**5,** 184-187, doi:DOI 10.1126/science.1169984 (2009).

31 Aharon, P. & Fu, B. S. Microbial sulphate reduction rates and sulphur and oxygen isotope fractionations at oil and gas seeps in deepwater Gulf of Mexico. Ge*ochimica Et Cosmochimica Acta 6*4**,** 233-246 (2000).

32 Joye, S. e*t al. T*he anaerobic oxidation of methane and sulphate reduction in sediments from Gulf of Mexico cold seeps. Ch*emical Geology 2*0**5,** 219-238, doi:DOI 10.1016/j.chemgeo.2003.12.019 (2004).

33 Niewohner, C., Hensen, C., Kasten, S., Zabel, M. & Schulz, H. D. Deep sulphate reduction completely mediated by anaerobic methane oxidation in sediments of the upwelling area off Namibia. Ge*ochimica Et Cosmochimica Acta 6*2**,** 455-464 (1998).

34 Hyndman, R. D. The Lithoprobe corridor across the Vancouver Island continental margin: the structural and tectonic consequences of subduction. Ca*nadian Journal of Earth Sciences 3*2**,** 1777-1802, doi:10.1139/e95-138 (1995).

35 Riddihough, R. Recent movements of the Juan de Fuca Plate System. Jo*urnal of Geophysical Research: Solid Earth 8*9**,** 6980-6994, doi:10.1029/JB089iB08p06980 (1984).

36 Hyndman, R. D. & Spence, G. D. A Seismic Study of Methane Hydrate Marine Bottom Simulating Reflectors. J. *Geophys. Res. 9*7**,** 6683-6698, doi:10.1029/92jb00234 (1992).

37 Yuan, T., Hyndman, R. D., Spence, G. D. & Desmons, B. Seismic velocity increase and deep-sea gas hydrate concentration above a bottom-simulating reflector on the northern Cascadia continental slope. Jo*urnal of Geophysical Research: Solid Earth 1*0**1,** 13655-13671, doi:10.1029/96jb00102 (1996).

38 Riedel, M., Spence, G. D., Chapman, N. R. & Hyndman, R. D. Seismic investigations of a vent field associated with gas hydrates, offshore Vancouver Island. Jo*urnal of Geophysical Research: Solid Earth 1*0**7,** 2200, doi:10.1029/2001jb000269 (2002).

39 Riedel, M., Novosel, I., Spence, G.D., Hyndman, R.D., Chapman, N.R., and Lewis, T. Geophysical and geochemical signatures associated with gas hydrate–related venting in the northern Cascadia margin. Ge*ol. Soc. Am. Bull 1*1**8(1-2) (**2006).

40 Riedel, M., Collett, T.S., Malone, M.J., and the Expedition 311 Scientists. Proc. IODP, 311: Washington, DC (Integrated Ocean Drilling Program Management International, Inc.). doi**:10.2204/iodp.proc.311.2006 (**2006b).

41 Paull, C. K., Ussler, W., Caress, W.D. Thomas, H., Lundsten, E., Riedel, M., and L. Lapham. Seafloor manifestations of gas venting and near seafloor gas hydrate occurrences. Eo*s Trans. AGU, 90(52), Fall Meet (*2009).

42 Novosel, I., Spence, G. D. & Hyndman, R. D. Reduced magnetization produced by increased methane flux at a gas hydrate vent. Ma*rine Geology 2*1**6,** 265-274, doi:http://dx.doi.org/10.1016/j.margeo.2005.02.027 (2005).

43 Pohlman, J., Spence, G.D., Chapman, N.R., Hyndman R.D., Grabowski, K.S., and Coffin R. B. Evidence for Anaerobic Methane Oxidation in Gas Hydrate Rich Sediments on the Northern Cascadia Margin Offshore Vancouver Island: Nice, France. EG*S-AGU-EUG Joint Assembly A*p**ril 6-11 (**2003).

44 Haacke, R., Hamilton, T., Enkin, R., Esteban, L., Pohlman, J. PGC2008007: Pacific Geoscience Centre marine gas hydrates cruise to the frontal ridge and mid-slope areas of the Vancouver Island accretionary wedge. PG*C2008007 Cruise report, Geological Survey of Canada,* 147 p (2008).

45 Pohlman, J. W. e*t al. A*naerobic methane oxidation in low-organic content methane seep sediments. Ge*ochimica et Cosmochimica Acta 1*0**8,** 184-201, doi:http://dx.doi.org/10.1016/j.gca.2013.01.022 (2013).

46 Harrison, A. G. & Thode, H. G. The kinetic isotope effect in the chemical reduction of sulphate. Tr*ansactions of the Faraday Society 5*3**,** 1648-1651 (1957).

47 Hulston, J. R. & Thode, H. G. Cosmic-Ray-Produced S36 and S33 in Metallic Phase of Iron Meteorites. J *Geophys Res 7*0**,** 4435-& (1965).

48 Farquhar, J., Bao, H. & Thiemens, M. Atmospheric Influence of Earth's Earliest Sulphur Cycle. Sc*ience 2*8**9,** 756-758, doi:10.1126/science.289.5480.756 (2000).

49 Boudreau, B. P. Di*agenetic models and their implementation: modelling transport and reactions in aquatic sediments.* (Springer, 1997).

50 Jørgensen, B. B., Weber, A. & Zopfi, J. Sulphate reduction and anaerobic methane oxidation in Black Sea sediments. De*ep Sea Research Part I: Oceanographic Research Papers 4*8**,** 2097-2120, doi:Doi: 10.1016/s0967-0637(01)00007-3 (2001).

51 Iversen, N. & Jorgensen, B. B. Anaerobic methane oxidation rates at the sulphate-methane transition in marine sediments from Kattegat and Skagerrak (Denmark). L*imnology and Oceanography 3*0**,** 944-955 (1985).

52 Claypool, G. E. in Th*e Geochemical Society Special Publications V*ol. 9 59-65 (Elsevier, 2004).

53 Brunner, B. & Bernasconi, S. M. A revised isotope fractionation model for dissimilatory sulphate reduction in sulphate reducing bacteria. Ge*ochimica et Cosmochimica Acta 6*9**,** 4759-4771, doi:DOI: 10.1016/j.gca.2005.04.015 (2005).

54 Boudreau, B. P. & Westrich, J. T. The dependence of bacterial sulphate reduction on sulphate concentration in marine sediments. Ge*ochimica et Cosmochimica Acta 4*8**,** 2503-2516, doi:Doi: 10.1016/0016-7037(84)90301-6 (1984).

55 Zerkle, A. L., Farquhar, J., Johnston, D. T., Cox, R. P. & Canfield, D. E. Fractionation of multiple sulphur isotopes during phototrophic oxidation of sulphide and elemental sulphur by a green sulphur bacterium. Ge*ochimica et Cosmochimica Acta 7*3**,** 291-306 (2009).

56 Johnston, D. T. e*t al. M*ultiple sulphur isotope fractionations in biological systems: A case study with sulphate reducers and sulphur disproportionators. Am*erican Journal of Science 3*0**5,** 645-660, doi:10.2475/ajs.305.6-8.645 (2005).

57 Briggs, B. R. e*t al. M*acroscopic Biofilms in Fracture-Dominated Sediment That Anaerobically Oxidize Methane. Ap*plied and Environmental Microbiology 7*7**,** 6780-6787, doi:10.1128/aem.00288-11 (2011).

58 van der Waals, J. & Platteeuw, J. C. in Ad*vances in Chemical Physics* (ed I. Prigorgine) 1-59 (John Wiley & Sons, 1959).

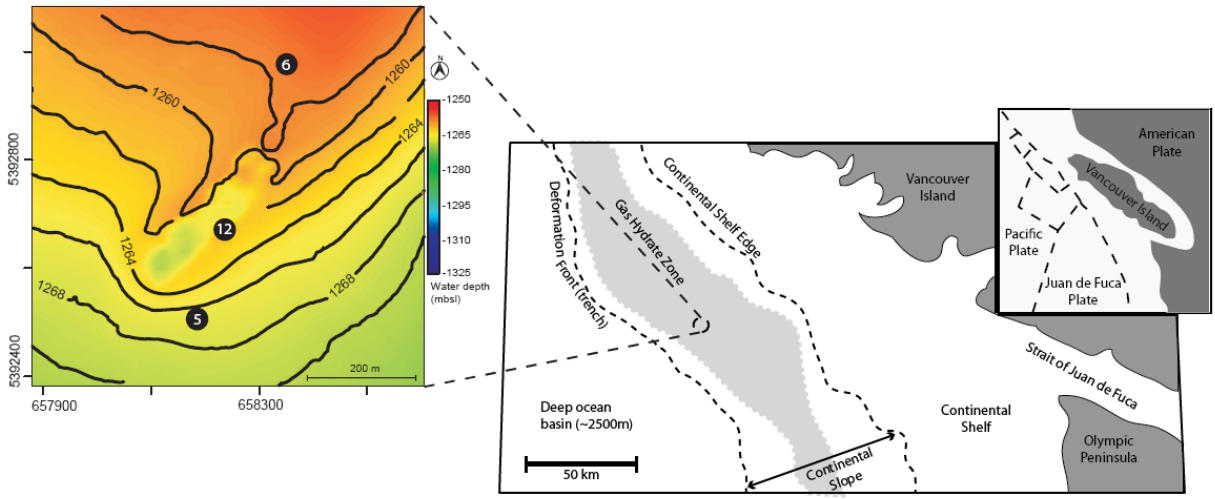

Fig. 2.1. Map of the continental margin offshore Vancouver Island, indicating the Northern Cascadia gas hydrate province. Inset shows seafloor topography in the Bullseye vent field where sediment cores (black dots with core-number) were collected.

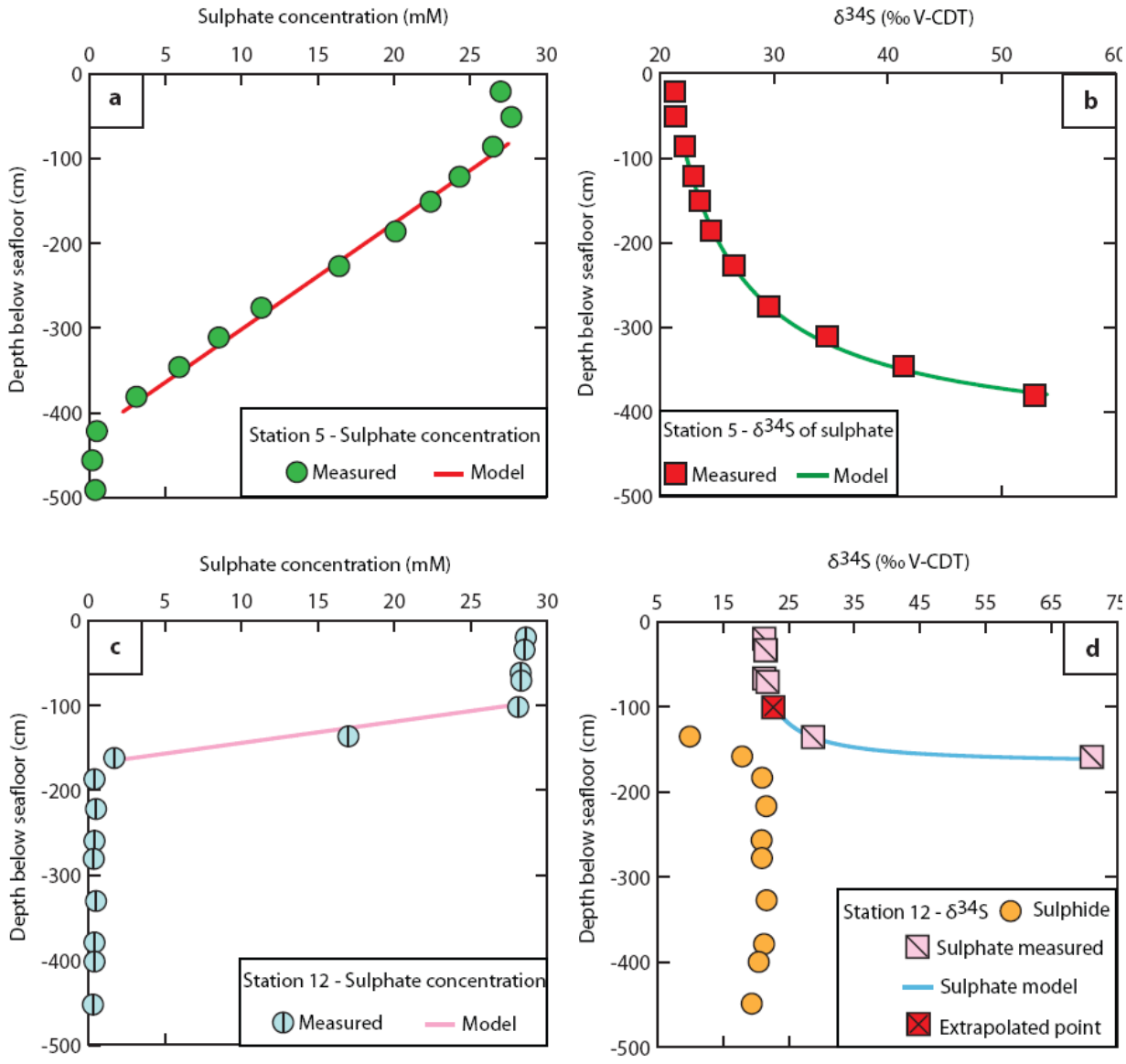

Fig. 2.2. Comparison of measured and modeled sulphur geochemistry above marine gas hydrates in the Bullseye vent field. (a) Pore water sulphate concentrations at station 5. (b) $\delta^{34}S$ values of pore water sulphate and sulphide at station 5. Material from the sulphate sample at ~100cm was unavailable for isotopic analysis. The $\delta^{34}S$ value at this level was extrapolated from the concentration-$\delta^{34}S$ relationship of the upper layer. (c) Pore water sulphate concentrations at station 12. (d) $\delta^{34}S$ values of pore water sulphate at station 12. In all cases, filled lines represent model reproductions of the measurements with a two-parameter diagenetic model. Values of $C_{SMT} \approx$ 2-3 mM and $^{34}\alpha = 0.95$ reproduce the trends at both stations.

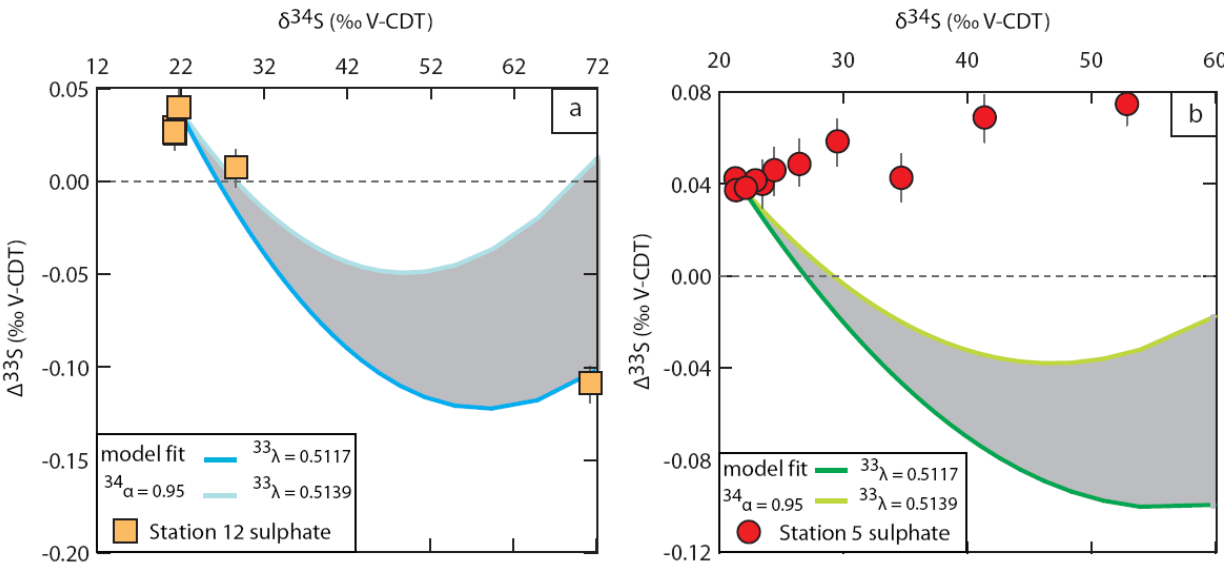

Fig. 2.3. Comparison of measured and modeled trajectories of $\Delta^{33}S$ and $\delta^{34}S$ values from pore water sulphate. (a) Measured $\Delta^{33}S$ – $\delta^{34}S$ trajectory at station 12 is within the field (in gray) predicted purely on the basis of sulphate reduction via AOM. (b) Measured $\Delta^{33}S$ – $\delta^{34}S$ trajectory at station 5 is nearly orthogonal to the model field (in gray) predicted purely on the basis of sulphate reduction via AOM. As such the model fits the sulphate concentration and $\delta^{34}S$ profiles well (Fig. 2b,c), the discrepancy highlights the presence of a hidden sulphur cycle at station 5.

Table S2.1. Sulphate concentration and sulphur isotope compositions of dissolved sulphate and sulphide at stations 5, 6, and 12. The (-) symbol indicates no data.

Table of sulphate concentrations associated with depth intervals and multiple S isotope data of dissolved sulphate and sulphide in pore water extracted from 3 sedimentary cores.								
Station	Depth (cmbsf)	$[SO_4^{2-}]$ (mM)	δ^{33}Sulphate (‰ V-CDT)	δ^{34}Sulphate (‰ V-CDT)	Δ^{33}Sulphate (‰ V-CDT)	δ^{33}Sulphide (‰ V-CDT)	δ^{34}Sulphide (‰ V-CDT)	Δ^{33}Sulphide (‰ V-CDT)
5	21	27.0	10.97	21.32	0.042	-	-	-
	51	27.7	10.98	21.37	0.037	-	-	-
	86	26.5	11.39	22.16	0.038	-	-	-
	122	24.3	11.79	22.93	0.042	-	-	-
	151	22.4	12.08	23.50	0.040	-	-	-
	186	20.1	12.57	24.46	0.046	-	-	-
	227	16.4	13.60	26.47	0.049	-	-	-
	276	11.3	15.17	29.55	0.058	-	-	-
	311	8.5	17.76	34.69	0.043	-	-	-
	346	5.9	21.18	41.40	0.069	-	-	-
	381	3.1	26.96	52.87	0.075	-	-	-
	422	0.5	-	-	-	-	-	-
	456	0.2	-	-	-	-	-	-
	491	0.4	-	-	-	-	-	-
6	33	26.7	11.18	21.74	0.041	-	-	-
	75	27.7	11.12	21.62	0.044	-	-	-
	137	25.0	11.70	22.74	0.051	-	-	-
	222	22.7	11.95	23.26	0.041	-	-	-
	237	18.2	13.10	25.55	0.022	-	-	-
	287	14.3	14.25	27.77	0.043	-	-	-
	342	9.1	18.07	35.31	0.044	-	-	-
	387	6.9	19.74	38.60	0.048	-	-	-
	437	6.0	20.06	39.27	0.031	-	-	-
	467	5.1	21.69	42.50	0.022	-	-	-
	502	0.9	20.73	40.73	-0.038	-	-	-
	527	0.3	-	-	-	-	-	-
	552	0.2	-	-	-	-	-	-
12	20.0	28.6	10.94	21.29	0.029	-	-	-
	34.0	28.5	10.97	21.37	0.026	-	-	-
	67.0	28.3	10.91	21.23	0.026	-	-	-
	71.0	28.3	11.20	21.78	0.040	-	-	-
	102	28.1	-	-	-	-	-	-
	137	17.0	14.68	28.69	0.007	5.20	9.93	0.100
	162	1.7	35.94	71.19	-0.109	9.24	17.90	0.066
	187	0.4	-	-	-	10.78	20.94	0.047
	222	0.5	8.22	16.18	-0.076	11.10	21.58	0.043
	262	0.4	8.54	16.84	-0.096	10.74	20.87	0.043
	284	0.4	-	-	-	10.76	20.91	0.048
	332	0.5	-	-	-	11.13	21.63	0.045
	384	0.4	-	-	-	10.93	21.24	0.042
	400	0.4	-	-	-	10.51	20.43	0.043
	449	0.3	-	-	-	9.97	19.37	0.041

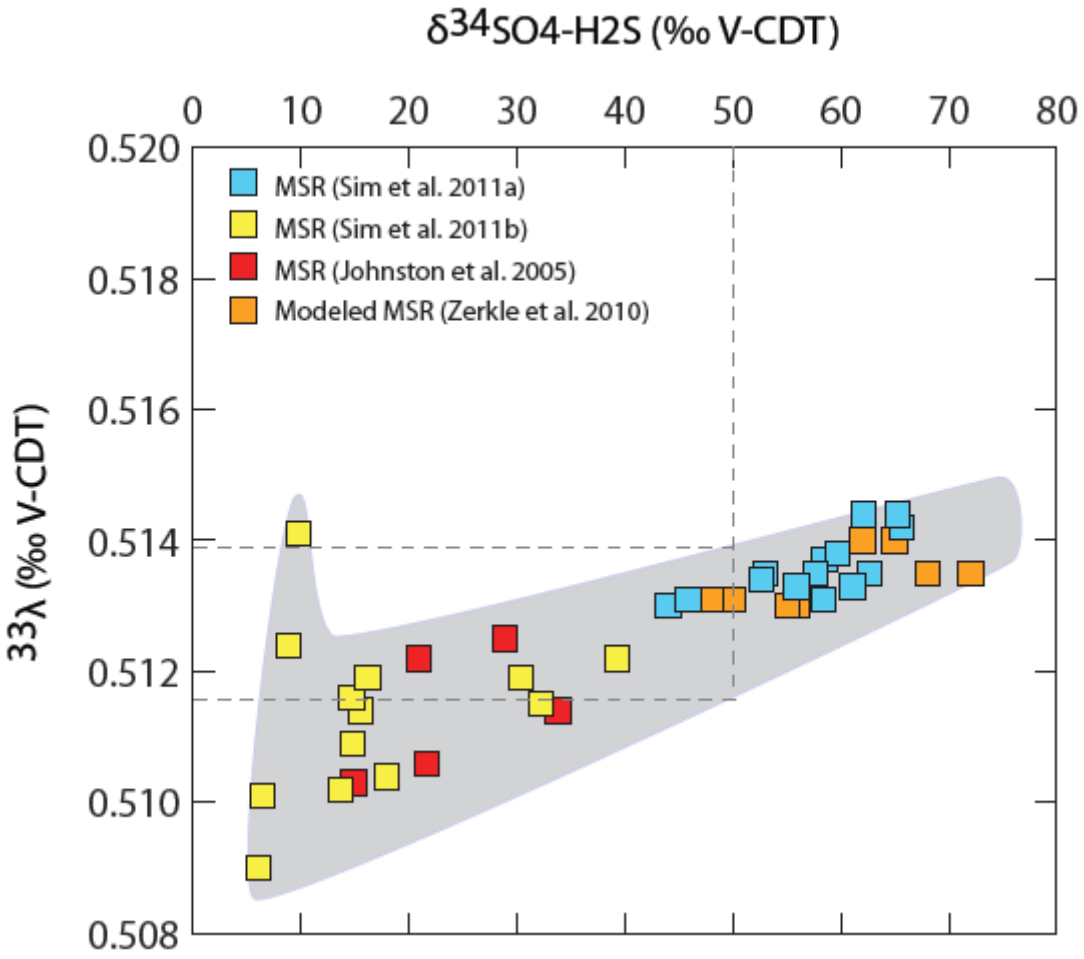

Fig. S2.1. Experimentally derived correlation of $\delta^{34}S_{SO_4^{2-},H_2S}$ [$= ({}^{34}\alpha - 1)\times 1000$] and ${}^{33}\lambda$ values. For an ${}^{34}\alpha$ value of 0.95 (dashed gray lines), the ${}^{33}\lambda$ value will be in the range of 0.5117 to 0.5139.

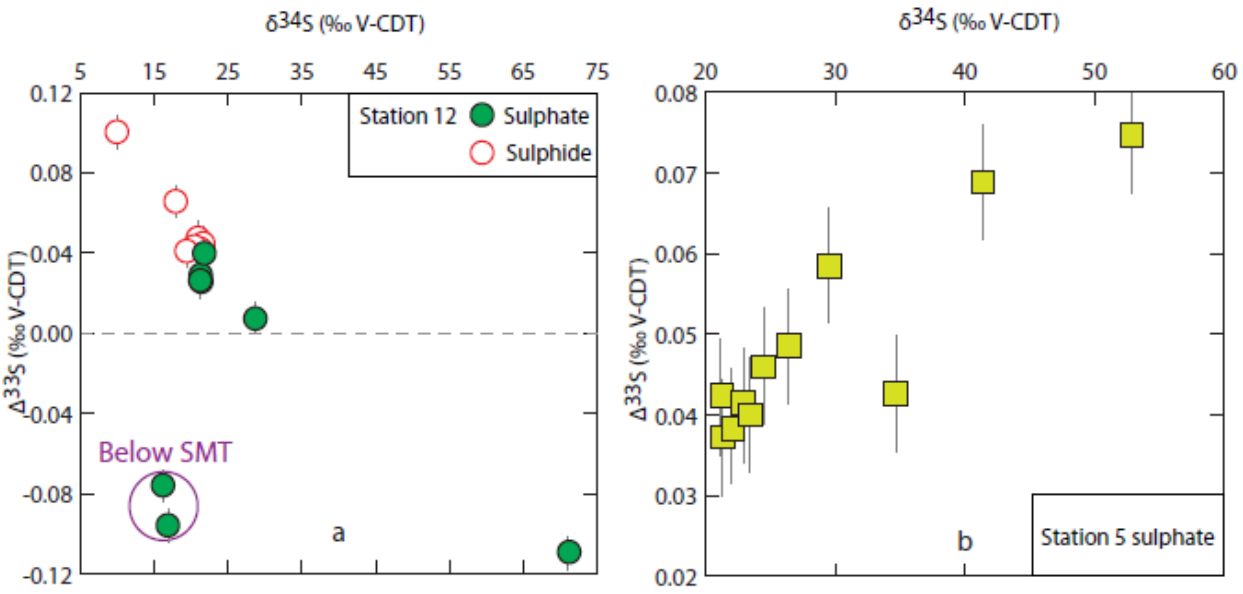

Fig. S2.2. Rare sulphur isotope compositions ($\Delta^{33}S$ values) of dissolved sulphate and sulphide show distinct trends with $\delta^{34}S$ values at station 12 (a) and station 5 (b).

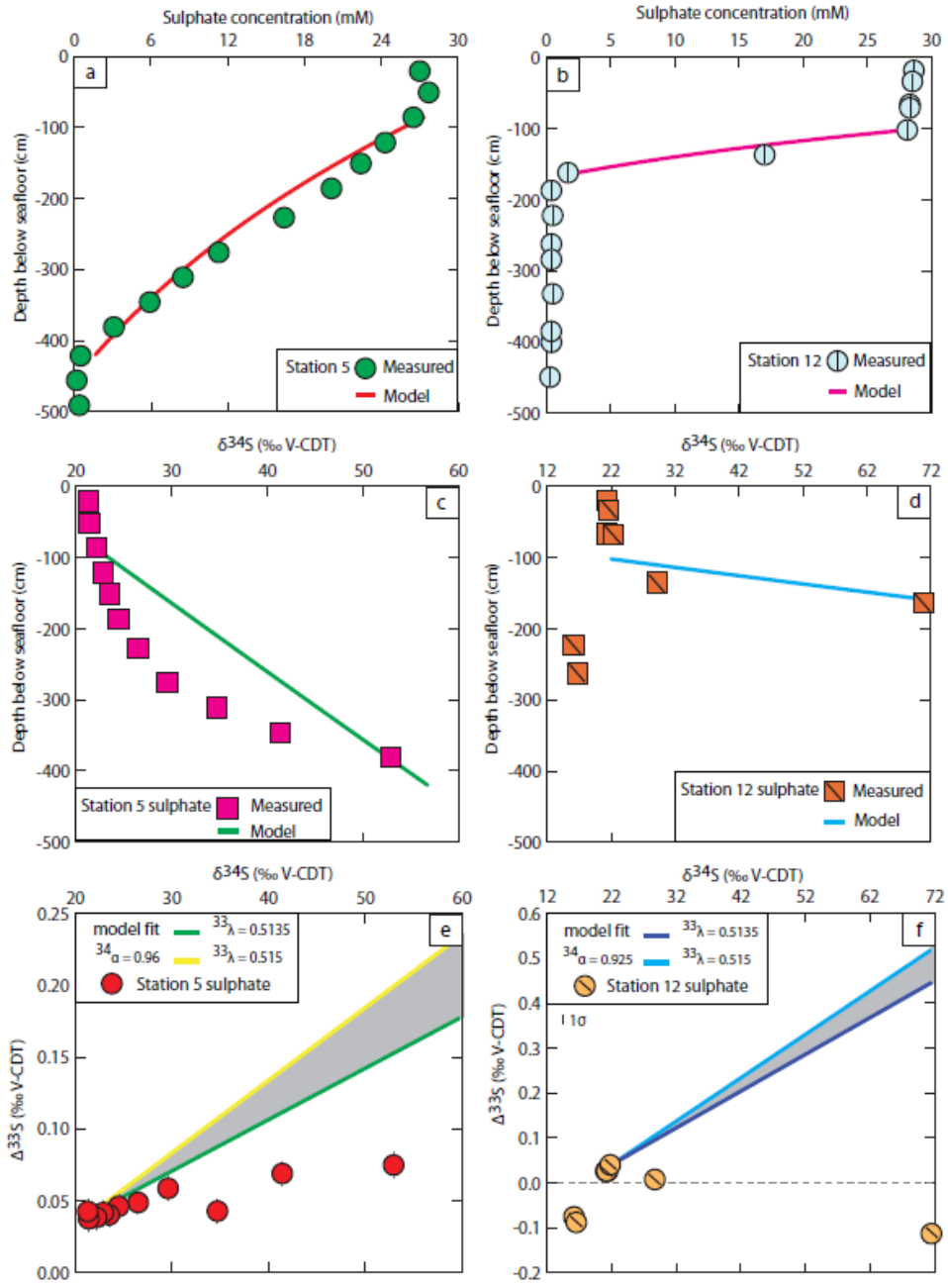

Fig. S2.3. Model of sulphate reduction coupled with organic matter oxidation. The observed straight sulphate concentration profiles are nearly reproduced at station 5 (a) and station 12 (b). However, the $\delta^{34}S$ profiles at both locations are reproduced poorly, even with ${}^{34}\alpha$ values that are on the extreme end of the measured range (c) station 5, ${}^{34}\alpha$=0.94; (d) station 12, ${}^{34}\alpha$=0.925. Predicted minor S isotope signals of pore water sulphate for station 5 (e) and station 12 (f). The predicted range of $\Delta^{33}S - \delta^{34}S$ trajectories for both alpha values are shown in gray and do not overlap with the measured trajectories.

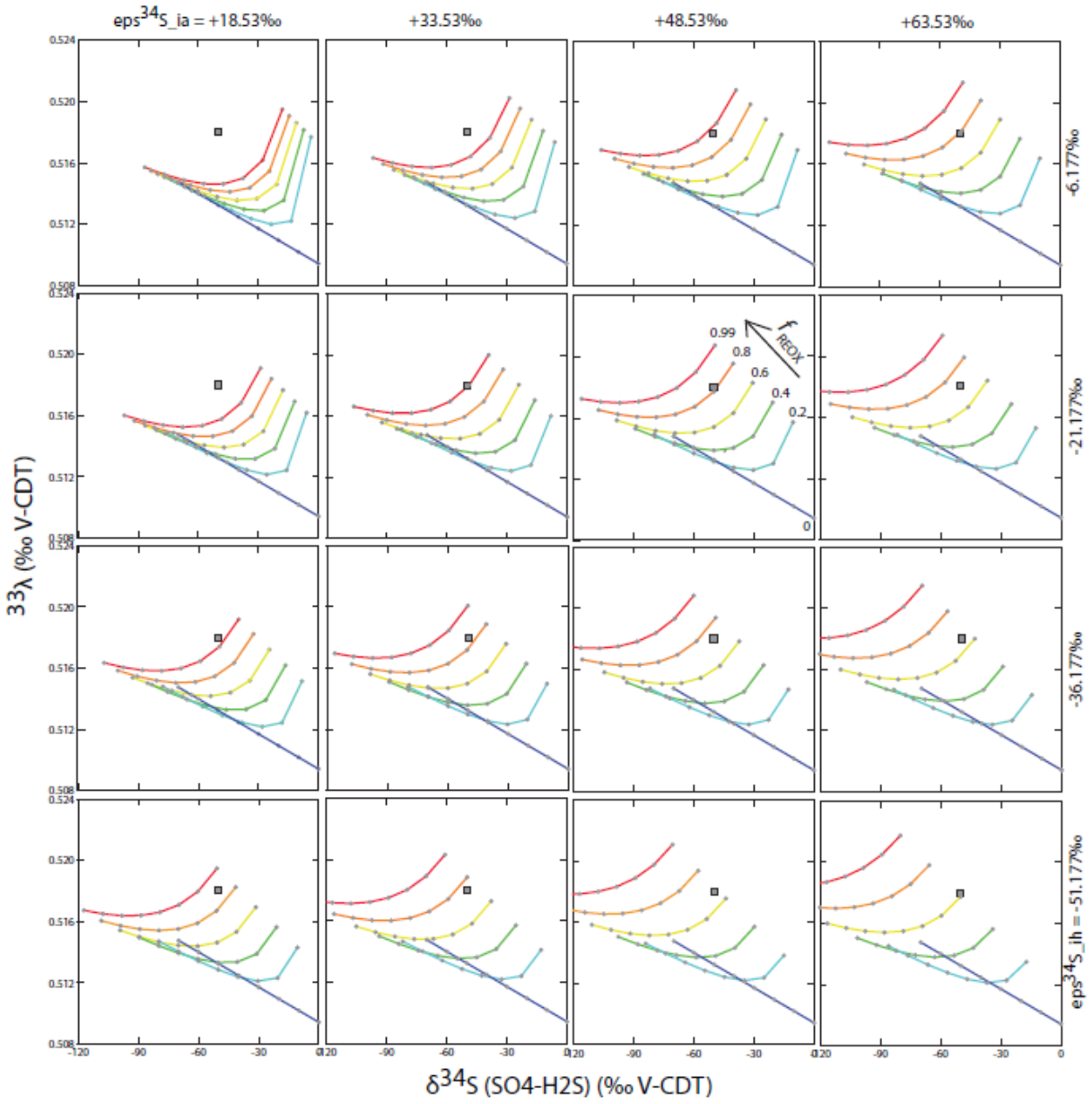

Fig. S2.4. Model of microbial sulphate reduction combined with sulphide reoxidation back to sulphate and sulphide on the ratio 1:3 when $^{34}\alpha_{IA}$ and $^{34}\alpha_{IH}$ are varied, $^{33}\lambda_{IA}$=0.5195071 and $^{33}\lambda_{IH}$ =0.5164677. Microbial sulphate reduction process has $^{34}\alpha_{MSR}$ =0.999-0.93 and $^{33}\lambda_{MSR}$=0.50942-0.51476, intermediate sulphur oxidizing to sulphate has $^{34}\alpha_{IA}$=0.98147-0.93647 and $^{33}\lambda_{IA}$=0.51951, intermediate sulphur oxidizing to sulphide has $^{34}\alpha_{IH}$=1.00617-1.02617 and $^{33}\lambda_{IH}$ =0.51647, at least 70% of the sulphide produced during sulphate reduction is reoxidized back to sulphate. Colored lines indicate different fractions of sulphide reoxidation in units of 20% and gray dots indicate values of $^{34}\alpha_{NET}$.

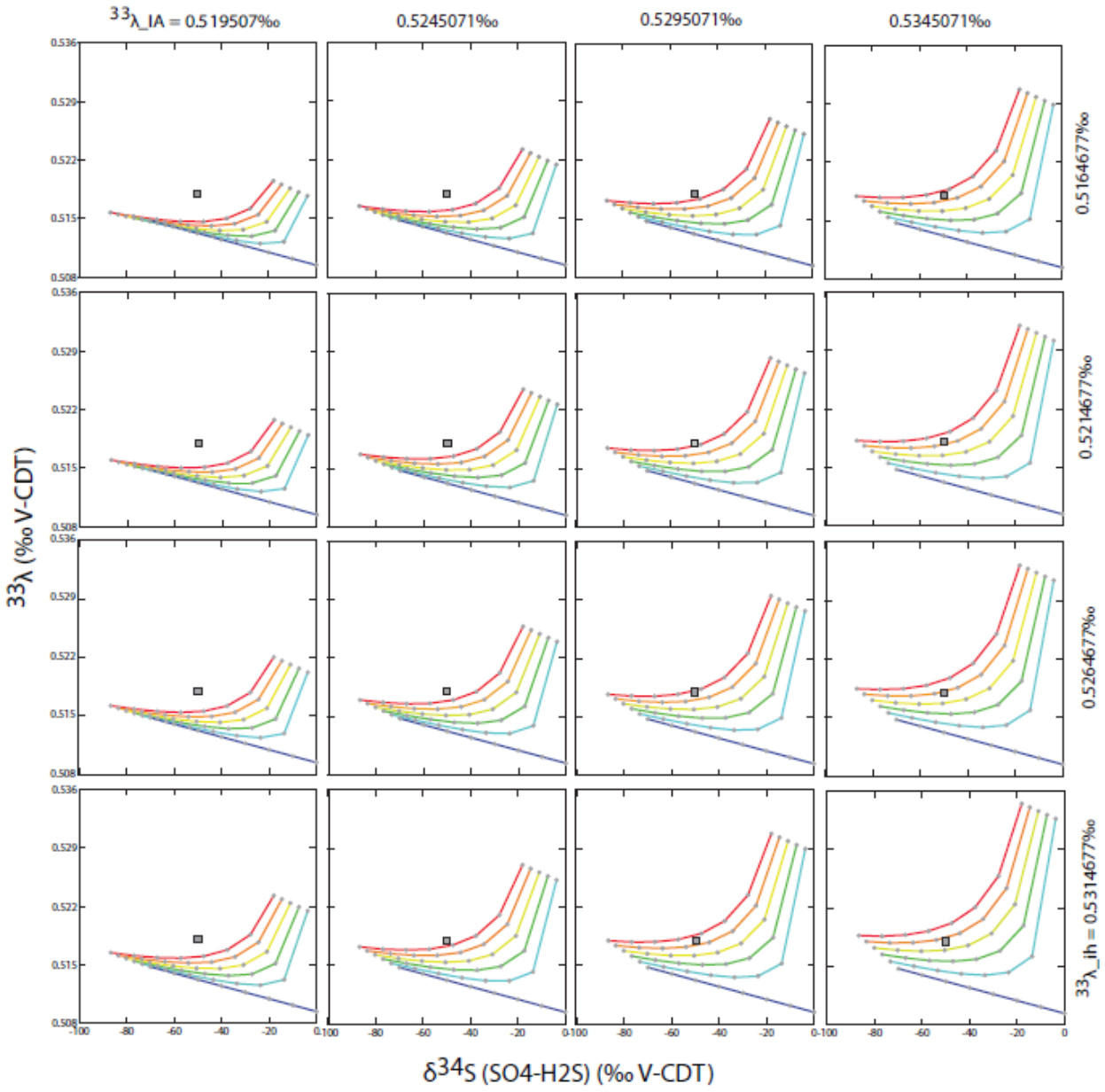

Fig. S2.5. Model of microbial sulphate reduction combined with sulphide reoxidation back to sulphate and sulphide on the ratio 1:3 when $^{34}\alpha_{IA}$=1.01853 and $^{34}\alpha_{IH}$ =0.993823, $^{33}\lambda_{IA}$ and $^{33}\lambda_{IH}$ are varied. Microbial sulphate reduction process has $^{34}\alpha_{MSR}$=0.999-0.93 and $^{33}\lambda_{MSR}$ =0.50942-0.51476, intermediate sulphur oxidizing to sulphate has $^{34}\alpha_{IA}$ =0.98147 and $^{33}\lambda_{IA}$ =0.51951-0.53451, intermediate sulphur oxidizing to sulphide has $^{34}\alpha_{IH}$=1.00617 and $^{33}\lambda_{IH}$=0.51647-0.52647, at least 60% of the sulphide produced during sulphate reduction is reoxidized back to sulphate. Colored lines indicate different fractions of sulphide reoxidation in units of 20% and gray dots indicate values of $^{34}\alpha_{NET}$.

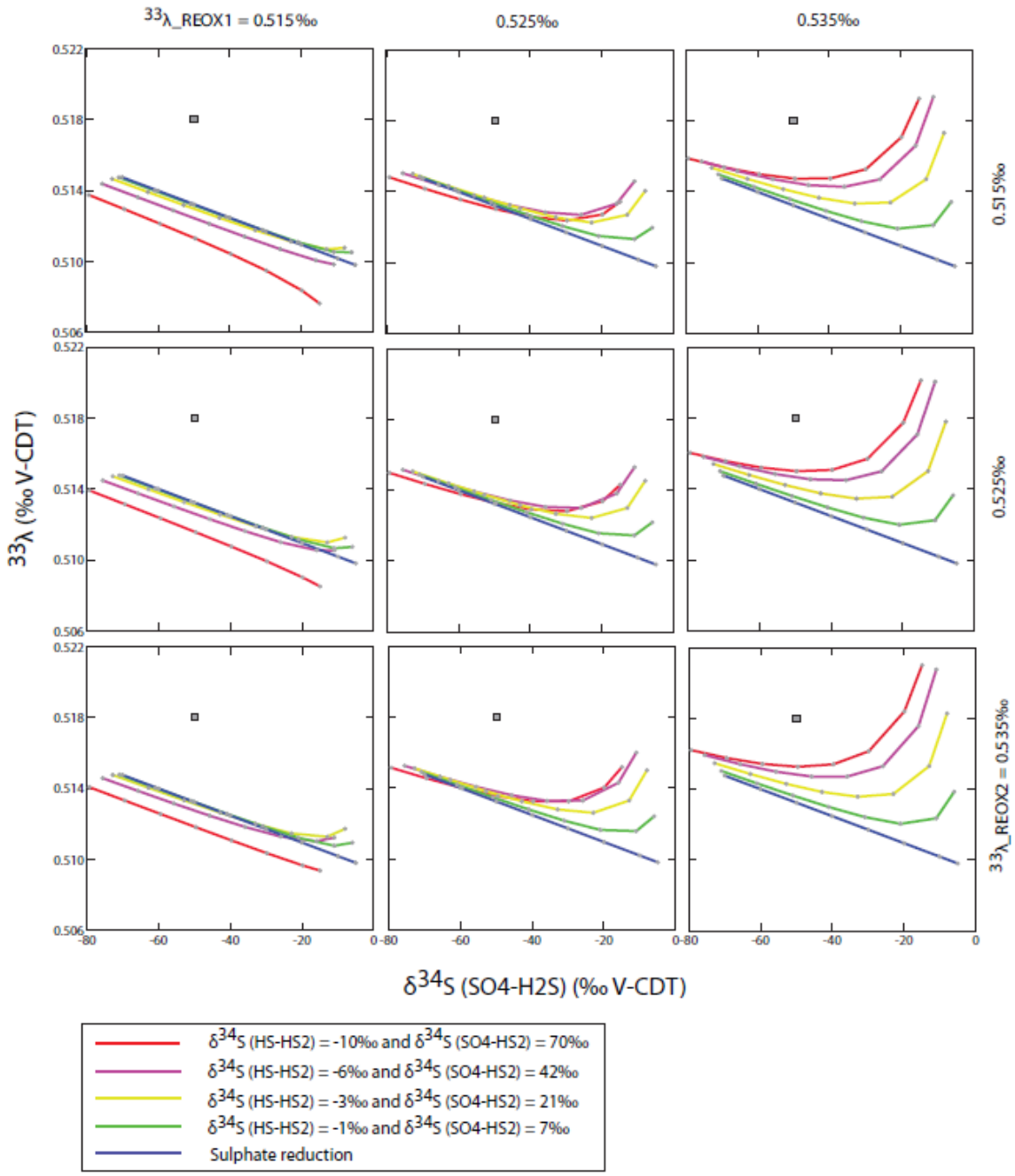

Fig. S2.6. Model of microbial sulphate reduction to disulphide followed by disulphide reoxidation to sulphate and sulphide on the ratio 1:7. Microbial sulphate reduction process has $^{34}\alpha_{MSR}$=0.995-0.93 and $^{33}\lambda_{MSR}$=0.50980-0.51476, $^{34}\alpha_{REOX1}$=1.007-1.07, disulphide oxidizing to sulphate has $^{33}\lambda_{REOX1}$=0.515-0.535 and $^{34}\alpha_{REOX2}$=0.999-0.99, disulphide oxidizing to sulphide has $^{33}\lambda_{REOX2}$=0.515-0.535, the model is unable to reproduce the net fractionation observed in station 5 ($^{34}\alpha_{NET}$=0.95, $^{33}\lambda_{NET}$=0.518).

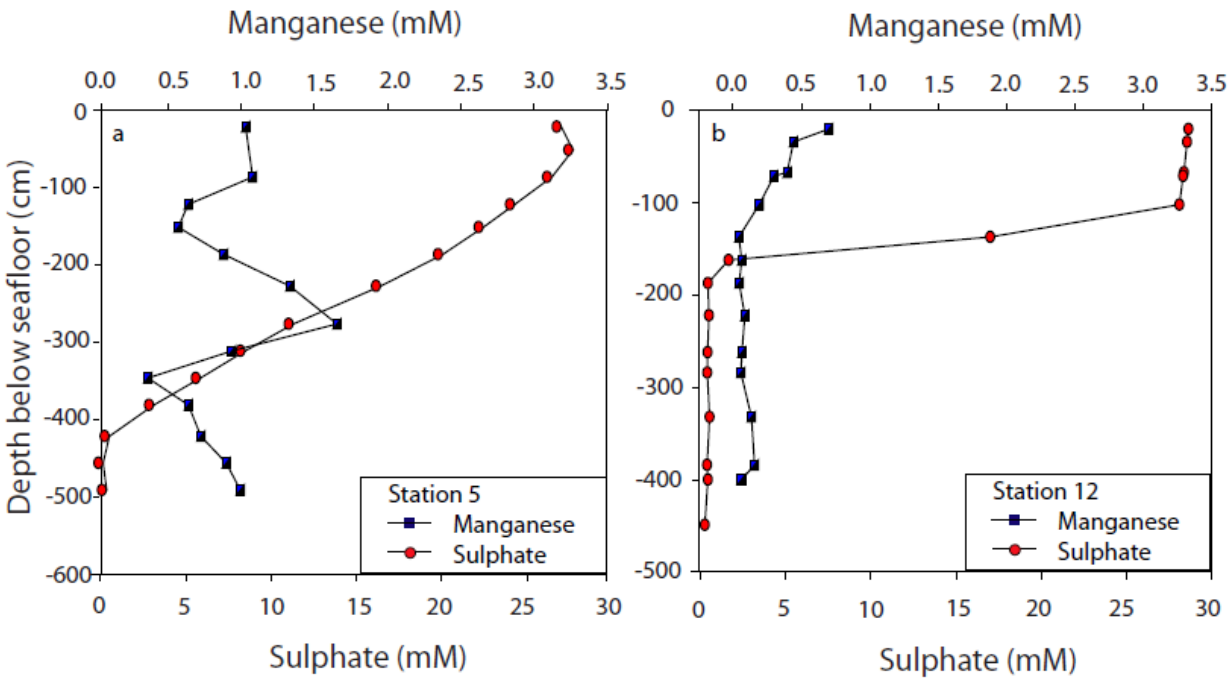

Fig. S2.7. Dissolved manganese (Mn) profile at station 5. Peaks surrounding the SMTZ reflect active Mn cycling and may indicate that manganese oxide reduction supports the sulphide reoxidation cycle identified here.

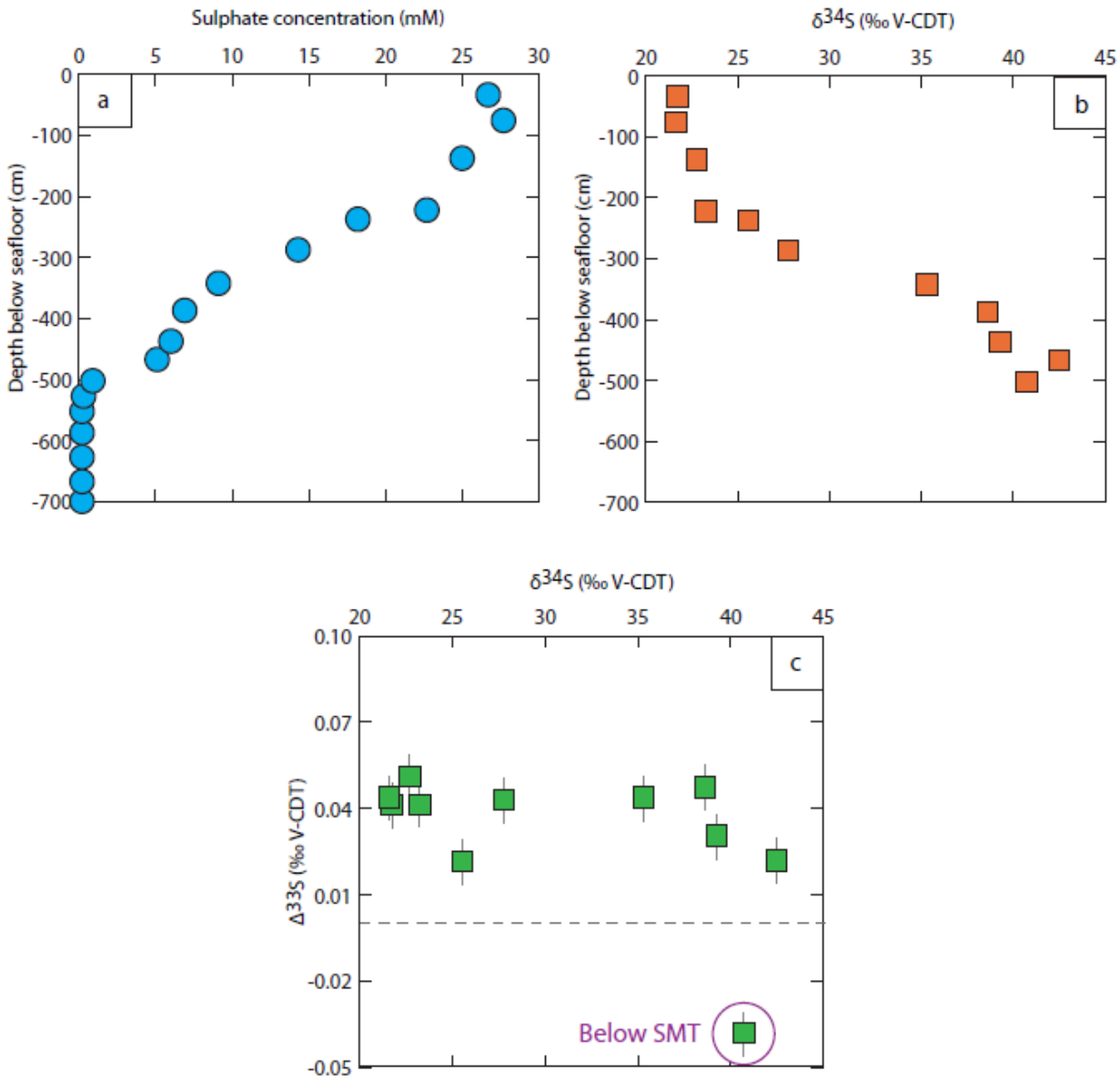

Fig. S2.8. Sulphur geochemistry at station 6. (a) Pore water sulphate concentrations. That sulphate does not vary smoothly with depth suggests that the system was not at steady state. (b) $\delta^{34}S$ values of pore water sulphate show similar trend as sulphate concentration profile. Sulphate concentrations and $\delta^{34}S$ values may be controlled by the same factor. (c) Measured $\Delta^{33}S - \delta^{34}S$ profile.

PREFACE TO CHAPTER 3

In chapter 2, we built three simple box models to understand the sulphur cycling in methane-rich sediments: (1) a model of sulphate reduction coupled with AOM at the SMTZ, (2) a model of sulphate reduction coupled with organic matter oxidation, and (3) a model to quantify sulphide reoxidation. In the first and second models, we assumed that the sulphur isotope composition of dissolved sulphate in pore water was only characterized by bacterial sulphate reduction. In the third model, when the produced sulphide was involved, we also assumed that sulphur isotope composition of sulphide was controlled solely by sulphide reoxidation process. In fact, the transport of sulphate from seawater into marine sediment might cause isotope fractionation. Similarly, the isotope composition of sulphide might change when it diffuses within the sediment from production depth to the depth where sulphide reoxidation occurs.

In chapter 3, we investigate the sulphur isotope fractionation of sulphate and sulphide during diffusion through a porous material (acrylamide gel) by setting up a series of sulphate/sulphide diffusion experiments in the laboratory. We measure sulphate/sulphide concentrations and their isotope compositions along the gel columns. From Fick's laws of diffusion, we build a model for the isotope composition of sulphate and sulphide. This model allows us to extract diffusion-associated sulphur isotope fractionation of sulphate and sulphide at temperatures from 5ºC to 45ºC. The results validate the assumptions of the models in chapter 2. Furthermore, the result provides valuable information for future studies on sulphur cycle in aqueous systems.

CHAPTER 3

Sulphur isotope effects of SO_4^{2-} and HS^- diffusion in water

Thi Hao Bui and Boswell Wing

3.1 Abstract

The sulphur isotope effect due to diffusion of S-bearing ions is thought to be small and is often ignored in studies of natural sediments. Simple kinetic models, however, have been used to suggest significant isotope fractionations associated with sulphate diffusion in sedimentary pore waters. To resolve this discrepancy, we designed an experimental study of S isotope-specific diffusion coefficients of dissolved sulphate (SO_4^{2-}) and bisulphide (HS^-) in a porous material (acrylamide gel). In these experiments the bulk diffusion coefficient of SO_4^{2-} is $4.33\pm0.10\times10^{-6}$ cm^2/s at room temperature, comparable to that reported in earlier studies, while the bulk diffusion coefficient of HS^- is $7.92\pm0.37\times10^{-6}$ cm^2/s. Although down core $\delta^{34}S$ values for pore water SO_4^{2-} were typically less than those of the SO_4^{2-} in the overlying solution, down profile S isotope fractionation in SO_4^{2-} was only slightly outside the external reproducibility of our analysis procedure. As a result we constrained the sulphur isotope effect of SO_4^{2-} diffusion, defined as ratio of the diffusion coefficient for the ^{34}S-subsituted isotopologue relative to that for the ^{32}S-subsituted isotopologue to lie between 0.9994 and 1.0000. On the other hand, the sulphur isotope effect of HS^- diffusion varied systematically from 0.9991 ± 0.0003 at 5ºC to 0.9990 ± 0.0002 at 22°C to 0.9987 ± 0.0002 at 45ºC. An increase in diffusive fractionation with increasing temperature is consistent with experimental evidence from other environmentally important anions. Measured fractionation of ^{33}S-^{32}S in pore water bisulphide suggests that a hydration shell of 1.5 to 4.5 water molecules accompanies HS^- when it diffuses. Sulphur isotope fractionations associated with diffusion of SO_4^{2-} in sedimentary pore waters are two or more orders of magnitude smaller than the typical fractionations produced by natural populations of sulphate reducing microbes, while fractionations associated with HS^- diffusion may become significant over diffusive distances greater than a meter.

3.2 Introduction

Sulphate is the second most abundant anion in seawater after chloride. In marine sediments, microbial sulphate reduction is responsible for the oxidation of most of the organic matter that makes it through oxic remineralization (Jorgensen, 1982). The topography of electron donors in the sediment column determines where sulphate reduction happens. For example, when coupled with organic matter oxidation, sulphate reduction rates are highest just below the sediment-water interface because organic matter is supplied from the water column. On the other hand, maximal sulphate reduction rates can occur much deeper in the sedimentary column when coupled with anaerobic oxidation of methane supplied from below (Devol and Ahmed, 1981). Just as these sinks are separated from the overlying seawater that ultimately sources sulphate, the sulphide produced during microbial sulphate reduction can also be consumed in regions far removed from the site of production. In iron-poor sediments, sulphide may diffuse upwards to near-surface reoxidative zones where it is oxidized back to sulphate through multiple diagenetic steps (Jorgensen and Bak, 1991). During diffusive transport from source to sink, isotopically-substituted sulphate and sulphide should be fractionated, with kinetic theory suggesting that less massive isotopologues (e.g., $^{32}SO_4^{2-}$) are transported more rapidly than their more massive counterparts (e.g., $^{34}SO_4^{2-}$) (Goldhaber and Kaplan, 1980).

Any sulphur isotope fractionation associated with diffusive transport is augmented by the sulphur isotope consequences of microbial sulphate reduction. Sulphate reducing microbes metabolize ^{32}S-substituted sulphate more rapidly than ^{34}S-substituted sulphate, leading to a residual sulphate pool that is isotopically heavier than the original source sulphate and product sulphide is isotopically lighter (Harrison and Thode, 1957). Microbial consumption of sulphate in marine sediments leads to pore water sulphate concentrations that decrease with sediment depth while becoming simultaneously enriched in heavy sulphur isotopes (Goldhaber and Kaplan, 1975; Jorgensen, 1979; Goldhaber and Kaplan, 1980). The interplay between this process and sedimentation rate would control the relative isotopic influences of diffusion and reduction on pore water sulphate (Goldhaber and Kaplan, 1980). The concentration gradient maintained by sulphate reduction pumps sulphate out of the effectively infinite seawater reservoir, potentially maximizing the impact of any diffusive fractionation, while higher sedimentation rates can isolate the local sulphate pool from any diffusive connections.

Although the potential importance of diffusive fractionation was recognized early (Goldhaber and Kaplan, 1980), most work considers the isotope effect of diffusion to be a

negligible component of isotope fractionation during sedimentary sulphur cycling (Jorgensen, 1979; Habicht and Canfield, 1997). More recently, however, the diffusive velocities of S-bearing molecules in marine sediments have been interpreted through an inverse square root model:

$$\frac{{}^{l}v}{{}^{h}v} = \sqrt{\frac{{}^{h}m_{eff}}{{}^{l}m_{eff}}}, \qquad (1)$$

where the superscripts indicate the heavy- or light-isotope substituted molecule, ${}^{i}v$ indicates the diffusive velocity of the isotopologue, and ${}^{i}m_{eff}$ indicates the effective mass of the isotopologue. Direct application of this square root model predicts that the diffusive isotope effect for sulphate could be characterized by a fractionation of ≈10‰ (Donahue et al., 2008). When the solute-solvent reduced mass as ${}^{i}m_{eff}$ in this model, smaller diffusive isotope fractionations are predicted (LaBolle et al., 2008). These sulphur isotope fractionations are comparable to those produced by pure cultures of sulphate-reducing microbes (Canfield, 2001). Theoretical considerations on the molecular scale (Bourg, 2008) as well as on the diagenetic scale (Wortmann and Chernyavsky, 2011), however, suggest that the square root model overestimates the transport-associated S isotope fractionation.

In this study, we present a series of experiments designed to determine the sulphur isotope fractionation associated with diffusion of sulphate and sulphide ions in seawater. We used a column of acrylamide gel with a porosity of ≈1 as the porous media to host the diffusing species. Experiments were undertaken at different temperatures to determine the effect of temperature on diffusion coefficients and on isotope fractionations.

3.3 Methodology

3.3.1 Gel preparation

We used polyacrylamide gel to set up sulphate and sulphide diffusion experiments (Eggenkamp and Cole, 2009; Davison et al., 1994). We did not use $K_2S_2O_8$ to catalyze the polymerizing reaction because sulphur in persulphate can be extracted together with sulphur in sulphate by the Thode reagent (Thode et al, 1961). We instead followed the protocol of photochemical polymerization (Technical note 1156, Bio-Rad). To prepare ~40mL of gel, we

mixed 14 ml of MilliQ-water with 6 ml N,N'-Methylene-bisacrylamide 2% aqueous solution (Sigma Chemical Co.) and 20 ml of acrylamide 30% aqueous solution (Fisher Scientific). The solution was degassed in a vacuum oven for 15 minutes at room temperature. Then we added initiators including 200µL of Riboflavine phosphate 0.14% (Sigma-Aldrich), 20mL of H_2O_2 30% (Fisher Scientific) and 60µL of TEMED (N,N,N',N'-Tetramethylethylenediamine, Sigma Chemical Co.) under a N_2 atmosphere. The solution was mixed thoroughly and was poured into clean dry glass tube of 1.8cm diameter. The polymerization process was completed under fluorescent lamps in less than 30 minutes.

3.3.2. Experimental set-up

After it set, the gel was left overnight with a Parafilm-covered top. To start the diffusion experiment, we filled the free space above the gel layer (about half the overall volume of the tube) with either a sulphate- or sulphide-bearing solution. All sulphide diffusion experiments were conducted in an anaerobic chamber to avoid sulphide oxidation. From preliminary experiments, diffusion times were estimated so that sulphate/sulphide ions would not reach the bottom of the gel, and the experiments were stopped before this time in order to satisfy the assumption of diffusion in an infinite half space. At the end of the experiment, we pipetted off the overlying solution, broke the glass tube, and removed the gel cylinder. Then we cut the gel into slices of ~1 cm with a razor-thin scalpel. Sulphide-bearing gels were immediately preserved in Zinc Acetate solution (4% w/w). The sulphide S was extracted with boiling HCl 6N and trapped as Ag_2S. Sulphur in the sulphate-bearing gels was extracted with a boiling 'Thode' solution (Thode et al, 1961) and trapped as Ag_2S. The concentrations of sulphate- and sulphide-S were determined gravimetrically by weighing the Ag_2S obtained from each gel slice and then normalizing to the mass of that slice.

3.3.3 Multiple sulphur isotope measurement

We weighed about 2-3mg of clean dry Ag_2S from each sample into aluminum foil pouches. These samples were loaded into Ni reaction bombs under Argon atmosphere. The bombs were evacuated to vacuum before being fluorinated with F_2. The Ag_2S reacted overnight with F_2 at 225ºC to form SF_6 gas. SF_6 was purified by cryogenic traps and gas chromatography. Clean SF_6 was loaded into a Finnigan MAT 253 to measure multiple sulphur isotope

compositions in dual inlet mode. Sulphur isotope compositions were referenced to V-CDT (Vienna-Canion Diablo Troilite) and reported as:

$$\delta^{3x}S = \left(\frac{R^{3x}_{Sample}}{R^{3x}_{V-CDT}} - 1\right) \times 1000, \qquad (2)$$

where 3x is 33, 34 or 36, and

$$\Delta^{33}S = \delta^{33}S - \left[\left(1 + \frac{\delta^{34}S}{1000}\right)^{0.515} - 1\right] \times 1000 \qquad (3)$$

We used international standards (IAEA-S-1, IAEA-S-2, IAEA-S-3) to calibrate the sulphur isotopic measurements. On the V-CDT scale, the sulphur isotope composition of IAEA-S-1 is $\delta^{34}S$=-0.3‰ and $\Delta^{33}S$=0.094‰. We report the uncertainty of our measurements based on replicate extractions of S-bearing gels. The total error of both sulphate and sulphide $\delta^{34}S$ values is 0.06‰ (1σ) and of $\Delta^{33}S$ values is 0.01‰ (1σ) and includes errors from the extraction process, purification and isotope measurement.

3.3.4 Diffusion models

We use a simple one-dimensional diffusion model to describe the evolution of ion concentrations and isotope compositions in the experiments. The change of ion concentrations through the gel column with time is described by Fick's second law:

$$\frac{\partial C}{\partial t} = D\frac{\partial^2 C}{\partial x^2} \qquad (4)$$

where C is the ion concentration, D is the diffusion coefficient of the ion in the gel, t is time and x is distance from the gel-solution interface. By design, sulphate or sulphide ions diffuse from the overlying solution into the gel. Because of its size, the solution acts as an effectively infinite source of ions with a homogeneous elemental and isotope composition. Over a limited timeframe of the experiments, the gel can be considered as having infinite length. Under these conditions, the solution for equation (4) is:

$$C(t,x) = C_0 erfc\left(\frac{x}{2\sqrt{Dt}}\right) \qquad (5)$$

where C_0 is the constant ion concentration in the overlying solution. Each experiment was run for a specified time, fixing t in this equation. This left two free parameters, C_0 and D to be constrained by the ion concentration profiles. We estimated these parameters for each

experiment by making a least-squares fit between the measured ion concentrations and those predicted from equation (5). The value for D from these fits is the diffusion coefficient of bulk sulphate or sulphide. Since more than 95% of sulphur in nature is ^{32}S, we considered that the D value extracted from our fits is equivalent to the diffusion coefficient for the ^{32}S-substituted ion (^{32}D), within the uncertainty of our ability to determine it (5-10% relative error, Table 1).

The relative diffusion coefficients of ionic isotopic analogues (isotopologues) are often well described by power-law relationship relative to the inverse ratio of their molecular mass (Richter el al., 2006):

$$\frac{^{h}D}{^{l}D} = \left(\frac{^{l}m_{eff}}{^{h}m_{eff}}\right)^{\beta}. \qquad (6)$$

Diffusive isotope fractionation has been quantified with β values that are specific to each ionic species (Richter el al., 2006), the ratio of ^{h}D to ^{l}D (Richter el al., 2006; Eggenkamp and Coleman, 2009), as well as an 'efficiency' factor E that is defined by $E = 2\beta$ (Watkins et al., 2011). Here we monitor isotope fractionation through $^{h}\alpha$, defined as the ratio of diffusion coefficients of heavy isotopologue versus the light isotopologue ($^{34}\alpha = {}^{34}D/{}^{32}D$). With this definition, isotopic ion profiles can be described by the following equation:

$$\delta^{34}S\ [‰] = \left[\left(\frac{\delta^{34}S_0}{1000} + 1\right) \times \frac{erfc\left(\frac{x}{2\sqrt{D^{34}\alpha t}}\right)}{erfc\left(\frac{x}{2\sqrt{Dt}}\right)} - 1\right] \times 1000 \qquad (7)$$

Once equation (7) has been fit to the measured isotopic composition profiles, the fractionation factor $^{34}\alpha$ and the initial isotope composition $\delta^{34}S_0$ are the two free parameters in this equation. We estimated these parameters for each experiment by making a least-squares fit between the measured $\delta^{34}S$ values and those predicted from equation (7). A similar procedure was used to estimate the fractionations associated with ^{33}S and ^{32}S.

3.4 Results

The initial sulphate solution that overlies the gel column has a concentration of ~100mM (slightly greater than three times seawater sulphate concentration). After the experiment, the

sulphate in the topmost gel layer is in elemental and isotopic equilibrium with sulphate in initial solution, illustrating that the infinite reservoir assumption is fulfilled within the uncertainty of our measurements (Figure 3.1). Within the gel, sulphate concentration decreases with distance from the gel-solution interface (Figure 3.1). Applying the diffusion model solution in equation (3) to the sulphate concentration profile results in an estimated diffusion coefficient of D_SO_4 of 4.33±0.10E-6 cm^2/s at 22ºC.

Although basic theory suggests that ^{32}S-sulphate diffuses faster than ^{34}S-sulphate (Equation 1), we did not observe systematic changes in the $\delta^{34}S$ values of sulphate in the gel with distance from the gel-solution interface (Figure 3.1). From our fits of equation (7) to the most variable measurements in the dataset, the upper boundary of fractionation is characterized by $^{34}\alpha = 0.9994$ while the lower boundary is consistent with no fractionation ($^{34}\alpha \sim 1$; Figure 3.1).

The sulphide experiments were performed in an anaerobic chamber in order to avoid sulphide loss and/or oxidation competing with sulphide diffusion. Extraction of the sulphide-S was not performed under anoxic conditions, however, possibly giving rise to sulphide concentration profiles that were not as smooth as the sulphate concentration profiles (Figure 3.2). We tested this possibility, and found that although oxidation and/or loss clearly fractionated sulphide isotopes, it took days (Figure 3.3). Because of this, the sulphide concentration profiles still clearly present diffusive behaviour (Figure 3.2). The best fit model (Equation 5) returns diffusion coefficients for sulphide that range from 4.69±0.42E-6 at 5°C to 14.56±0.85E-6 cm^2/s at 45°C (Table 3.1).

Along the gel column, the $\delta^{34}S$ values of sulphide decrease by ~3‰ to 5‰ over a distance of ~15 cm for the experiments at different temperatures (Figure 3.2). Fitting the diffusion model to these profiles shows that diffusive sulphur isotope fractionation is present, and characterized by $^{34}\alpha = 0.9991$ at 5°C ranging to $^{34}\alpha = 0.9987$ at 45ºC.

3.5 Discussion

3.5.1 Sulphate and sulphide speciation

For noble gases, the β value appropriate to equation (4) is in the range of 0.05 to 0.2 (Bourg and Sposito, 2008). But the mass dependence of isotopologue-specific diffusion of

monovalent and divalent ions is much weaker (β ~ 0-0.05) (Richter et al., 2006; Bourg and Sposito, 2007; Eggenkamp and Coleman, 2009). For example, there is no measurable isotope fractionation during the experimental diffusion of the divalent cation Mg^{2+} while Li^{+} is fractionated (Richter et al., 2006). This observation suggests there may be a link between the charge density of dissolved species and diffusion-associated isotope fractionation (Watkins et al., 2011). Therefore, it is necessary to identify the speciation of sulphate and sulphide in the solutions studied here.

Sodium sulphide dissolving in water will dissociate as follows:

$$Na_2S \rightarrow 2Na^{+} + S^{2-}$$

$$S^{2-} + H_2O \leftrightarrow HS^{-} + OH^{-}$$

$$HS^{-} + H_2O \leftrightarrow H_2S + OH^{-}$$

Hydrogen sulphide (H_2S) is a weak acid when dissolved in water. It has a first acid dissociation constant (Ka_1) ~10^{-7} (Ellis and Golding, 1959; Goldhaber and Kaplan, 1975; Millero et al., 1988). But estimates of its second acid dissociation constant (Ka_2) vary over five orders of magnitude, from 10^{-13} to 10^{-18} (Ellis and Golding, 1959; Licht et al., 1990; Migdisov et al., 2002). In order to calculate the dominant dissolved sulphide species in the initial solution, we use a Ka_2 value in the middle of the reported range =$10^{-15.5}$. From these values, we calculate that dissolved H_2S is dominant in solutions with pH<7 while ion S^{2-} is dominant at pH>14 and HS^{-} is the primary species at intermediate pH values.

According to these speciation calculations, sulphide in the initial Na_2S solution (C ≈ 200mM, pH ≈ 12.7) is mostly HS^{-} (~98.4%). The pH of acrylamide gel solution is ~9 and this value does not change during the polymerization process. Therefore, even if there is no pH adjustment when sulphide diffuses from overlying solution to the gel, most of sulphide is still in the form of HS^{-} (>98%).

The sulphate solution has pH~6.5. The Na_2SO_4 may dissociate according to:

$$Na_2SO_4 \rightarrow 2Na^{+} + SO_4^{2-}$$

$$SO_4^{2-} + H_2O \leftrightarrow HSO_4^{-} + OH^{-}$$

$$HSO_4^{-} + H_2O \leftrightarrow H_2SO_4 + OH^{-}$$

Sulphuric acid (H_2SO_4) is a strong acid with very high first dissociation constant (Ka_1=2.4E+6). It means that dissolved H_2SO_4 species is very unstable and it dissociates completely. The second acid dissociation constant is 10^{-2}. Therefore at pH<2, HSO_4^- is dominant and at pH>2, SO_4^{2-} is the dominant ion. At pH 6.5 (pH of 100mM Na_2SO_4 solution), more than 99.99% of dissolved sulphate species is SO_4^{2-}.

3.5.2 Isotope fractionation during sulphide loss

In our study, during the preparation process (cutting and weighing gel), sulphide in the gel was exposed to the open atmosphere, potentially leading to sulphide oxidation and/or loss. To test if this process affected the sulphur isotope composition of the remaining sulphide, we prepared a gel in equilibrium with our starting sulphide solution. We cut the gel into small pieces, stored them in the open atmosphere, and periodically extracted sulphur from a piece of gel to determine sulphide concentration and isotope composition.

In general, sulphide concentration decreases with increasing storage time (Figure 3.3), while sulphur isotope measurements showed that ^{32}S-sulphide is lost faster than ^{34}S-sulphide with net isotope fractionation factor of ~0.9978 (Figure 3.4). This is larger than the fractionation factor associated with sulphide diffusion. To avoid the isotopic complications of sulphide loss, we set up the experiment in anoxic conditions, and exposed the gel to the open atmosphere during sample preparation for only a short time (<1 hour) compared to the timescale of sulphide loss (>1day; Figure 3.3).

3.5.3 Diffusion coefficients

3.5.3.1 SO_4^{2-} diffusion coefficient

From our two sulphate experiments, we estimate a $D\_SO_4^{2-}$ value of 4.33±0.10E-6 cm^2/s at 22ºC. This value is comparable to sulphate diffusion coefficients in marine sediment obtained by previous studies in the temperature range from 4 to 23.7ºC (Krom and Berner, 1980; Li and Gregory, 1973) (Table 2).

3.5.3.2 HS^- diffusion coefficient

At 22ºC, the model concentration profile best describes the measured concentration profile with the diffusion coefficient of 7.92±0.37E-6 cm^2/s. Because the porosity of the

acrylamide gel is approximately equal 1, this value should be equal to the diffusion coefficient of HS^- in water (Eggenkamp and Coleman, 2009).

The diffusion coefficient of HS^- strongly depends on temperature and this dependence is linear in the range of studied temperature (Figure 5). The change in the diffusion coefficient of HS^- is 0.25E-6 cm^2/s per °C. This rate is comparable to, but somewhat lower than that of Cl^- (0.37E-6 cm^2/s per °C) (Eggenkamp and Coleman, 2009), suggesting that the size of the hydration shells of each ion may decrease in a similar fashion as temperature increases (Eggenkamp and Coleman, 2009).

3.5.4 Sulphur isotope fractionation

3.5.4.1 Sulphur SO_4^{2-} isotope fractionation

No measureable systematic isotope fractionation due to SO_4^{2-} diffusion was observed in our study (Figure 3.1). The range of $\delta^{34}S$ values in the gel column constrains the diffusive fractionation factor to lie between 0.9994 and 1, with most measurements consistent with the upper end of this range. Even the maximum possible fractionation factor, which corresponds to an $^{34}\varepsilon$ ($=[^{34}\alpha - 1] \times 1000$) value of 0.6‰, is more than an order of magnitude smaller than the fractionation that has been recently proposed for sulphate diffusion (Donahue et al., 2008; LaBolle et al., 2008).

According to kinetic theory, $D(^{34}SO_4^{2-})/ D(^{32}SO_4^{2-}) = (96/98)^{\beta}$. From the measurements reported here, $^{34}\alpha = D(^{34}SO_4^{2-})/ D(^{32}SO_4^{2-}) > 0.99940$, which implies that $\beta < 0.029$. Such a small value has been previously suggested from theoretical considerations (Bourg, 2008). Aqueous diffusive isotope fractionation appears to be greater for uncharged solutes than for ions and is greater for monovalent ions than for divalent ions (Rodushkin et al., 2004; Richter et al., 2006; Zeebe, 2011), leading to the speculation that the larger and longer-lived hydration shells associated with more highly charged species limits diffusion-associated isotope fractionation (Watkins et al., 2011). It seems that the data provided here for relative $^{34}SO_4^{2-}$ and $^{32}SO_4^{2-}$ diffusion support this hypothesis.

3.5.4.2 Sulphur HS^- isotope fractionation

The three experiments at 5°C, 22°C and 45°C suggest that diffusive HS^- isotope fractionation decreases slightly with temperature (Figure 6). Diffusive fractionation factors for

HS^- are comparable to those for the diffusive fractionation of ionic chlorine, bromine, and mono-valent cations (e.g. Richter el al., 2006; Eggenkamp and Coleman, 2009) (Table 3). The β value calculated for HS^- is 0.0170±0.0085.

3.5.4.3 Multiple sulphur isotopes

The magnitude of an isotope-specific diffusion coefficient is proportional to its effective molecular mass (m_{eff}, Richter et al., 2005; Bourg and Sposito, 2008):

$$^{x}D = {}^{x}m_{eff}^{-\beta} \qquad (8)$$

where x = 32, 33, or 34 for the sulphur isotope system.

From this relationship we have:

$$^{33}\alpha = \frac{^{33}D}{^{32}D} = \left(\frac{^{33}m_{eff}}{^{32}m_{eff}}\right)^{-\beta} \qquad (9)$$

and

$$^{34}\alpha = \frac{^{34}D}{^{32}D} = \left(\frac{^{34}m_{eff}}{^{32}m_{eff}}\right)^{-\beta} \qquad (10)$$

Accordingly, the exponent that relates the diffusive isotope fractionation factors for ^{33}S-^{32}S and ^{34}S-^{32}S is (cf. Young et al., 2001):

$$^{33}\lambda = \frac{ln(^{33}\alpha)}{ln(^{34}\alpha)} = \frac{\ln\left(\frac{^{33}m_{eff}}{^{32}m_{eff}}\right)}{ln\left(\frac{^{34}m_{eff}}{^{32}m_{eff}}\right)} \qquad (11)$$

When the diffusing species does not interact with its surroundings, m_{eff} can be calculated as the molecular mass of the ion plus any H_2O molecules in its hydration shell. When solute-solvent collisions are taken into account, the effective mass in equation (9) and (10) is often replaced by the reduced mass μ (Richter et al., 2005; LaBolle et al., 2008) where:

$$^{x}\mu = \frac{^{x}m_{eff,solute} \times M_{solvent}}{^{x}m_{eff,solute} + M_{solvent}} \qquad (12)$$

where $M_{solvent}$ is equal to the mass of a water molecule for aqueous solutions. As above, ${}^{x}m_{eff,\ solute}$ is the molecular mass of the ^{34}S-, ^{33}S-, and ^{32}S-substituted ion plus any H_2O molecules in its hydration shell.

A negative relationship between $\Delta^{33}S$ and $\delta^{34}S$ values has been observed in the sulphide diffusion experiments, as exemplified by the experiment at 45ºC because of the larger overall fractionation in this experiment. The negative correlation is characterized by a $^{33}\lambda$ of 0.5047 and an R^2=0.71 (Figure 3.7). Using the molecular mass of the bare HS^- ion as m_{eff} yields a $^{33}\lambda$ value of 0.5081 while using the bare ion reduced mass model, without any hydration shell, predicts a $^{33}\lambda$ value of 0.5129.

In order to obtain the experimental value ($^{33}\lambda$=0.5047), a hydration shell is required to increase the overall molecular mass of the diffusing species. The molecular mass model suggests that ~1.5 water molecules on average surround each HS^- ion while the reduced mass model suggests a hydration shell of ~4.5 water molecules around each HS^- ion. These estimates agree well with a recently computed coordination number for the HS^- ion of ~4.5 (Liu et al., 2013). A larger and longer lived hydration shell reduces the effect of mass differences of the ions, which in turn, leads to the lower overall diffusion-associated fractionation (Watkins et al., 2011).

3.6 Conclusions

We constrained the diffusion coefficients of SO_4^{2-} and HS^- in through a water-saturated polyacrylamide gel at 22ºC as 4.33±0.10E-6 cm^2/s and 7.92±0.37E-6 cm^2/s, respectively. The diffusion coefficient of HS^- increases with temperature in the same range as that of Cl^-. The SO_4^{2-} diffusion does not cause significant sulphur isotope fractionation (β<0.029 at the temperature of 22ºC). The lack of diffusion-associated fractionation of ion SO_4^{2-} is similar to that of ion Mg^{2+} (Richter et al., 2005) strengthening the inverse linkage between ion charge density and the diffusion-associated isotope fractionation. This low fractionation means that one can ignore the impact of SO_4^{2-} diffusion on the overall isotope fractionation of SO_4^{2-} in marine sedimentary pore waters. The isotope fractionation of ion HS^- is detectable and varies between 0.99909±0.00030 and 0.99869±0.00020 in the temperature range of 5ºC to 45ºC. Fractionation of ^{33}S-^{32}S reveals that, at 45ºC, HS^- is surrounded by a hydration shell of 1.5 to 4.5 water

molecules. However, the overall magnitude of this fractionation is significantly smaller than the sulphur isotope fractionation produced by sulphate reducing bacteria (Canfield, 2001). If HS^- occurs over centimeter scales, this suggests that the isotope effect of HS^- can be ignored in sedimentary pore waters. However, HS^- diffusion on the meter scale is likely to induce a diffusive isotope fractionation that may need to be taken into account when interpreting S isotope records in modern and ancient sediments.

3.7 References

Beekman, H. E., Appelo, C. A. J., Eggenkamp, H. G. M., and Kreulen, R. (1992) ^{37}Cl–^{35}Cl transport modelling in accumulating sediments of a former brackish lagoonal environment. In *Proc. 7th Int. Symp. Water–Rock Interaction* (eds. Y. K. Kharaka and A. S. Maest), pp. 209–212. Boudreau B. P. (1997) Diagenetic models and their implementation (Vol 505.) Berlin: Springer.

Bourg I. C. and Sposito G. (2007). Molecular dynamics simulations of kinetic isotope fractionation during the diffusion of ionic species in liquid water. *Geochim. Cosmochim. Acta* **71**, 5583-5589.

Bourg I. C. and Sposito G. (2008). Isotope fractionation of noble gases by diffusion in liquid water: Molecular dynamics simulations and hydrologic applications. *Geochim. Cosmochim. Acta* **72**, 2237-2247.

Bourg I. C. (2008) Comment on "Modeling sulphur isotope fractionation and differential diffusion during sulphate reduction in sediments of the Cariaco Basin" by M.A. Donahue, J.P. Werne, C. Meile and T.W. Lyons. *Geochim. Cosmochim. Acta* **72**, 5852-5854.

Canfield D. E. (2001) Isotope fractionation by natural populations of sulphate-reducing bacteria. *Geochim. Cosmochim. Acta* **65**, 1117-1124.

Davison W., Zhang H., and Grime G. W. (1994) Performance characteristics of gel probes used for measuring the chemistry of pore waters. *Environ. Sci. Technol.* ***28***, 1623-1632.

Desaulnier, D. E., Kaufmann, R. S., Cherry, J. A., and Bentley, H. W. (1986) ^{37}Cl-^{35}Cl variations in a diffusion-controlled groundwater system. *Geochimica et Cosmochimica Acta* **50**, 1757-1764.

Devol A. H. and Ahmed S. I. (1981) Are high rates of sulphate reduction associated with anaerobic oxidation of methane? *Nature* **291**, 407-408.

Donahue M. A., Werne J. P., Meile C. and Lyons T. W. (2008) Modeling sulphur isotope fractionation and differential diffusion during sulphate reduction in sediments of the Cariaco Basin. *Geochim. Cosmochim. Acta* **72**, 2287-2297.

Eggenkamp H. G. M and Coleman M. L. (2009) The effect of aqueous diffusion on the fractionation of chlorine and bromine stable isotopes. *Geochim. Cosmochim. Acta* **73**, 3539-3548.

Eggenkamp, H. G. M., Middelburg, J. J., and Kreulen, R. (1994) Preferential diffusion of ^{35}Cl relative to ^{37}Cl in sediments of Kau Bay, Halmahera, Indonesia. *Chemical Geology* **116**, 317-325.

Ellis A. J. and Golding R. M. (1959) Spectrophotometric determination of the acid dissociation constants of hydrogen sulphide. *J. Chem. Soc. 1959,* 127-130.

Goldhaber M. B. and Kaplan I. R. (1975) Apparent dissociation constants of hydrogen sulphide in chloride solutions. *Marine chemistry **3***, 83-104.

Goldhaber M. B. and Kaplan I. R. (1980) Mechanisms of sulphur incorporation and isotope fractionation during early diagenesis in sediments of the Gulf of California. *Marine chemistry 9*, 95-143.

Groen, J., Velstra, J., and Meesters, A. G. C. A. (2000) Salinization processes in paleowaters in coastal sediments of Suriname: Evidence from $\delta^{37}Cl$ analysis and diffusion modeling. *Journal of Hydrology* **234**, 1-20.

Habicht K. S. and Canfield D. E. (1997) Sulphur isotope fractionation during bacterial sulphate reduction in organic-rich sediments. *Geochim. Cosmochim. Acta* **61**, 5351-5361.

Harrison A. G. and Thode H. G. (1958) Mechanism of the bacterial reduction of sulphate from isotope fractionation studies. *Transactions of the Faraday Society* **54**, 84-92.

Iversen N. and Jorgensen B. B. (1993) Diffusion coefficients of sulphate and methane in marine sediments: influence of porosity. *Geochim. Cosmochim. Acta* **57**, 571-578.

Jorgensen B. B. (1979) A theoretical model of the stable sulphur isotope distribution in marine sediments. *Geochim. Cosmochim. Acta* **43**, 363-374.

Jorgensen B. B. (1982) Mineralization of organic matter in the sea bed - the role of sulphate reduction. *Nature* **296**, 643-644.

Jorgensen B. B. and Bak F. (1991) Pathways and microbiology of thiosulphate transformations and sulphate reduction in a marine sediment (Kattegat, Denmark). *Appl. Environ. Microbiol.* ***57(3)***, 847-856.

Krom M. D. and Berner R. A. (1980) The diffusion coefficients of sulphate, ammonium, and phosphate ions in anoxic marine sediments. *Limnol. Oceanogr.* ***25(2),*** 327-337.

Li Y. H. and Gregory S. (1974) Diffusion of ions in sea water and in deep-sea sediments. *Geochim. Cosmochim. Acta* **38**, 703-714.

Licht S., Forouzan F., and Longo K. (1990) Differential densometric analysis of equilibria in highly concentrated media: determination of the aqueous second acid dissociation constant of H_2S. *Anal. Chem.* ***62***, 1356-1360.

Liu X., Sprik M., and Cheng J. (2013) Hydration, acidity and metal complexing of polysulphide species: A first principles molecular dynamics study. *Chemical Physics Letter* **563**, 9-14.

Migdisov A. A., William-Jones A. E., Lakshtanov L. Z., and Aleknin Y. V. (2002) Estimates of the second dissociation constant of H_2S from the surface sulfidation of crystalline sulphur. *Geochim. Cosmochim. Acta* **66**, 1717-1725.

Millero F. J., Plese T., and Fernandez M. (1988) The dissociation of hydrogen sulphide in seawater. *Limnol. Oceanogr.* ***33(2),*** 269-274.

Pikal, M. J. (1972) Isotope effect in tracer diffusion: Comparison of the diffusion coefficients of $^{24}Na^+$ and $^{22}Na^+$ in aqueous electrolytes. *Journal of Physical Chemistry* **76**, 3038-3040.

Richter, F. M., Mendybaev, R. A., Christensen, J. N., Hutcheon, I. D., William, R. W., Sturchio, N. C., and Beloso Jr., A. D. (2006) Kinetic isotope fractionation during diffusion of ionic species in water. *Geochimica et Cosmochimica Acta* **70**, 277-289.

Rodushkin, I., Stenberg, A., Andren, H., Malinovsky, D., and Baxter, D. C. (2004) Isotope fractionation during diffusion of transition metal ions in solution. *Analytical Chemistry* **76**, 2148-2151.

Schulz H. D. (2000) Quantification of early diagenesis: dissolved constituents in marine pore water. *Marine geochemistry* (pp. 85-128). Springer Berlin Heidelberg.

Thode H. G., Monster J. and Dunford H. B. (1961) Sulphur isotope geochemistry. *Geochim. Cosmochim. Acta* **25**, 159-174.

Wortmann U. G. and Chernyavsky B. N. (2011) The significance of isotope specific diffusion coefficients for reaction-transport models of sulphate reduction in marine sediments. *Geochim. Cosmochim. Acta* **75**, 3046-3056.

Young E. D., Galy A., and Nagahara H. (2002) Kinetic and equilibrium mass-dependent isotope fractionation laws in nature and their geochemical and cosmochemical significance. *Geochim. Cosmochim. Acta* **66**, 1095-1104.

Zeebe, R. E. (2011) On the molecular diffusion coefficients of dissolved CO_2, HCO_3^-, and CO_3^{2-} and their dependence on isotopic mass. *Geochimica et Cosmochimica Acta* **75**, 2483-2498.

Table 3.1. Sulphide diffusion experiments.

Experiment	Temperature (ºC)	time (days)	D_HS^- (cm^2/s)	Fractionation (D^{34}/D^{32})
1	5	45	4.69±0.42E-6	0.99909±0.00030
2	22	21	7.92±0.37E-6	0.99900±0.00022
3	45	12	14.56±0.85E-6	0.99869±0.00020

Table 3.2. Diffusion coefficient of sulphate in different environments at different temperatures.

Source	**T (ºC)**	**Material**	**D_sulphate (*E-6 cm^2/s)**
Iversen and Jorgensen (1993)	4	Marine sediment, φ=0.90	3.7±0.02
Krom and Berner (1980)	20	Marine sediment, φ=0.64	5.0±1.4
Li and Gregory (1973)	5	Pacific red clay, φ=0.70-0.85	3.3±0.2
Li and Gregory (1973)	23.7	Pacific red clay, φ=0.70-0.85	5.3±0.2
This study	22	Acrylamide gel, φ~1	4.33±0.10

Table 3.3. Comparing diffusive isotope fractionation of hydrogen sulphide with other mono-valent anions and cations.

Species	**Source**	**Material**	**Fractionation $(1-D_l/D_h)*1000$**	**T_estimated (ºC)**
Cl^-	Eggenkamp and Coleman, 2009	Acrylamide gel	1.28‰	2ºC
	Eggenkamp and Coleman, 2009	Acrylamide gel	1.66‰	21ºC
	Eggenkamp and Coleman, 2009	Acrylamide gel	1.65‰	54ºC
	Eggenkamp and Coleman, 2009	Acrylamide gel	1.92‰	80ºC
	Desaulnier et al., 1986	Ground water	1.2‰	5 ºC
	Beekman et al., 1992	Sediment	2.3‰	10 ºC
	Eggenkamp et al., 1994	Sediment	2.3‰	25 ºC
	Groen et al., 2000	Sediment	2.7‰	25 ºC
	Richter et al., 2006	Water	1.4‰	21 ºC
Br^-	Eggenkamp and Coleman, 2009	Acrylamide gel	0.98‰	2ºC
	Eggenkamp and Coleman, 2009	Acrylamide gel	0.64‰	21ºC
	Eggenkamp and Coleman, 2009	Acrylamide gel	0.78‰	80ºC
Li^+	Richter et al., 2006	Water	2.3‰	21 ºC
Na^+	Pikal, 1972	Water	2‰	21 ºC

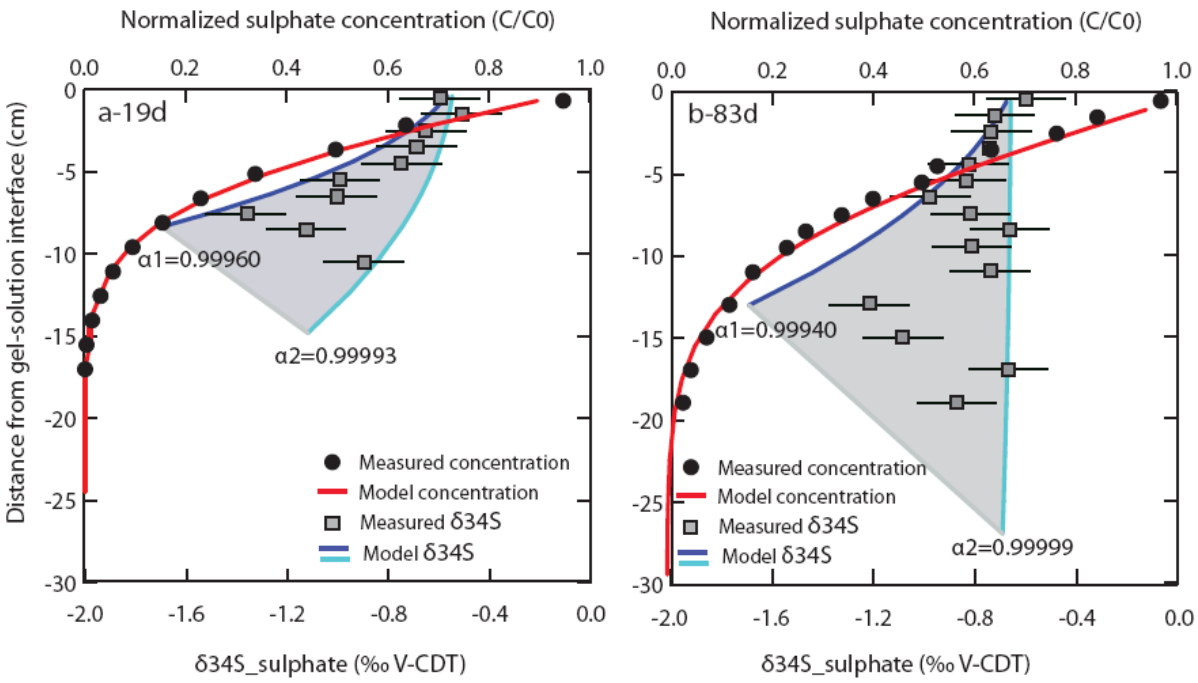

Fig. 3.1. Sulphate concentration profile (circle) and sulphate $\delta^{34}S$ profile (square) at room temperature – (a) 19-day experiment and (b) 83-day experiment, error bar 1σ=0.15‰

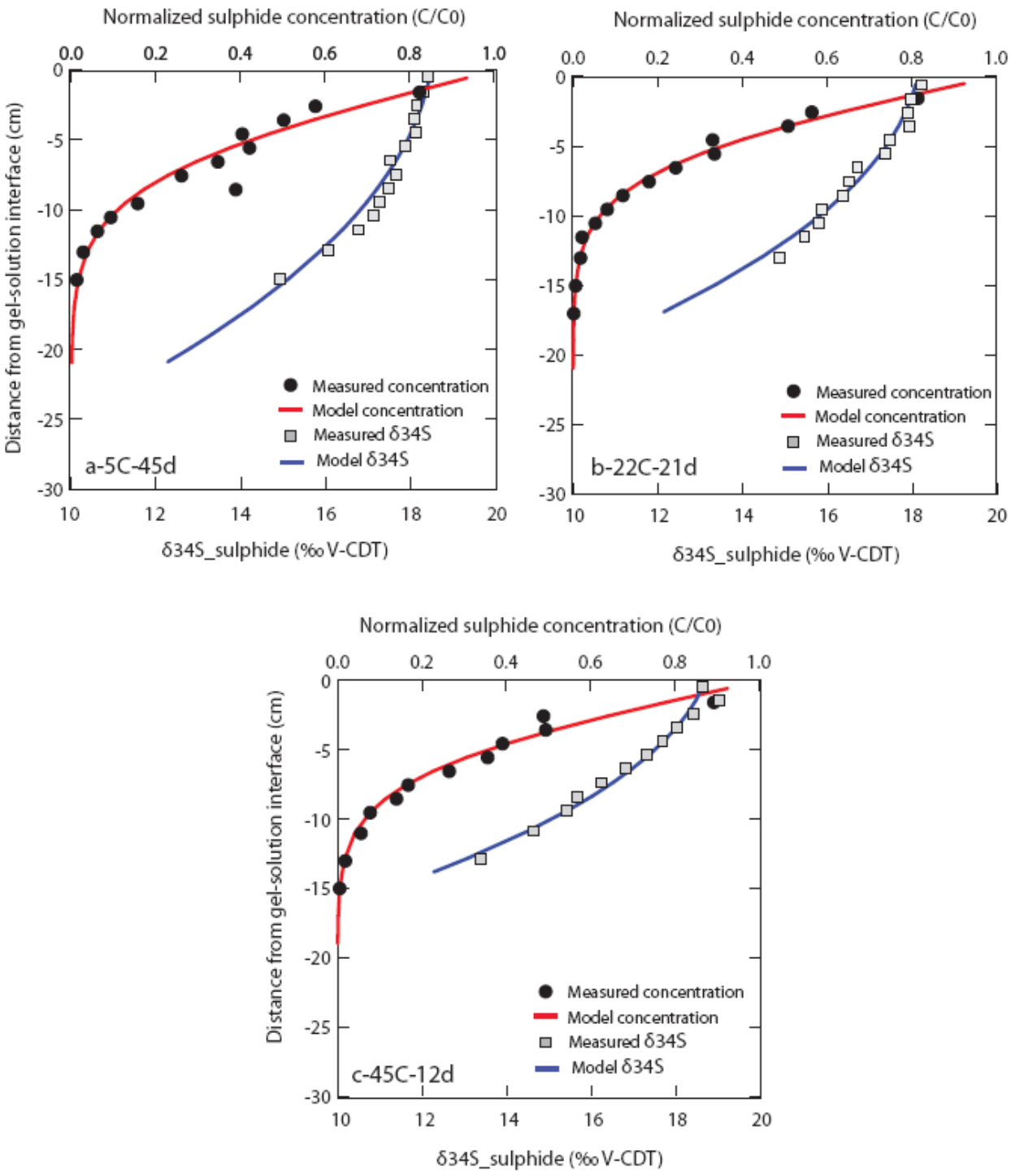

Fig.3.2. Sulphate concentration profile (circle) and sulphate $\delta^{34}S$ profile (square) at 5ºC (a), 22ºC (b) and 45°C (c)

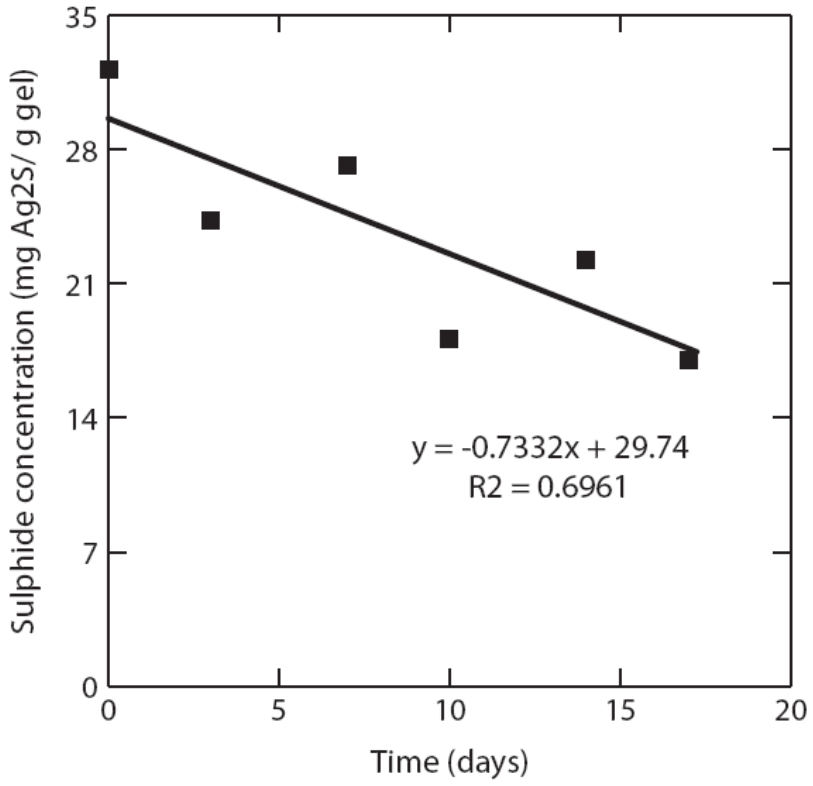

Fig. 3.3. Sulphide concentration decreases with storage time

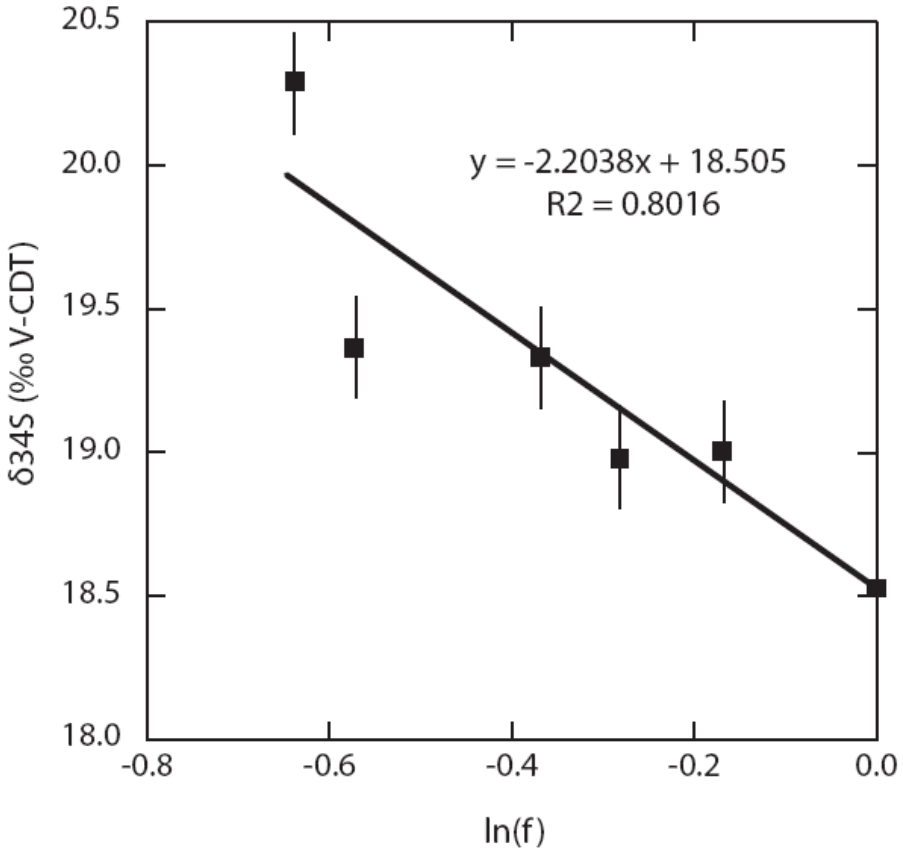

Fig. 3.4. The $\delta^{34}S$ value of sulphide decreases with the remaining fraction with 1σ error bar (0.15‰)

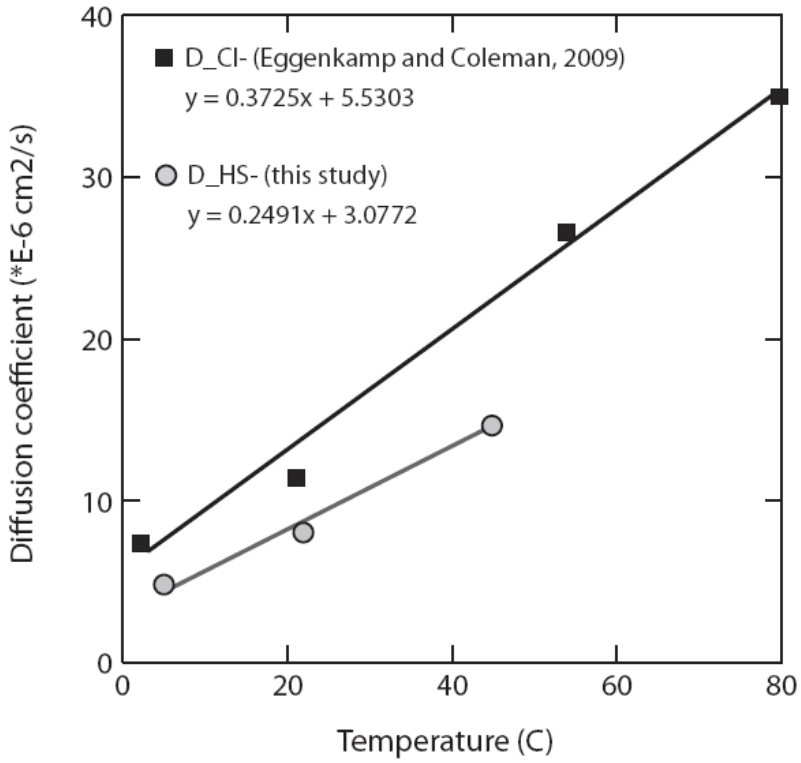

Fig. 3.5. Dependence of diffusion coefficient of ion HS^- (white circle) and Cl^- (black square) on temperature (1σ error bars in our study are smaller than symbols)

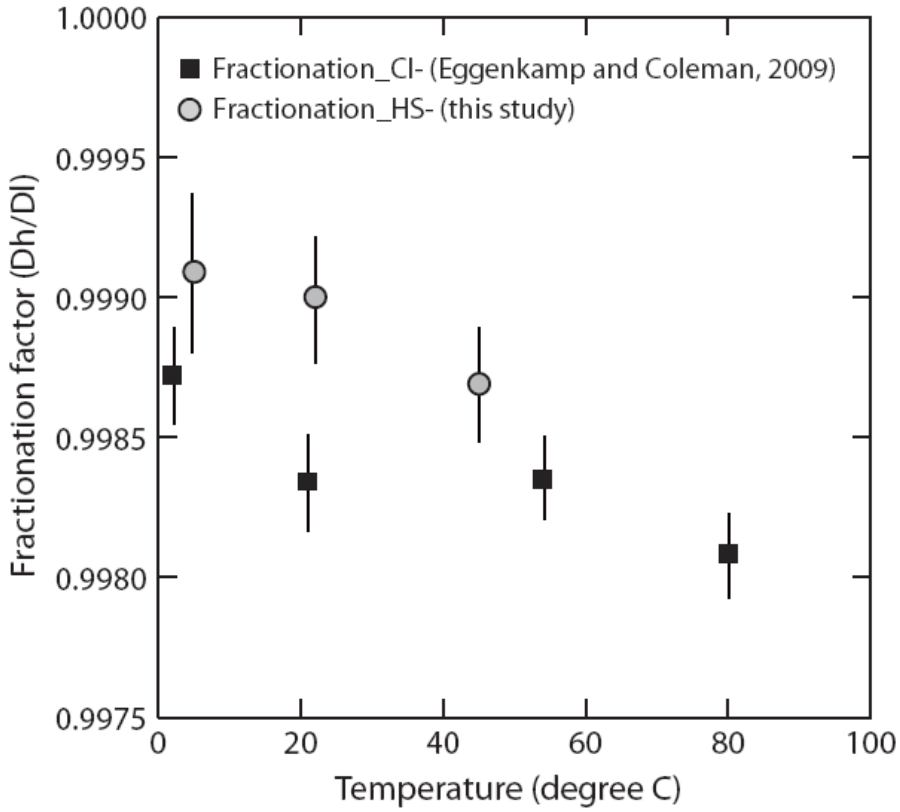

Fig. 3.6. Dependence of isotope fractionation of HS^- and Cl^- ions on temperature with 1σ error bars

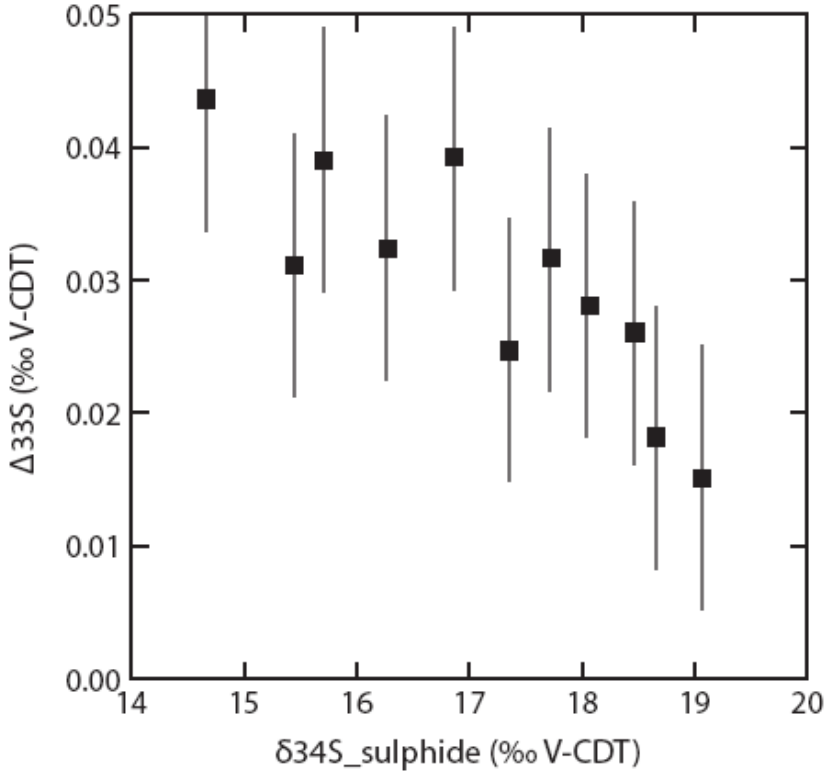

Fig. 3.7. $\Delta^{33}S - \delta^{34}S$ profile of sulphide diffusion experiment at 45ºC with 1σ error bar of $\Delta^{33}S$ (0.01%)

PREFACE TO CHAPTER 4

In chapters 2, we have highlighted the application of multiple sulphur isotopes to investigate the combination of different microbiological pathways in modern marine sediments. In chapter 3, we examined the effect of the transportation processes, in particular diffusion, on the isotope fractionation of ions. Sulphur in marine sediments is sourced from seawater sulphate. This source is stable because the concentration and isotope composition of seawater sulphate did not change significantly during last several tens of thousands of years. On the other hand, terrestrial sediments receive little sulphur from the water column because fresh water contains much less sulphate. Therefore, the enrichment of sulphur in terrestrial sediment indicates an abrupt input from either atmosphere or a sulphur-rich water source.

In chapter 4, we investigate the multiple sulphur isotope records of ancient terrestrial sediments collected in the Karoo Basin at the Permian-Triassic boundary (~252 Ma). Previous studies have shown an enrichment of sulphur content in this period and have proposed a link between this observation and the concurrent mass extinction (Maruoka et al., 2003). Yet the implications remain speculative. Multiple sulphur isotope data of the enriched sulphur may reveal the sources of this sulphur. Based on our results, we propose the cause as well as mechanism of the extinction event at Permian-Triassic boundary.

Maruoka T., Koeberl C., Hancox P., and Reimold W. (2003) Sulphur geochemistry across a terrestrial Permian-Triassic boundary section in the Karoo basin, South Africa. *Earth and Planetary Science Letters* **206**, 101-117.

CHAPTER 4

Sulphur and carbon isotope records across the terrestrial Permian-Triassic (P-T) boundary

Thi Hao Bui and Boswell Wing

4.1 Abstract

A full picture of the end-Permian mass extinction remains incomplete because of the continuing debate about a satisfying cause and mechanism. Studies on marine and terrestrial P-T strata in the last few decades have shown a strongly disturbed carbon and sulphur cycle during the extinction event. In this work, we study carbon and sulphur isotope records across the terrestrial P-T boundary. We collected sedimentary rock samples and carbonate nodules along two sections of ~10 meters in two locations, Commando Drift Dam and Wapadsberg, in the Karoo Basin (South Africa). We determined the carbon and sulphur contents as well as the carbon and sulphur isotope signatures of those samples. The total carbon contents of sedimentary rocks at Commando Drift Dam were quite low, typically <<1 wt %, but they showed two peaks up to ≈4 wt % total carbon. Corresponding to these two peaks of total carbon content, we observed two peaks of sulphur contents at the same depths. Coincident with the first peak in carbon content, the $\delta^{13}C$ values of both sedimentary rocks and carbonate nodules show a negative shift of ~-3‰. The two sulphur peaks have $\delta^{34}S$ values that are significantly higher than background $\delta^{34}S$ values by ~5 ‰. Although only the first carbon peak is identified in our Wapadsberg section, it shows similar elemental and isotopic associations. We examined different possible mechanisms for heavy sulphur injections into the terrestrial aquatic system around the P-T boundary in the Karoo basin.

4.2 Introduction

The end-Permian mass extinction (~252.3Ma (Shen et al., 2011)) is known as the greatest biotic crisis in the Earth history with the loss of more than 90% of marine species and 70% of terrestrial vertebrate families (Erwin, 1994). This event is characterized by a prominent negative carbon isotope excursion with a general shift in $\delta^{13}C$ values of -3 to -5‰ that has been observed

worldwide in both marine and terrestrial sediments (Jinshi et al., 1984; Holser et al., 1987, 1989; Ward et al., 2005; Krull et al., 2000; Wit et al., 2002). Because the $\delta^{13}C$ excursion happened on a relatively short time scale, it is unlikely to be explained by changes in the mass balance between burial and reoxidized organic carbon (Korte and Kozur, 2010). Therefore, additional factors have been proposed to explain this observation, such as a bolide impact (Becker et al., 2001, 2004; Kaiho et al., 2001), oceanic anoxia (Wignall and Hallam, 1992; Kajiwara et al., 1994), massive methane release from the deep ocean (Krull et al., 2000), volcanism (Lo et al., 2002; Renne et al., 1995; Kamo et al., 2003) or some combination of above sources (Berner, 2002; Sephton et al., 2005).

The Meishan section in South China is the most thoroughly investigated marine P-T section in the world (Jin et al., 2000). In this section, both pyrite and carbonate-associated sulphate (CAS) are enriched at the P-T boundary (Riccardi et al., 2006). The CAS concentration increases from a background of ~1000 ppm to >5000 ppm and the pyrite sulphur weight percent increases ten times from less than 0.2% to 2%. Corresponding to this sulphur are sulphur isotope fluctuations of these two species (Riccardi et al., 2006). An earlier study on this location inferred an abrupt decrease in $\delta^{34}S$ of seawater sulphate coinciding with the extinction horizon (Kaiho et al., 2001). These isotope variations have been explained by the presence of euxinic deep water that overturned at the P-T boundary, bring isotopically depleted H_2S into the surface ocean (Riccardi et al., 2006; Kaiho et al., 2001).

Sulphur enrichments around the P-T boundary have also been observed in other marine sections. Total sulphur content is enriched in the rocks near the P-T boundary at the Chichibu and Sasayama sections, Japan and this enrichment is associated with heavier isotope composition (Kajiwara et al., 1994). Similar observations have been reported at the Siusi section (Italy) with total sulphur content increases from ~0.05% to 0.37% and the $\delta^{34}S$ of CAS increases at the extinction level depth (Newton et al., 2004). The co-variation of sulphur content and sulphur isotope in these locations has been attributed to the increase of oceanic anoxia, during which the activity of sulphate reducing microbial populations might be enhanced (Kajiwara et al., 1994; Newton et al., 2004).

The background total sulphur content in marine environments is quite high because of the abundance of marine sulphate. As a result, volcanism and bolide impacts can only provide

enough sulphur to slightly perturb sulphur isotope signatures (Kaiho et al., 2006). In contrast, the low sulphur abundance in terrestrial aqueous environments makes them a sensitive recorder of any sulphur additions with distinct isotope compositions. Therefore, in this study, we analyze carbon and sulphur content as well as carbon and sulphur isotope compositions in two terrestrial P-T strata in southern Karoo Basin.

Among terrestrial P-T sites, Karoo Basin of South Africa appears to be the ideal location to study terrestrial P-T geochemistry because it exposes a complete succession of Upper Permian to Lower Triassic strata (Ward et al., 2005). At Senekal section in the northern Karoo, a sulphide enrichment at the P-T boundary has been reported (Maruoka et al., 2003). The enhanced accumulation of sulphide was interpreted as the result of the sulphate enrichment in the basin waters, largely because the ratios of organic carbon to sulphide resembled those of marine sections. Here we build on this work and use carbon isotopes to correlate our stratigraphic variations with those from previous studies. Sulphur contents are measured to indicate possible periods of sulphur enrichment and multiple sulphur isotopes are measured to give unique clues about possible sulphur sources.

4.3 Methodology

Samples were collected from two locations in Karoo Basin, Commando Drift Dam (CDD) and Wapadsberg (WP) (Fig. 4.1). The CDD sample set includes 27 sedimentary rock samples at average resolution of 35 cm and 9 carbonate nodules along a ~10 meter vertical section. The magnetostratigraphy of this section has been well constrained (De Kock and Kirschvink, 2003). The WP sample set includes 42 sedimentary rock samples along a section of ~9 meters. No carbonate nodules were collected. Elemental geochemistry and mineralogy of the Wapadsburg samples were investigated in previous study (Coney et al., 2007). Sedimentary rock samples and carbonate nodules were ground to fine powder for the analyses reported here.

Total carbon and total sulphur contents of these samples were analyzed with an Eltra CS-800 in the Stable Isotope Lab at McGill. The instrument has a detection limit of ~0.05% for both carbon and sulphur. Reproducibility calculated from triplicate measurements was less than 7%.

To measure the organic C isotopes of sedimentary rocks, we weighted 1 to 2 grams of powder samples in clean glass tubes. About 5 mL of HCl 1N was added to convert carbonates into CO_2. Samples were left overnight before centrifuging and pouring out the liquid. This acidifying step was repeated until all carbonates were removed. Samples then were rinsed > 4 times with Milli-Q water to remove the excess acid. Sample powders were dried in oven at 70°C. Dry samples were ground again to homogenize and were weighed in tin cups. Carbon isotope measurements were performed with a Carlo Erba NC 1500™ elemental analyzer coupled to a Micromass Isoprime™ mass spectrometer in continuous-flow mode at GEOTOP, University of Québec at Montréal. Based on the inorganic carbon content of carbonate nodules, precise amounts of carbonate samples were weighted in glass cups. Samples were acidified with 100% orthophosphoric acid under vacuum. Carbonates were converted into gaseous CO_2. These CO_2 were purified and were then transferred to a VG-Prism™ triple-collector mass spectrometer for carbon isotope measurements. The $\delta^{13}C$ values of carbonate and organic C are reported relative to the Vienna Pee Dee Belemnite (V-PDB) with analytical error of ±0.1‰ and reproducibility better than ±0.04‰.

Because the amounts of WP samples are small, we could only extract bulk sulphur with the Kiba reagent (Kiba et al., 1955) while sulphur in CDD samples was extracted in bulk form (with Kiba reagent) or in a sequential fashion. To extract multiple sulphur pools of CDD samples, about 30 grams of rock powders were weighed in 150 mL glass beakers. One hundred mL of Milli Q water was added in each beaker and samples were shaken for 1-2 days. Samples then were centrifuged. The liquids were filtered with 0.45 μm filter paper. This water leaching step was repeated 2 times. The water solutions were condensed and acidified with HCl (0.5N) to pH~3 to remove dissolved carbonates and bicarbonates. A few drops of $BaCl_2$ solution (10% w/w) were added to precipitate the water-leachable sulphates as $BaSO_4$. The remaining powders were dried and were ground for sulphide extraction with a boiling mixture of 6N HCl and Cr(II) reduction solution (Fossing and Jorgensen, 1989). The leftover residue was cooled down and filtered to separate liquid and solid components. Sulphur from sulphates in the residual liquid phase ("acid-soluble" sulphates) or solid phase ("acid-insoluble" sulphate), as well as from the water-leachable sulphates, was extracted with Thode reagent (Thode et al., 1961). The H_2S gas produced from the extractions was trapped in 4% zinc acetate solution and then was converted into Ag_2S by the reaction with 0.1N $AgNO_3$. The Ag_2S precipitates were well rinsed with diluted

NH_4OH and Milli-Q water and were dried at 70°C for at least 24 hours. Approximately 3 mg of Ag_2S were weighted into clean Al foil pouches. They then were dropped into Ni bombs and reacted with excess F_2 at 225°C overnight to form SF_6 gas. The SF_6 was purified by cryogenic separation and gas chromatography. Sulphur isotopes were measured with a Finnigan MAT 253 in dual inlet mode in the McGill Stable Isotope Lab. The sulphur isotope compositions are reported relative to Vienna Canyon Diablo Troilite (V-CDT) as:

$$\delta^{3x}S = \left(\frac{R^{3x}_{Sample}}{R^{3x}_{V-CDT}} - 1\right) \times 1000,$$

where 3x is 33, 34 or 36, and

$$\Delta^{33}S = \delta^{33}S - \left[\left(1 + \frac{\delta^{34}S}{1000}\right)^{0.515} - 1\right] \times 1000$$

The 2σ uncertainty of $\delta^{34}S$ values is 0.1‰ and of $\Delta^{33}S$ values is 0.015‰ based on repeated analyses of standard materials.

4.4 Results

4.4.1 Permian-Triassic boundary

Magnetostratigraphic records are commonly used to correlate the stratigraphy of different sections in the Karoo basin (Ward et al., 2005; De Kock and Kirschvink, 2003). Here, we use carbon isotope signatures of carbonates and organic carbon to relate our sections to others from previous studies. We use the lithological transition of green-grey mudstone to red-brown mudstone as a zero depth datum. This transition has been interpreted as the paleontological P-T boundary (Coney et al., 2007), as well as the boundary between Permian and Triassic strata located below the main extinction level in the Karoo basin (DeKock and Kirschvink, 2003). Because of these conflicting interpretations, we do not attribute any relationship between this lithological change and extinction dynamics.

4.4.2 Carbon and sulphur content

Background carbon and sulphur contents in both CCD and WP are normally lower than the detection limit of our measurements (Fig. 4.2a,d; Fig. 4.3a,c). In the CCD section, there are

two enrichments of total carbon content. The first enrichment is right at the depth of the lithological transition (Fig. 4.2a). Here the total carbon content is 4.5 wt %, which is ~10-fold higher than background levels. Corresponding to this enrichment of total carbon, we also observe a peak of total sulphur content (Fig. 4.2d). Our analysis of different sulphur pools shows that most of sulphur is in the form of acid insoluble sulphate (98.8%; Fig. 4.4d). The second carbon enrichment is at 3.5 meters above the transition (Fig. 4.2a). Associated with it is a small peak in sulphur content (Fig. 4.2d) with 82.4% of total sulphur in the form of acid-insoluble sulphate (Fig. 4.4d).

In WP section, we also observe an enrichment of total carbon content at depth zero with similar magnitude as in CCD (Fig. 4.3a). However, the sulphur content peak is nearly 10 times smaller than sulphur peak in CDD section (0.08% versus 0.6%) (Fig. 4.3c).

4.4.3 Carbon isotopes

The $\delta^{13}C$ values of the CDD samples have an average of -25‰. At depth zero, the $\delta^{13}C$ values are at their maximum value (-23‰) before shifting down to their minimum value (-26.5‰). After the -3.5‰ shift, the $\delta^{13}C$ profile quickly recovers its background level (Fig. 4.2b). Similar to organic carbon, inorganic carbon also shows a negative shift from -8.5‰ to -11.5‰ at depth zero (Fig. 4.2c). These negative carbon isotope excursions correspond to the peak of total carbon content. At +3.5 meters, where the second peak of total carbon content is, no $\delta^{13}C$ change in either organic or inorganic carbon is observed (Fig. 4.2b,c).

The organic carbon isotopes of WP samples show two distinct negative excursions. The $\delta^{13}C$ decreases from -22.5‰ to -25.5‰ right before the transition depth. It then recovers to the background level (-23‰) for a while before shifting again to -26.5‰ (Fig. 3b).

4.4.4 Sulphur isotopes

The bulk $\delta^{34}S$ values of CDD samples vary from +3.8‰ to +21.8‰ with the average of 13‰ (Fig. 4.2e). There are two $\delta^{34}S$ maximums corresponding to the two sulphur content peaks. At the first sulphur content peak (at depth zero), the bulk $\delta^{34}S$ value is +19.2‰ and at the second sulphur content peak (at depth +3.5 meters), the bulk $\delta^{34}S$ value is +21.8‰.

WP samples have background $\delta^{34}S$ values from ~ +2‰ to +9‰ with the highest $\delta^{34}S$ value at depth zero, corresponding to the sulphur content peak (Fig. 4.3). In general, bulk sulphur in WP samples is lighter than bulk sulphur in CDD samples (Fig. 4.5).

Almost all CDD samples contain small amounts of water-leachable sulphates and acid-soluble sulphates (Fig. 4.4a,c). The $\delta^{34}S$ values of water-leachable sulphates vary from +1.2‰ to 17.0‰ with the maximum at the transition depth. The $\delta^{34}S$ values of acid-soluble sulphates are in the same range as water-leached sulphates. Sulphides are rare and have significantly lower $\delta^{34}S$ values (from -7.3‰ to +6.6‰) than the rest of the pools (Fig. 4.4b). Similarly, acid-insoluble sulphates only appear in some samples above the depth zero, and occur in high proportion at the two peaks of total sulphur content (Fig. 4.4d). The $\delta^{34}S$ values of acid-insoluble sulphates are relatively higher than those of other sulphur pool, ranging from +10.2‰ to +21.3‰.

Multiple sulphur isotope signatures of bulk sulphur in CDD and WP sections do not completely overlap with each other. WP bulk sulphur in general has lower $\delta^{34}S$ and $\Delta^{33}S$ values compared to CDD bulk sulphur. Most WP samples are on negative $\Delta^{33}S$ side as well (Fig. 4.5).

4.5 Discussion

4.5.1 Carbon and sulphur enrichments

Carbon and sulphur enrichments were observed at the transition depth in both study sections, CDD and WP. A common explanation for these enrichments is volcanic activity because volcanic eruption will inject both carbon (as CO_2) and sulphur (as sulphate aerosol) into the atmosphere while atmospheric transport will bring them to sediments where they are captured in the form of carbonate and sulphate precipitates (Maruoka et al., 2003). However, carbon and sulphur may come from different sources. Marine incursions into a terrestrial basin can bring sulphate into the terrestrial environment during sea level fluctuations (Forney, 1975). Sulphide gas also can escape from euxinic water columns to the atmosphere, where wet and dry deposition might allow it to be preserved in terrestrial sedimentary systems (Kump et al., 2005). Alternatively, it has been proposed that sulphur can be ejected from the mantle by bolide impact (Kaiho et al., 2001). In a similar fashion, carbon enrichments in terrestrial sediment can be the

result of enhanced carbon release into the atmosphere by various mechanisms (e.g. Faure et al., 1995; Retallack and Jahren, 2008; Krull et al., 2000).

In addition to the main carbon and sulphur spikes at the transition depth, another less intense carbon and sulphur addition period was also observed at +3.5 meters in the CDD section. Similar to the first sulphur enrichment, the second sulphur enrichment is also associated with a peak in the $\delta^{34}S$ value of total sulphur. But the carbon isotope signature remains stable. These observations may suggest two different mechanisms for the two carbon and sulphur enrichment periods.

4.5.2 Correlation of the negative $\delta^{13}C$ excursion

The P-T boundary at marine sections has been characterized by a rapid, negative $\delta^{13}C$ excursion in both organic and inorganic samples (Magaritz et al., 1992; Wang et al., 1994). However, in non-marine sections, the relationship between $\delta^{13}C$ changes and the P-T boundary is not well established (MacLeod et al., 2000). In the Karoo Basin, the $\delta^{13}C$ excursion has been observed in organic and inorganic samples from Lootsberg and Carlton Heights (Ward et al., 2005). The absence of an organic $\delta^{13}C$ excursion in sections from Wapadsburg and Bethulie has been explained by the intrusion of Mesozoic dolerite dikes and sills, which have homogenized the original $\delta^{13}C$ record (Ward et al., 2005). Even though the Bethulie organic $\delta^{13}C$ record does not show any negative excursion, soil nodules in this site show a large shift of $\delta^{13}C$ at the extinction level (MacLeod et al., 2000). However, these negative carbonate nodule $\delta^{13}C$ values (~ -17‰) have been proposed to reflect calcite crystallization under poorly drained, swampy conditions rather than to provide a record of atmospheric $\delta^{13}C$ values (Tabor et al., 2007).

In our study, we observed the negative shift (-3.5‰) of both organic and inorganic $\delta^{13}C$ right at the transition depth in CDD section. The negative $\delta^{13}C$ excursion of organic carbon in WP section is the same magnitude with CDD section (-3.5‰) even though the shift is less sharp. We were probably able to identify this shift at WP, in spite of the igneous intrusions there, because we determined the variation of carbon isotopes at a much finer scale (~0.1 meters) compared to previous studies (e.g. Ward et al., 2005; MacLeod et al., 2000). Despite this difference in resolution, it appears that the most straightforward interpretation of our profiles is that we have located the carbon isotope anomalies that are linked to the initiation of protracted terrestrial extinctions in the Karoo basin (Ward et al., 2005). Although the C isotope excursion

associated with the marine extinction interval was abrupt and brief, occurring over less than ~60 ka, about 500 ka of carbon cycle instability followed this period (Burgess et al., 2013). Linking our sections to the marine extinction interval, therefore, remains problematic.

4.5.3 Potential sulphur sources

4.5.3.1 Mantle sulphur

Sulphur enrichment across the P-T boundary has also been proposed to result from mantle S ejection due to a bolide impact (Kaiho et al., 2001). Mantle S has a $\delta^{34}S$ value that is near zero (Sakai et al., 1984) to slightly less than zero (Labidi et al., 2013). This sulphur is isotopically lighter than the background $\delta^{34}S$ values in the CDD and WP sections. Barring a complicated scenario of oxidation, microbial sulphate reduction, and isotopic enrichment of the residual sulphate, mantle S is unlikely to be the source of the isotopically heavy sulphur in the Karoo sediments.

4.5.3.2 Volcanic sulphur

Another possible source of sulphur enrichment in Karoo basin is from volcanic activity. The temporal coincidence between the massive Siberian Trap basaltic eruptions and the P-T extinctions has led to detailed investigations of the cause-effect relationship between the two events (Kamo et al., 2003; Campbell et al., 1992; Renne et al., 1991; Jin et al., 2000). Detailed studies on Siberian Traps have suggested that the eruption released huge amount of S, Cl and F into the atmosphere over relatively short time period (Campbell et al., 1992; Kamo et al., 2003; Black et al., 2012).

The SO_2 released from the Siberian Traps might come from two sources: (1) degassing from the flood basalts themselves or from the Ni-Cu-PGE sulphide ore deposits hosted by the flood basalts (Naldrett et al., 1992), and (2) fluid-driven dissolution and volatilization of Devonian and Carboniferous anhydrite in the wall rocks of the Traps (Campbell et al., 1992). The sulphide ores are enriched in heavy sulphur isotopes, with the maximum $\delta^{34}S$ values of sulphide minerals in the range of 10 to 14‰ (Ripley et al., 2010). These sulphides coexist with magmatic anhydrite that has $\delta^{34}S$ values of ~19-23 ‰ (Ripley et al, 2010). Devonian evaporites like those found in the wall rocks of the traps have $\delta^{34}S$ values that typically vary from +19.0‰

to +26.5‰ (Wu et al., 2010) with a minimum of +15.0‰ and a maximum of +34.0‰ in the global evaporite dataset (Claypool et al., 1980).

At CDD, the first sulphur enrichment (at the transition depth) has a bulk $\delta^{34}S$ value of +19.2‰. The great disparity in the sulphur content of this peak and the background profile means that the sulphur added to the CDD system had approximately this $\delta^{34}S$. Although the weaker sulphur enrichment at ~3.5 meters above the transition depth in the CDD section makes a similar linkage less strong there, the second sulphur enrichment does have a $\delta^{34}S$ value of +21.8‰. These values are in the range of $\delta^{34}S$ values of Devonian evaporites and magmatic anhydrite from the Siberian Traps. However, the $\Delta^{33}S$ values of CDD samples are higher than those reported from Devonian evaporites $\Delta^{33}S$ (0.022‰ - 0.042‰ compared to 0.000‰ – 0.007‰). In addition, recent modeling of global climate and atmospheric chemistry suggests that the very little volcanic input from the Siberian Traps was transported to the Southern Hemisphere at PT times, because of efficient sedimentation in the Northern Hemisphere as well as limited interhemispheric atmospheric circulation (Black et al., 2013). Finally, transport and chemistry of S-bearing atmospheric species is isotopically selective (Castleman et al., 1974; Harris et al., 2013). It would seem to be a fortuitous coincidence if the isotopic consequences of atmospheric processing led to S deposition with the same isotope composition as the sulphur that was originally input into the atmosphere.

4.5.3.3 Marine sulphate

Seawater is rich in dissolved sulphate while terrestrial aquatic systems contain much less sulphate (>100-fold less). Marine incursions into a terrestrial aquatic system will add a significant amount of sulphur into the terrestrial sediments as a result. If the sulphur enrichment observed in Karoo Basin originates from a seawater source, the sulphur isotopes of this enriched sulphur must reflect the isotope composition of marine sulphate. The $\delta^{34}S$ value of bulk sulphur at the first sulphur enrichment period is 19.2±0.10‰ and the $\Delta^{33}S$ value is 0.042±0.015‰. This isotope composition is comparable to the estimated multiple sulphur isotope composition of marine sulphate at 250 Ma ($\delta^{34}S$ = 19.2‰ and $\Delta^{33}S$ = 0.022‰) (Wu et al., 2010).

From our analysis of individual sulphur pools, it turns out that most of sulphur enrichment is in the form of mineral sulphates that are insoluble in hydrochloric acid 6N (Fig. 4.4). The acid-insoluble sulphate has isotopic characteristics that are extremely similar to those

inferred for seawater sulphate at 250 Ma with $\delta^{34}S$ = 18.15‰ and $\Delta^{33}S$ = 0.023‰. A potential difficulty with a marine sulphate source for the sulphur enrichment we have identified here is that the deposition in the Karoo Basin at this time was distinctly non-marine (Hancox, 2000). It is unclear therefore whether a direct marine incursion would have been possible to account for the addition of sulphate with a seawater sulphur isotope signal in this retro-foreland basin.

4.5.3.4 Volatilization of aqueous H_2S

Chemocline upward excursions have been proposed as a kill mechanism to explain the end-Permian extinction event (Kump et al., 2005). This mechanism provides a link between marine and terrestrial extinctions through the effect of sulphide toxicity in aqueous environments (Bagarinao, 1992) and the impact of accumulated atmospheric H_2S on the ozone shield (Visscher et al., 2004). Biomarker studies of marine P-T sections have suggested that photic-zone euxinia was common in marine environments around the time of the P-T boundary (Grice et al., 2005; Cao et al., 2009), suggesting that H_2S-charged seawater was present at this time.

While the other sulphate pools in the CDD section have isotope compositions that correlate positively with the dominant acid-insoluble sulphate pool (Figs. 4.6, 4.7), the sulphide in this section has extremely negative $\Delta^{33}S$ values compared to the sulphate pools (Fig. 4.7). In addition, this sulphide is a rare component of the CDD section, present only right at the sulphur enrichment layer and a few meters above (Fig. 4.4). Calculations of the exponent that relates the $\Delta^{33}S$–$\delta^{34}S$ values of the average sulphides and sulphates ($\delta^{34}S_{sulphide}$ = -5‰, $\Delta^{33}S_{sulphide}$ = -0.08‰, $\delta^{34}S_{sulphate}$ = 15‰, $\Delta^{33}S_{sulphate}$ = 0.03‰) is 0.522, which is far too high to be produced by a combination of microbial sulphate reduction and microbial S disproportionation for a difference in $\delta^{34}S$ values of ~20‰ (Chapter 2).

However, the negative $\Delta^{33}S$ values that characterize the CDD sulphide can result from isotope mixing processes (Shen et al., 2011). We demonstrate this with an illustrative model that takes, as one end member, sulphide with an isotope composition that is equal to that of the sulphate in the CDD section (Fig. 4.7). Sulphide with this composition may have originated during diagenetic sulphide production in the sulphate-poor CDD sedimentary environment sometime after sedimentary deposition. We consider two other possible end-member sulphide compositions: (1) the average sulphide in a global compilation of P-T marine sediments ($\delta^{34}S \approx$ -25.6‰, $\Delta^{33}S \approx 0.087$; Wu et al., 2010) and (2) an end member with an extremely negative $\delta^{34}S$

value and a $\Delta^{33}S$ value that is near zero ($\delta^{34}S \approx -55‰$, $\Delta^{33}S \approx 0.00$). The latter end member resembles the extremely low $\delta^{34}S$ sulphide found in some P-T marine sediments with evidence of photic-zone euxinia (Grice et al., 2005), and takes on a $\Delta^{33}S$ value that is consistent with recent evidence of thermodynamic fractionation by microbial sulphate reducers once $\delta^{34}S_{sulphate}$ - $\delta^{34}S_{sulphide} \approx 75$ ‰ (Canfield et al., 2010; Sim et al., 2011). Mixing of these end members with the proposed diagenetic sulphide in proportions of ~25-50% can reproduce the isotopic characteristics of the CDD sulphides (Fig. 4.7). Atmospheric injections of sulphide through the proposed chemocline upward excursions apparently can explain the $\delta^{34}S$ and $\Delta^{33}S$ values of the CDD sulphides. If these injections were driven by the oceanic versions of limnic eruptions (Zhang and Kling, 2006), it is not inconceivable that concurrent enrichments in sulphate with a marine sulphate isotope composition (Figs. 4.4, 4.7) as well as carbonate carbon with anomalously low $\delta^{13}C$ values (Knoll et al., 1996) might also occur.

4.6 Conclusions

We observed the carbon and sulphur enrichment period at the transition depth from green-grey mudstone to red-brown mudstone in both studied sections, CDD and WP. Organic and inorganic carbon isotope excursions at this depth allow us to correlate the carbon and sulphur enrichment period to have been likely to occur within the 500 ka period of C-cycle instability after the P-T extinction event (Burgess et al., 2013). We have considered four different sulphur sources that might inject sulphur into the Karoo sediments. A marine source for both sulphate and sulphide provides support for a common injection mechanism associated with oceanic gas-driven eruptions.

4.7 References

Bagarinao T. (1992) Sulphide as an environmental factor and toxicant: tolerance and adaptations in aquatic organisms. *Aquatic Toxicology* **24**, 21-62.

Becker L., Poreda R. J., Hunt A. G., Bunch T. E., and Rampino M. (2001) Impact event at the Permian-Triassic boundary: Evidence from extraterrestrial noble gases in fullerenes. *Science* **291**, 1530-1533.

Becker L., Poreda R. J., Basu A. R., Pope K. O., Harrison T. M., Nicholson C., and Lasky R. (2004) Bedout: A possible end-Permian impact crater offshore of northwestern Australia. *Science* **304**, 1469-1476.

Berner R. A. (2002) Examination of hypotheses for the Permo-Triassic boundary extinction by carbon cycle modelling. *Proceedings of National Academy of Sciences* **99**, 4172-4177.

Black B. A., Elkins-Tanton L. T., Rowe M. C., and Peate I. U. (2012) Magnitude and consequences of volatile release from the Siberian Traps. *Earth and Planetary Science Letters* **317-318**, 363-373.

Black B. A., Lamarque J. F., Shields C. A., Elkins-Tanton L. T., and Kiehl J. T. (2013) Acid rain and ozone depletion from pulsed Siberian Traps magmatism. *Geology* **42**, 67-70.

Burgess S. D., Bowring S., and Shen S. Z. (2013) High-precision timeline for Earth's most severe extinction. *Proceedings of the National Academy of Sciences of the United States of America* **111**,

Campbell I. H., Czamanske G. K., Fedorenko V. A., Hill R. I., and Stepanov V. (1992) Synchronism of the Siberian Traps and the Permian-Triassic boundary. *Science* **258**, 1760-1763.

Canfield D. E., Farquhar J., and Zerkle A. L. (2010) High isotope fractionations during sulfate reduction in a low-sulfate euxinic ocean analog. *Geology* **38**, 415-418.

Cao C., Love G. D., Hays L. E., Wang W., Shen S., and Summons R. E. (2009) Biogeochemical evidence for euxinic oceans and ecological disturbance presaging the end-Permian mass extinction event. *Earth and Planetary Science Letters* **281**, 188-201.

Castleman A. W., Munkelwitz H. R., and Manowitz B. (1974) Isotopic studies of the sulfur component of the stratospheric aerosol layer. *Tellus* **26**, 222-234.

Chaussidon M., Albarede F., and Sheppard S. M. F. (1989) Sulphur isotope variations in the mantle from ion microprobe analyses of micro-sulphide inclusions. *Earth and Planetary Science Letters* **92**, 144-156.

Coney L., Reimold W. U., Hancox P. J., Mader D., Koeberl C., McDonald l., Struck U., Vajda V., and Kamo S. L. (2007) Geochemical and mineralogical investigation of the Permian-Triassic boundary in the continental realm of the southern Karoo basin, South Africa. *Palaeoworld* **16**, 67-104.

De Kock M. O. and Kirschvink J. L. (2003) Paleomagnetic constraints on the Permian-Triassic boundary in terrestrial strata of the Karoo Supergroup, South Africa: Implications for the causes of the end-Permian extinction event. *Gondwana Research* **7**, 175-183.

de Wit M. J., Ghosh J. G., de Villiers S., Rakotosolofo N., Alexander J., Tripathi A., and Looy C. (2002) Multiple organic carbon isotope reversals across the Permo-Triassic boundary of terrestrial Gondwana sequences: Clues to extinction patterns and delay ecosystem recovery. *The Journal of Geology* **110**, 227-240.

Erwin D. H. (1994) The Permo-Triassic extinction. *Nature* **367**, 231-236.

Farley K. A. and Mukhopadhyay S. (2001) An extraterrestrial impact at the Permian-Triassic boundary? *Science* **293**, 2343.

Faure K., de Wit M. J., and Willis J. P. (1995) Late Permian global coal hiatus linked to ^{13}C-depleted CO_2 flux into the atmosphere during the final consolidation of Pangea. *Geology* **23**, 507-510.

Forney G. G. (1975) Permo-Triassic sea-level change. *The Journal of Geology* **83**, 773-779.

Fossing H. and Jorgensen B. B. (1989) Measurement of bacterial sulphate reduction in sediments: Evaluation of a single-step chromium reduction method. *Biogeochemistry* **8**, 205-222.

Grice K., Cao C., Love G. D., Bottcher M. E., Twitchett R. J., Grosjean E., Summons R. E., Turgeon S. C., Dunning W., and Jin Y. (2005) Photic zone euxinia during the Permian-Triassic superanoxic event. *Science* **307**, 706-709.

Hancox P. (2000) The continental Triassic of South Africa. *Zbl. Geol. Palaont. Teil I*, 1285-1324.

HarrisE., Sinha B., Pinxteren D. v., Tilgner A., Fomba K. W., Schneider J., Roth A., Gnauk T., Fahlbusch B., Mertes S., Lee T., Collett J., Foley S., Borrmann S., Hoppe P., Hermann H. (2013) Enhanced role of transition metal ion catalysis during in-cloud oxidation of SO_2. *Science* **340**, 727-730.

Holser W. T. and Magaritz M. (1987) Events near the Permian-Triassic boundary. *Modern Geology* **11**, 155-180.

Holser W. T., Schonlaub H. P., JR M. A., Boeckelmann K., Klein P., Magaritz M., Orth C. J., Fenninger A., Jenny C., Kralik M., Mauritsch H., Pak E., Schramm J. M., Stattegger K.,

and Schmoller R. (1989) A unique geochemical record at the Permian/Triassic boundary. *Nature* **337**, 39-44.

Jin Y. G., Wang T., Wang W., Shang Q. H., Cao C. Q., and Erwin D. H. (2000) Pattern of marine mass extinction near the Permian-Triassic boundary in south China. *Science* **289**, 432-436.

Jinshi C., Maorong S., Weiguo H., and Yuyuan Y. (1984) Carbon isotope of carbonate strata at Permian-Triassic boundary in Changxing, Zhejiang. *Scientia Geologica Sinica* **19**, 88-93.

Kajiwara Y., Yamakita S., Ishida K., Ishiga H., and Imai A. (1994) Development of a largely anoxic stratified ocean and its temporary massive mixing at the Permian/Triassic boundary supported by the sulphur isotopic record. *Palaeogeography, Palaeoclimatology, Palaeoecology* **111**, 367-379.

Kaiho K., Kajiwara Y., Nakano T., Miura Y., Kawahata H., Tazaki K., Ueshima M., Chen Z., and Shi G. R. (2001) End-Permian catastrophe by a bolide impact: Evidence of a gigantic release of sulphur from the mantle. *Geology* **29**, 815-818.

Kaiho K., Kajiwara Y., Chen Z. Q., and Gorjan P. (2006) A sulphur isotope event at the end of the Permian. *Chemical Geology* **235**, 33-47.

Kajiwara Y., Yamakita S., Ishiga H., and Imai A. (1994) Development of a large anoxic stratified ocean and its temporary massive mixing at the Permian/Triassic boundary supported by the sulphur isotopic record. *Palaeogeography, Palaeoclimatology, Palaeoecology* **111**, 367-379.

Kamo S. L., Czamanske G. K., Amelin Y., Fedorenko V. A., Davis D. W., and trofimov V. R. (2003) Rapid eruption of Siberian flood-volcanic rocks and evidence for coincidence with the Permian-Triassic boundary and mass extinction at 251 Ma. *Earth and Planetary Science Letters* **214**, 75-91.

Kiba T., Takagi T., Yoshimura Y., and Kishi I. (1955) Tin (II)-strong phosphoric acid. A new reagent for the determination of sulphate by reduction to hydrogen sulphide. *Bulletin of the chemical society of Japan* **28**, 641-644.

Korte C. and Kozur H. W. (2010) Carbon isotope stratigraphy across the Permian-Triassic boundary: A review. *Journal of Asiantic Earth Sciences* **39**, 215-235.

Krull E. S. and Retallack G. J. (2000) $\delta^{13}C$ depth profiles from paleosols across the Permian-Triassic boundary: Evidence for methane release. *Geological Society of America Bulletin* **112**, 1459-1472.

Kump L. R., Pavlov A., and Arthur M. A. (2005) Massive release of hydrogen sulphide to the surface ocean and atmosphere during intervals of oceanic anoxia. *Geology* **33**, 397-400.

Lo C. H., Chung S. L., Lee T. Y., Wu G. (2002) Age of Emeishan flood magmatism and relations to Permian-Triassic boundary events. *Earth and Planetary Science Letters* **198**, 449-458.

MacLeod K. G., Smith R. M. H., Koch P. L., and Ward P. D. (2000) Timing of mammal-like reptile extinctions across the Permian-Triassic boundary in South Africa. *Geology* **28**, 227-230.

Magaritz M., Krishnamurthy, R. V., and Holser W. T. (1992) Parallel trends in organic and inorganic carbon isotopes across the Permian/Triassic boundary. *American Journal of Science* **292**, 727-739.

Maruoka T., Koeberl C., Hancox P., and Reimold W. (2003) Sulphur geochemistry across a terrestrial Permian-Triassic boundary section in the Karoo basin, South Africa. *Earth and Planetary Science Letters* **206**, 101-117.

Morante R. (1996) Permian and early Triassic isotopic records of carbon and strontium in Australia and a scenario of events about the Permian-Triassic boundary. *Historical Biology: An international Journal of Paleobiology* **11**, 289-310.

Naldrett A. J., Lightfoot P., Fedorenko V., Doherty W., and Gorbachev N. (1992) Geology and geochemistry of intrusions and flood basalts of the Noril'sk region, USSR, with implications for the origin of the Ni-Cu-ores. *Economic Geology* **87**, 975-1004.

Newton R. J., Pevitt E. L., Wignall P. B., and Bottell S. H. (2004) Large shifts in the isotopic composition of seawater sulphate across the Permo-Triassic boundary in northern Italy. *Earth and Planetary Science Letters* **218**, 331-345.

Renne P. R. and Basu A. R. (1991) Rapid eruption of the Siberian Traps flood basalts at the Permo-Triassic boundary. *Science* **253**, 176-179.

Renne P. R., Black M. T., Zichao Z., Richards M. A., and Basu A. R. (1995) Synchrony and causal relations between Permian-Triassic boundary crises and Siberian flood volcanism. *Science* **269**, 1413-1416.

Retallack G. J. and Jahren A. H. (2008) Methane release from igneous intrusion of coal during Late Permian extinction events. *The Journal of Geology* **116**, 1-20.

Retallack G. K., Seyedolali A., Krull E. S., Holser W. T., Ambers C. P., and Kyte F. T. (1998) Search for evidence of impact at the Permian-Triassic boundary in Antarctica and Australia. *Geology* **26**, 979-982.

Retallack G. J., Metzger C. A., Greaver T., Jahren A. H., Smith R. M. H., and Sheldon N. D. (2006) Middle-late Permian mass extinction on land. *Geological Society of America Bulletin* **118**, 1398-1411.

Riccardi A. L., Arthur M. A., and Kump L. R. (2006) Sulphur isotopic evidence for chemocline upward excursions during the end-Permian mass extinction. *Geochimica et Cosmochimica Acta* **70**, 5740-5752.

Sephton M. A., Looy C. V., Brinkhuis H., Wignall P. B., de Leeuw J. W., and Visscher H. (2005) Catastrophic soil erosion during the end-Permian biotic crisis. *Geology* **33**, 941-944.

Shen S. Z., Crowley J. L., Wang Y., Bowring S. A., Erwin D. H., Sadler P. M., Cao C. Q., Rothman D. H., Henderson C. M., Ramezini J., Zhang H., Shen Y., Wang X. D., Wang W., Mu L., Li W. Z., Tang Y. G., Liu X. L., Liu L. J., Zeng Y., Jiang Y. F., and Jin Y. G. (2011) Calibrating the end-Permian mass extinction. *Science* **334**, 1367-1372.

Sim M. S., Bosak T., and Ono S. (2011) Large sulfur isotope fractionation does not require disproportionation. *Science* **333**, 74-77.

Tabor N. J., Montanez I. P., Steiner M. B., and Schwindt D. (2007) $\delta^{13}C$ values of carbonate nodules across the Permian-Triassic boundary in the Karoo supergroup (South Africa) reflect a stinking sulphurous swamp, not atmospheric CO_2. *Palaeogeography, Palaeoclimatologu, Palaeoecology* **252**, 370-381.

Thackery J. F., Van Der Merwe N. J., Lee-Thorp J. A., Sillen A., Lanham J. L., Smoth R., Keyser A., and Monteiro P. M. S. (1990) Changes in carbon isotope ratios in the late Permian recorded in therapsid tooth apatite. *Nature* **347**, 751-753.

Thode H. G., Monster J., and Dunford H. B. (1961) Sulphur isotope geochemistry. *Geochimica et Cosmochimica Acta* **25**, 159-174.

Visscher H., Looy C. V., Collinson M. E., Brinkhuis H., Cittert J. H. A. v. K., Kurschner W. M., and Sephton II M. A. (2004) Environmental mutagenesis during the end-Permian

ecological crisis. *Proceedings of the National Academy of Sciences of the United States of America* **101**, 12952-12956.

Wang K., Geldsetzer H. H. J., and Krouse H. R. (1994) Permian-Triassic extinction: Organic $\delta^{13}C$ evidence from British Columbia, Canada. *Geology* **22**, 580-584.

Ward P. D., Botha J., Buick R., DeKock M. O., Erwin D. H., Garrison G. H., Kirschvink J. L., and Smith R. (2005) Abrupt and gradual extinction among Late Permian land vertebrates in Karoo basin, South Africa. *Science* **307**, 709-713.

Wignall P. and Hallam A. (1992) Anixia as a cause of the Permian/Triassic mass extinction: facies evidence from northern Italy and the western United States. *Palaeogeography, Palaeoclimatology, Palaeoecology* **93**, 21-46.

Wu N., Farquahar J., Strauss H., Kim S. T., and Canfield D. E. (2010) Evaluating the S-isotope fractionation associated with Phanerozoic pyrite burial. *Geochimica et Cosmochimica Acta* **74**, 2053-2071.

Zhang Y. and Kling G. W. (2006) Dynamics of lake eruptions and possible ocean eruptions. *Annual review of Earth and Planetary Sciences* **34**, 293-324.

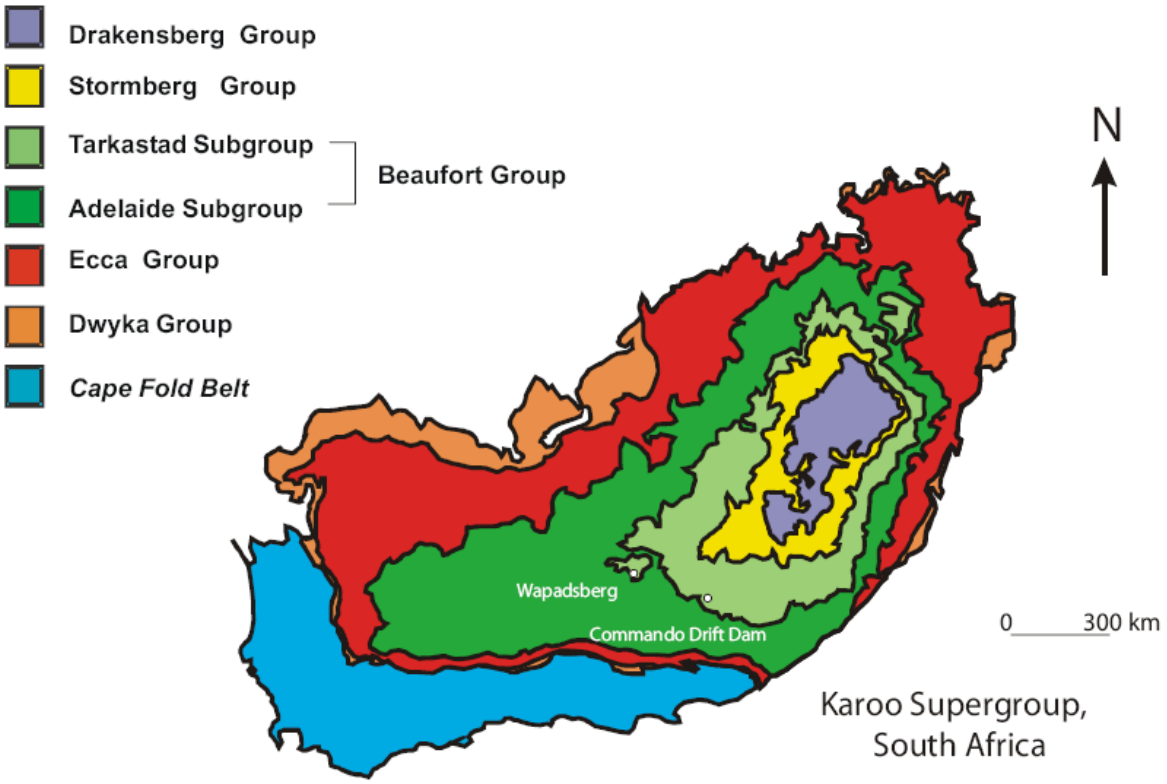

Fig. 4.1. Karoo Basin map and location of the 2 study sites (revised after Coney, 2005).

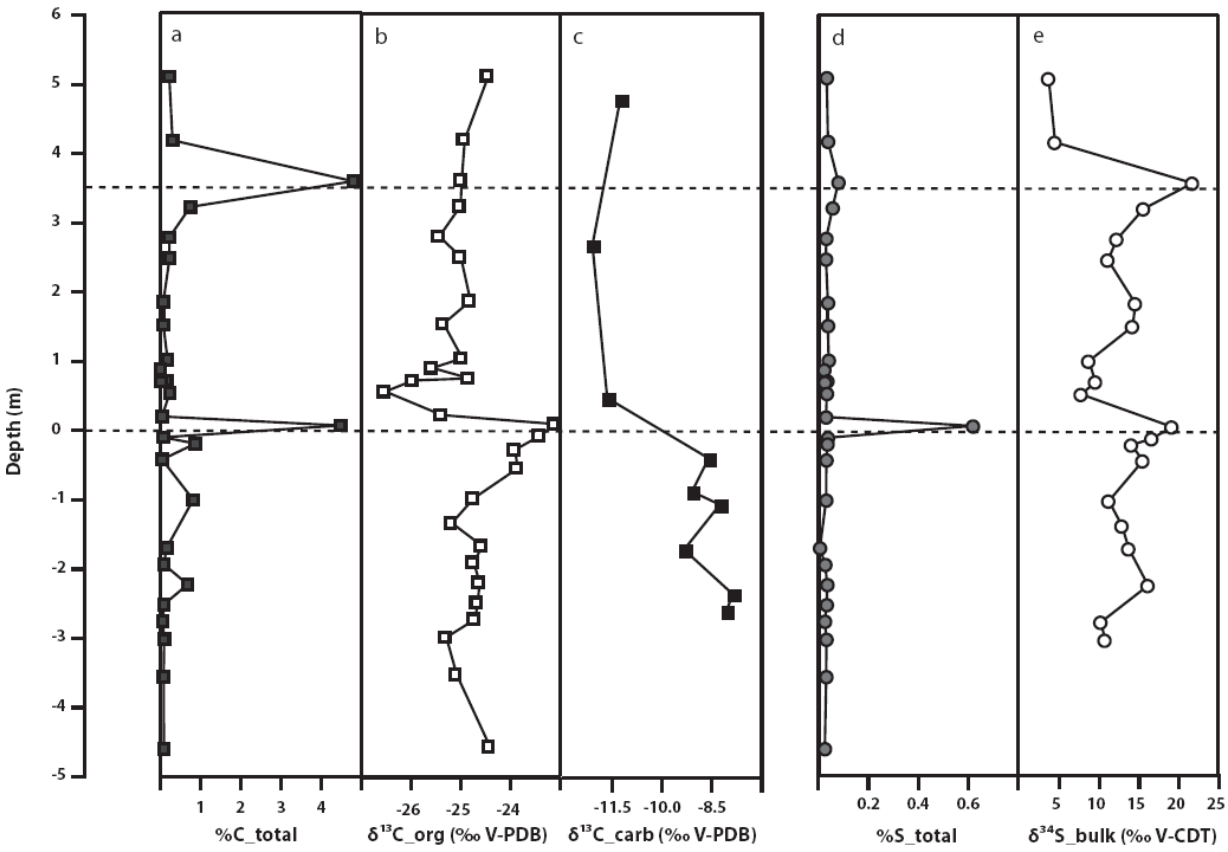

Fig. 4.2. C and S contents and isotope signatures of CCD samples

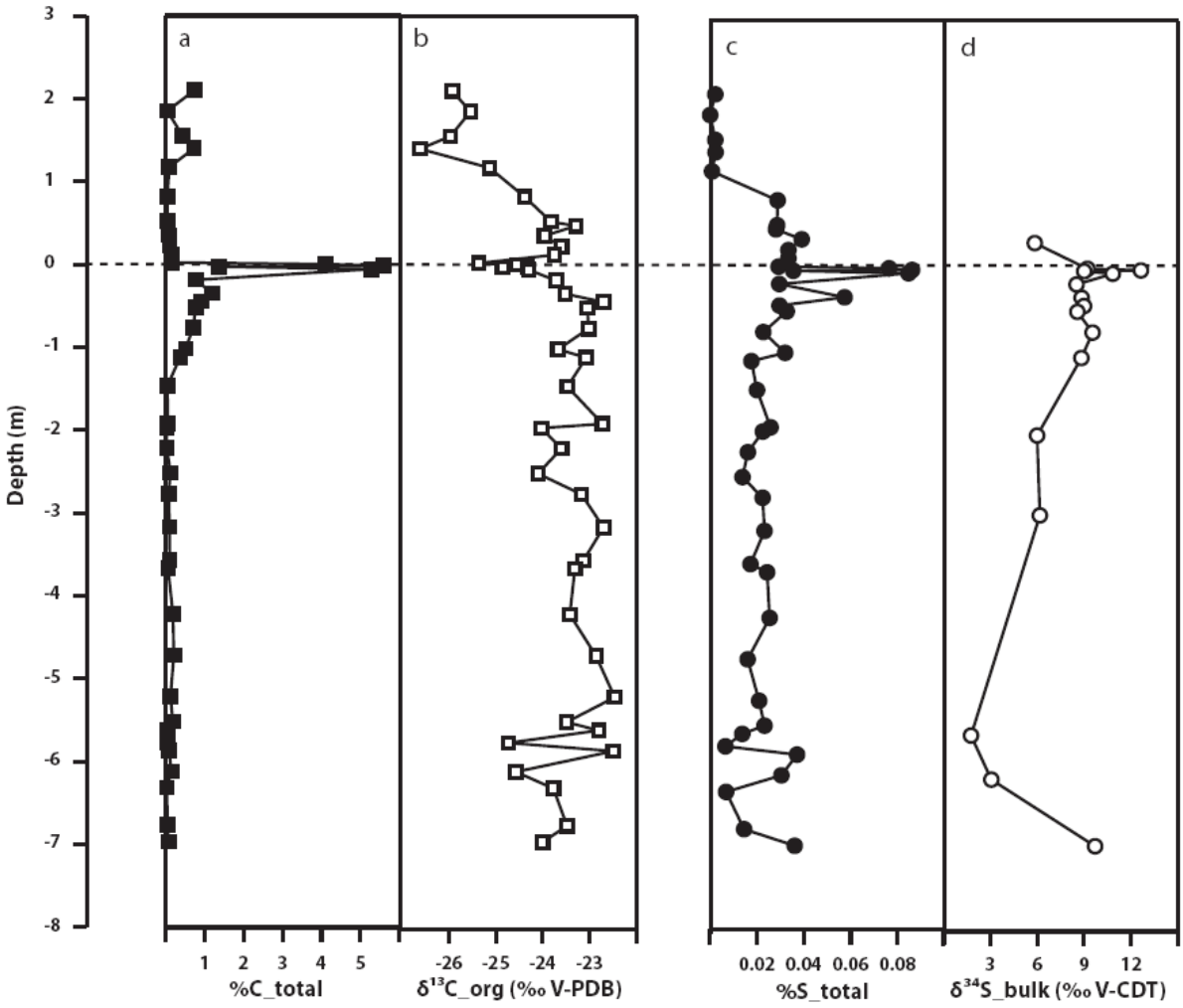

Fig 4.3. C and S contents and isotope signatures of WP samples

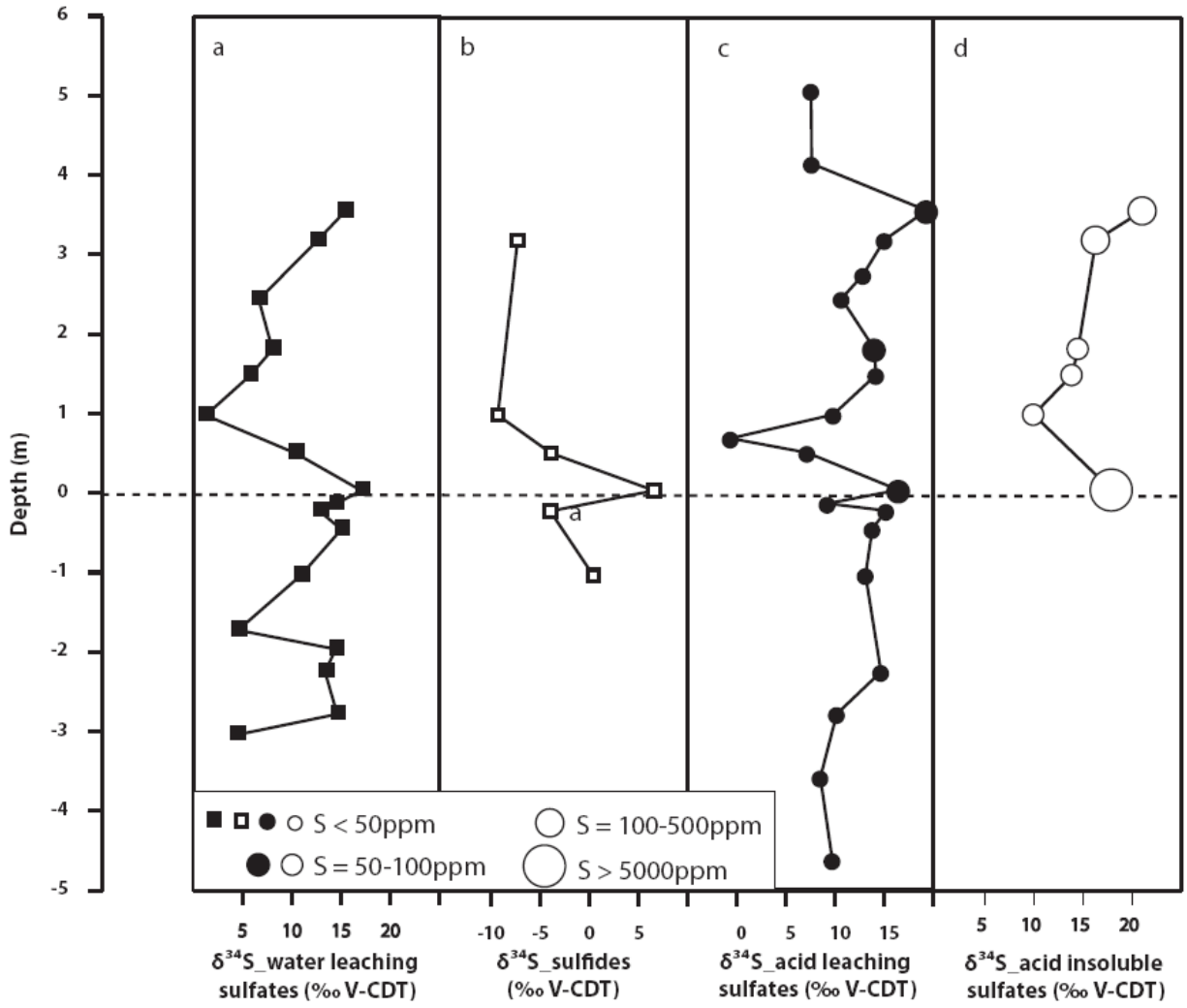

Fig. 4.4. Different sulphur pools in CDD

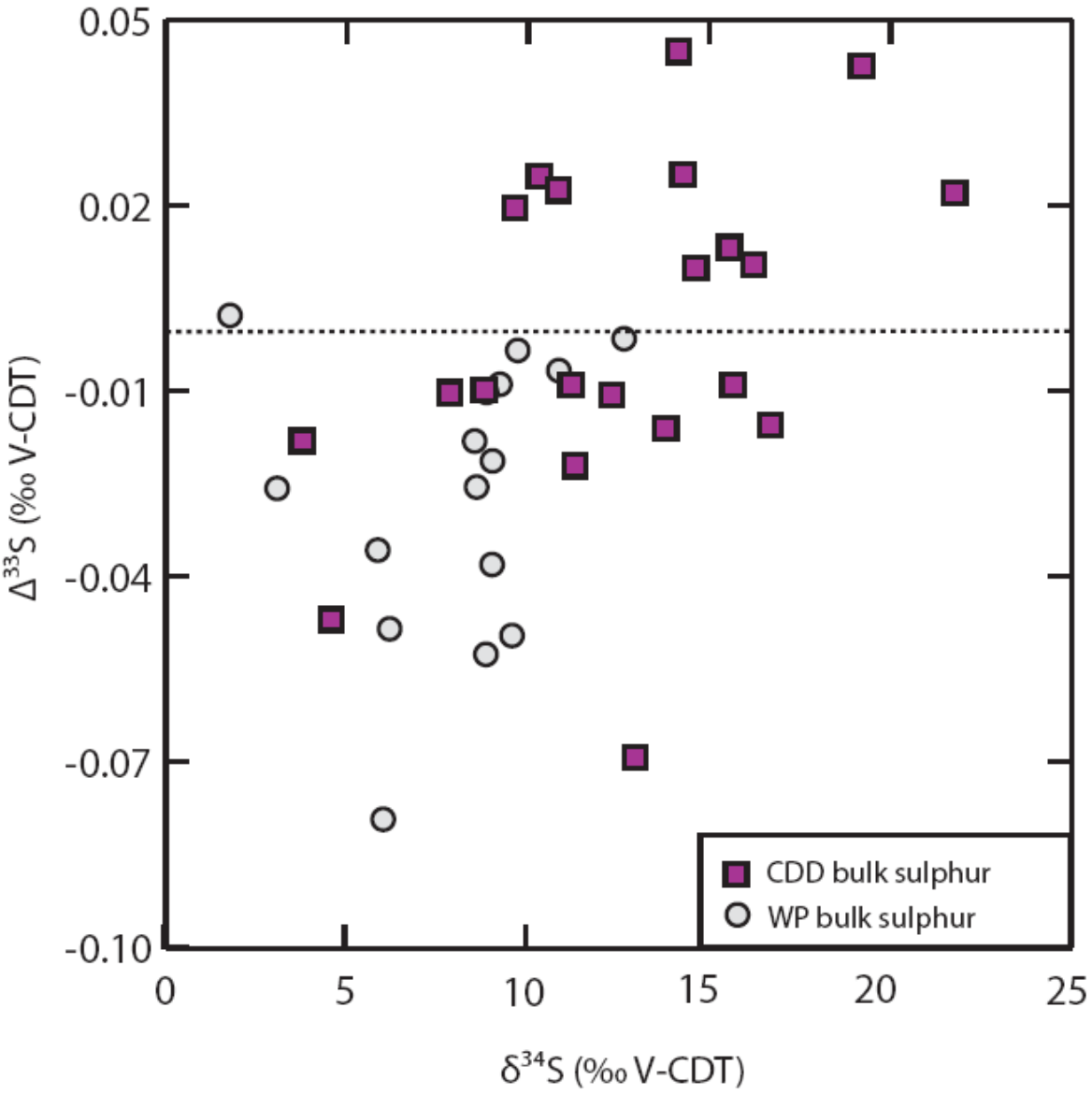

Fig. 4.5. Multiple S isotope signatures of bulk sulphur in CDD and WP

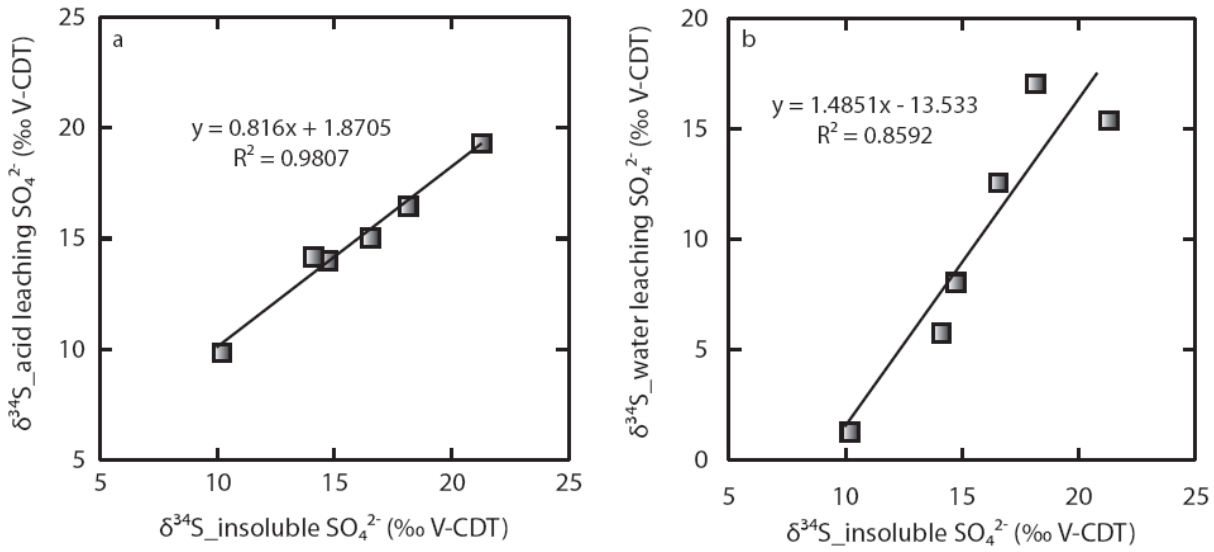

Fig. 4.6. The $\delta^{34}S$ relationships between three sulphate pools in CDD; (a) correlation between $\delta^{34}S$ of acid-leachable sulphate and $\delta^{34}S$ of acid-insoluble sulphate; (b) correlation between $\delta^{34}S$ of water-leachable sulphate and $\delta^{34}S$ of acid-insoluble sulphate.

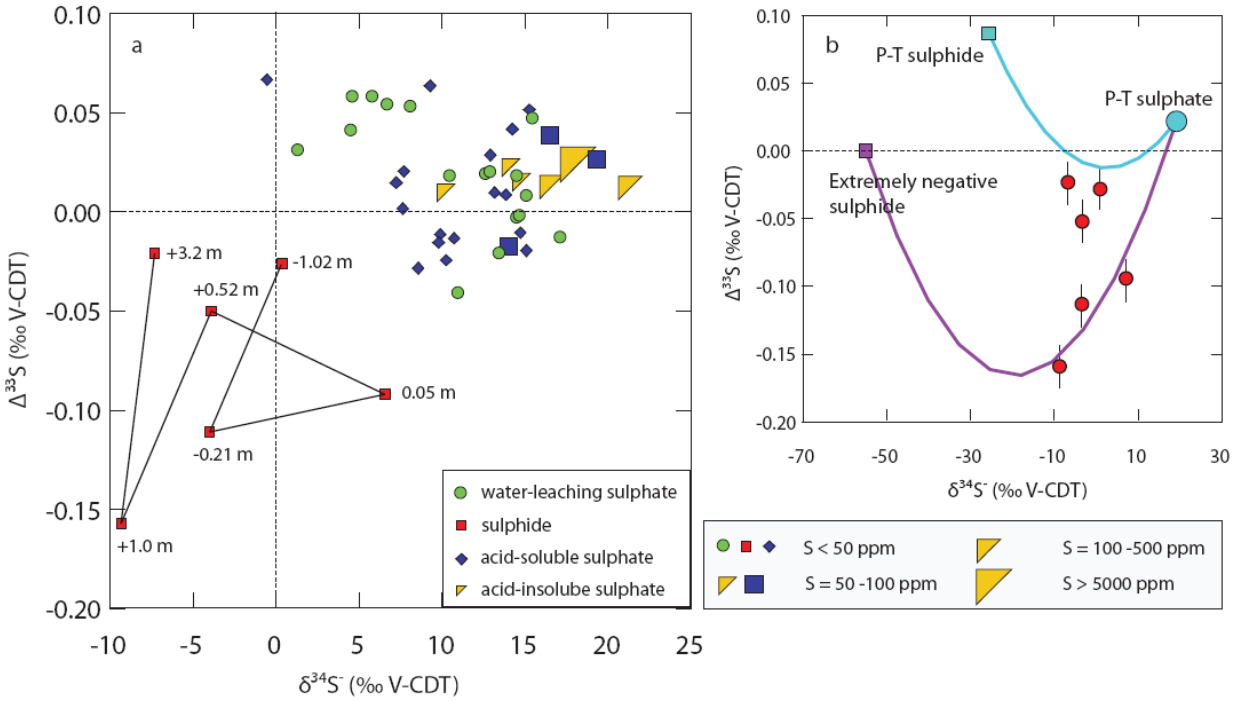

Fig. 4.7. Multiple sulphur isotope signatures of different sulphur pools in CDD (a) and 2 end-member mixing model to reproduce CDD sulphide multiple sulphur isotope signatures (b)

CHAPTER 5

Summary

5.1 Conclusions

The interpretive potential of multiple sulphur isotopes to the study of complex microbial pathways involved in the sulphur cycle of methane-rich marine sediments allows us to identify the contribution of each of these processes in such a complex natural system. This led us to conclude that the sedimentary methane flux is larger than estimates based on microbial sulphate reduction alone when an active reoxidative cycle is present. A natural limitation of the first study led us to inquire on the effect of transport by diffusion. The isotope fractionation of dissolved sulphur species (sulphate and sulphide) during diffusive transport in aqueous systems was investigated with multiple sulphur isotopes. No significant isotope fractionation was observed during sulphate diffusion leading us to suggest that one can ignore the impact of sulphate diffusion on the overall isotope fractionation of sulphate in sedimentary pore waters. In contrast, a clear fractionation develops in sulphide diffusion and needs to be taken into account on meter scale studies. Multiple sulphur isotopes, applied to seemingly mass-dependent processes allowed us to trace the source of sulphur injected into terrestrial P-T sediments. The interpretation of these signatures allowed us to propose different mechanisms that explain the cause and mechanism of Earth's largest recorded extinction event.

5.2 Statement of original contributions

5.2.1 Manuscript 1: Hidden sulphur cycle stimulates the microbial methane biofilter in deep marine sediments

Multiple sulphur isotopes have shown the presence of sulphur cycling in two similar study sites where an active reoxidative cycle was not identified with traditional sulphur isotope measurements. The conclusions obtained via multiple sulphur isotopes suggest that sulphide reoxidation may play an important role in the sulphur cycle which in turn leads to the under-estimation of methane fluxes based on conventional interpretation of the sulphate concentration profiles. The microbial sulphate reduction, coupled with a sulphide reoxidation model allows us

to correct the methane fluxes by determining the relative fraction of the sulphide flux back to sulphate. In station 5 of the Cascadia margin, at least 60% of the sulphide is recycled which amounts to a methane flux 2.5 times higher than the flux estimated from sulphate concentration profile alone.

5.2.2 Manuscript 2: Sulphur isotope effects of SO_4^{2-} and HS^- diffusion in water

To our knowledge, this is the first investigation which reports the experimental determination of the diffusion-associated fractionations of dissolved sulphate and sulphide. In opposition to kinetic theory, the experimental results show very small to negligible sulphur isotope fractionation of the sulphate ion during diffusion. The tiny diffusion-associated fractionation of dissolved sulphate confirms our assumption for the sulphate reduction models in chapter 2. The mono-hydrogen sulphide ion has a fractionation of 1.0±0.5‰, which is comparable to other mono-valent cations and anions, such as Na^+ and Cl^-. The isotope fractionation associated with the diffusion of sulphide can therefore be ignored in centimeter-scale processes. But it needs to be taken into account at the meter scale resolution. Finally, this fractionation does not change significantly in the studied temperature range (5ºC to 45ºC).

5.2.3 Manuscript 3: Sulphur and carbon isotope records across the terrestrial Permian-Triassic (P-T) boundary

In this study, we discussed the sources of sulphur enrichment at two study sites, CCD and WP in the Karoo Basin. We determined that four different sulphur sources; marine sulphates, volatized sulphide from euxinic marine water, mantle sulphur and volcanic sulphur, may have contributed to the sulphur enrichments observed. However, each individual sulphur source did not explain satisfactorily the multiple sulphur isotope characteristics of all sulphur fractions isolated from the sediments. A complex sulphur cycle during the P-T period may be to blame. Thus, no single sulphur deposition and corresponding event can be identified from the multiple S isotopes deposited during the end Permian mass extinction.

5.3 Future work

To expand the scope of the study elaborated in this thesis:

- In chapter 2, we built two separate models for MSR coupled with AOM at the SMTZ and for MSR coupled with organic matter oxidation. However, the coexistence of organic matter at the upper sediment layer and methane at deep sediment is widely observed. Therefore, it is necessary to develop a sulphur isotope model for MSR coupled with both AOM and OM oxidation in marine sediments.
- Following chapter 3, we would like to investigate the diffusion-associated fractionation of dissolved H_2S which is the main species of sulphide in aqueous solutions at pH <7. It might also be interesting to examine if the diffusion-associated fractionation changes with pH of the environment.
- Following chapter 4, we would like to study the sulphur content and the multiple sulphur isotope record in other terrestrial P-T boundary locations in order to determine if the sulphur enrichment at the P-T boundary is a global signal and if the provenance of the enriched sulphur detected in our study is from the same source.